Modelli ed esperimenti per la dinamica non lineare di dischi palettati con mistuning e contatti con attrito

ScuDo

Scuola di Dottorato ~ Doctoral School

WHAT YOU ARE, TAKES YOU FAR

Doctoral Dissertation

Doctoral Program in Mechanical Engineering (32^{th}cycle)

Models and Experiments for Nonlinear Dynamics of Mistuned Bladed Disks with Friction Contacts

By

S. Mehrdad Pourkiaee

******

Supervisor(s):

Prof. Stefano Zucca

Doctoral Examination Committee:

Prof. Paolo Tiso, Referee, ETH Zurich

Prof. Ender Cigeroglu, Referee, Middle East Technical University

Politecnico di Torino

April 2020

Declaration

I hereby declare that, the contents and organization of this dissertation constitute my own original work and does not compromise in any way the rights of third parties, including those relating to the security of personal data.

S. Mehrdad Pourkiaee
April 2020

* This dissertation is presented in partial fulfillment of the requirements for **Ph.D. degree** in the Graduate School of Politecnico di Torino (ScuDo).

I would like to dedicate this thesis to my lovely parents,
I love you beyond words,
I hope you will always feel that, even when I'm not around to tell you so.

Acknowledgements

I cannot begin to express my gratitude to my PhD advisor Prof. Stefano Zucca. I honestly do not have the proper words but thank you for going beyond what I asked of you. I will always be grateful for your professionalism and what you have done to help me.

I would like to extend my sincere thanks to Prof. Teresa Berruti who made enormous contribution to the experimental activities in my PhD study. Thank you for your guidance and persistent help.

I also had great pleasure of working with Prof. Robert G. Parker when he was a visiting professor at the Department of Mechanical and Aerospace Engineering in Politenico di Torino. I have greatly benefited from his insightful comments and constructive suggestions.

I also very much appreciate Prof. Malte Krack for welcoming me in his research group at the Institute of Aircraft Propulsion Systems, in University of Stuttgart. Many thanks to my fellow friends in the Structural Dynamics group for all the fruitful discussions and moments.

Special thanks to my fellows in the AerMec lab for all the support and friendship.

Finally, I would like to express my deepest gratitude to my lovely parents and to my beloved brother. Such a journey abroad, would not have been possible without your love, support and encouragement. Thank you from the bottom of my heart. To you I dedicate this thesis.

Abstract

Bladed disks can be found in engines used to power aircrafts and power plants. Due to their high modal density and the broad frequency range of the aerodynamic excitation forces, resonance-crossings on Campbell diagram are very likely during the design phase. High cycle fatigue (HCF) failure of turbine/compressor blades due to high vibration amplitudes in resonance frequency is one of the main concerns in their design stage. To suppress excessive vibrations in the blades and prevent HCF, dry friction damping has been widely incorporated into the design of bladed disks. However, due to the nonlinear nature of friction contacts, analysis of such systems becomes complicated. In addition to that, the inevitable presence of small variations between blades and consequently the loss of cyclic symmetry properties, known as mistuning, could considerably affect the dynamic behavior of bladed disks. Compared with that of a tuned bladed disk, which is a bladed disk with identical blades/sectors, the vibration response levels of a mistuned system can be much higher, that can ultimately result in premature HCF of blades.

Motivated by the turbomachinery community's need for practical design tools that can account for realistic operating conditions, one main focus of this dissertation is to develop models for nonlinear forced response analysis of bladed disks with friction interfaces. The developed models can be constructed by minimal computational effort (sector-level) and are suitable for statistical analyses, tailored for industrial applications. In addition, this dissertation faces the inherent complexity of experimental investigations of nonlinear dynamics of mistuned bladed disks. To this end, a detailed experimental campaign is conducted to evaluate the effects of mistuning on nonlinear forced response levels of an integrally bladed disk. The provided experimental benchmark can be used to validate the tools developed for nonlinear forced response of mistuned bladed disks.

Contents

List of Figures

List of Tables

Chapter 1

Introduction

1.1 Dynamics of Bladed Disks

In turbomachinery applications, bladed disks are critical components subjected to high levels of oscillating forces (e.g. unbalancing, fluctuating fluid flow) [2]. Because of their high modal density and the broad operating range of the engine, critical resonance crossings on the Campbell diagram are inevitable. This results in high amplitude vibrations and ultimately the high cycle fatigue (HCF) failure of the system. Accordingly, forced response calculations for predicting the maximum response levels, evaluating high stress situations and finally estimating the fatigue life is of crucial importance in the bladed disks design [3].

To reduce the vibration amplitude of the bladed disks, dry friction damping has been extensively incorporated into their design, since:

- Bladed disks are typically found lacking material damping.
- Other external damping sources like viscous and aerodynamic damping are usually very small. The latter one might even transfer the energy, conversely into the system (negative aerodynamic damping).

Friction damping is introduced into bladed disks through contact interfaces (i.e. mating surfaces with relative motion) and in different forms such as: blade attachments [4–6], shrouds [7, 8] or underplatform dampers [9–12]. Common types of friction joints used in bladed disks can be seen in Fig. 1.1.

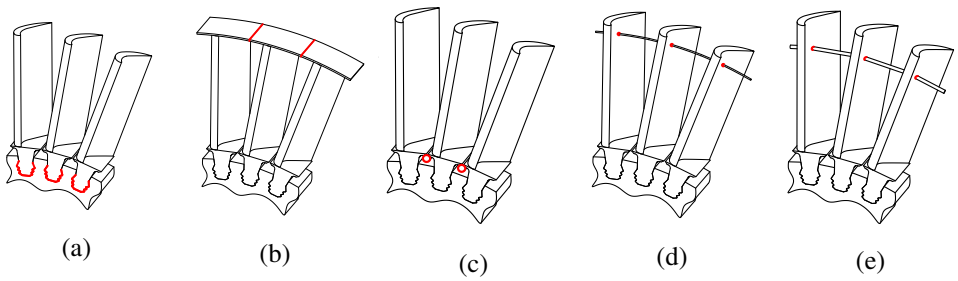

Fig. 1.1 Common friction joints in bladed disks [1]: (a) root joints, (b) shrouds, (c) under-platform dampers, (d) damper wires, (e) damper pins.

Boundary conditions at contact interfaces, and as a result the friction damping and the system natural frequencies, are highly dependent on vibration amplitudes. In other words, contact forces are state-dependent and nonlinear in nature [13]. Therefore, to accurately assess the amount of the friction damping and changes in natural frequencies, nonlinear analysis is mandatory.

Ideally, bladed disk sectors are designed to be identical. By assuming symmetry and in the absence of geometric nonlinearities, a single sector model is sufficient to compute the nonlinear forced response levels of the full system by defining the proper phase conditions at sector interfaces [14, 15].

Forced response calculations become more challenging in the presence of mistuning. The word mistuning refers to the differences which exist between the blades/sectors due to geometrical tolerances, material inhomogeneity, assembly process or due to the operating conditions such as the wear phenomena [16].

According to the literature, mistuning can be divided into two categories, namely small and large. There is no solid metric to quantify the level of mistuning, but it can be stated that in the presence of small mistuning, linear vibration modes of a mistuned system can be represented as a linear combination of its tuned vibration modes.

Small mistuning is basically modeled as small deviations of a structural property of the system from its nominal value. The most commonly varied structural properties are Young's modulus (this type of mistuning is also called stiffness or frequency mistuning) [17], damping [18] and even contact stiffness [19].
Large mistuning on the other hand, refers to significant changes in structural properties of the bladed disk (usually mass and stiffness) such that the assumption of

small mistuning fails to accurately predict system dynamics. Large mistuning, is usually modeled by using some modal properties of the underlying tuned system plus complementary bases which overall can predict the vibratory response of the original mistuned system [20].

Mistuning may have considerable effects on vibratory response of bladed disks. It is shown that, in the presence of mistuning vibration energy can be localized around few number of blades which can result in premature HCF of the blades [16].

From computational point of view, mistuning destroys cyclic symmetry and makes the full wheel model essential to predict the possible vibration localization and to correctly assess the HCF life of blades. On top of that, the random nature of mistuning demands Monte Carlo simulations to statistically characterize its effect on the response levels, which simply makes the nonlinear analysis of highly refined industrial finite element (FE) models unaffordable [21].

In the last three decades, nonlinear methods [22] based on Harmonic Balance Method (HBM) have established themselves as highly accurate and numerically efficient methods to compute the steady-state response of assemblies with contact interfaces, such as bladed disks [1].

Despite the huge time savings achievable by using the HBM with respect to Time Domain Analysis (TDA), the typical size of industrial finite element (FE) models of bladed disks (i.e. millions of degrees of freedom per sector) makes the analysis unfeasible for design purposes, unless reduced order models (ROMs) [23] are implemented to shorten the computational time.

In this regard, many ROMs have been developed for forced response analysis of *linear mistuned* bladed disks [16, 1, 24].

Based on their construction, they can be divided into component-mode-based [25, 26] or system-mode-based [27, 28] ROMs. The component-mode-based ROMs are developed based on Component Mode Synthesis (CMS) and substructuring techniques and by dividing the bladed disk system into blades and the disk components. In general, the CMS-based ROMs are suitable for any types of mistuning.
It is well known in the literature that any time a CMS-based approach is used, the interface degrees of freedom (DOFs) of the components may become the largest portion of the ROM, although their contribution to the dynamics of the system may be marginal. In order to overcome this problem, interface reduction (also known as

secondary reduction) methods have been developed [29, 30, 26] to reduce the size of the interface DOFs.

The system-mode-based ROMs are developed by incorporating the system-level vibration modes of the tuned system, into the reduction basis. This idea was initially introduced by Yang and Griffin [27] and was referred to as the subset of nominal modes (SNM).
The SNM was tailored for integrally bladed disks (also called blisk) with small frequency mistuning and by assuming that normal modeshapes of the mistuned blisks in a high modal density region, can be represented as a linear combination of its tuned vibration modes in the same frequency range.

This hypothesis implies that one can compute the reduction basis (i.e. the modeshapes of the tuned system) only once at the beginning of the forced response analysis, by performing single sector (called fundamental sector) computations, with the appropriate cyclic symmetry boundary conditions [31], without any need to develop the FE model of the full system.

The fundamental assumption of SNM was widely used and extended in further reduced order modeling techniques such as the: fundamental mistuning model (FMM) [32], component mode mistuning (CMM) [17], integral mode mistuning (IMM) [33], pristine–rogue–interface modal expansion (PRIME) [20] and nodal energy weighted transformation (NEWT) [28]. Compared to CMS-based techniques, system-mode-based reductions result in a very compact ROM with no retained interface DOFs.

A detailed description of ROMs developed for linear mistuned bladed disks can be found in [24, 34]. In both cases (either component-mode or system-mode based ROMs), the winning strategies are those which end up with a ROM in which:

- The reduction basis includes the modes of the tuned system, since only single-sector analysis is sufficient.
- The reduction basis is invariant of the mistuning pattern and is only computed once (necessary for statistical analyses).
- Interface degrees of freedom (DOFs) that are shared between adjacent components are not retained in the ROM, otherwise, performing extra secondary reductions is mandatory to reduce the ROM size.

1.2 Nonlinear Dynamics of Mistuned Bladed Disks

One cannot naturally extend the ROMs developed for linear systems to the nonlinear case, since:

- There is no proof that any set of modeshapes of the tuned system are a suitable basis for nonlinear forced response.
- The equivalent stiffness provided by the contact interfaces depends on the vibration amplitude and therefore there is not a single tuned linear system suitable as a projection basis for the governing equations of the nonlinear mistuned system.

In CMS-based ROMs for systems with localized nonlinearities master DOFs not only include the boundary DOFs that are used for CMS assembly but also contact DOFs at friction interfaces. Consequently, the performance of the final ROM will be tightly dependent on the choice of component normal modes and their assumed boundary conditions at boundary DOFs. Additionally, the effect of mistuning on statically condensed partitions of the ROM (that are associated with the retained master DOFs) should be addressed and needs more clarification, especially for different configurations of bladed disks.

In system-mode-based ROMs, that are developed for linear analysis of bladed disks (i.e. no contact DOF is retained in the ROM), it is not clear how to retain contact DOFs in the final ROM and yet be able to perform a system-level modal synthesis. This needs to be addressed in developing system-mode-based ROMs for nonlinear analysis of bladed disks with localized nonlinearities.

The literature about nonlinear mistuned bladed disks is much smaller, compared to the literature on linear mistuned systems [16] and nonlinear tuned systems [1], the reasons for that being the difficulties either in performing nonlinear analyses of full systems or in developing effective ROMs for the mistuned system.

Tang et al. [35] developed a ROM for nonlinear dynamics of blisks with ring dampers; the so-called coherent ring damper (CoRiD) method. They also combined the CoRiD with the method of N-PRIME [36] and were able to model the effect of both small and large mistuning, simultaneously.

In [37], Tang et al. introduced an extension of the Craig-Bampton [38] component mode synthesis (CB-CMS) with the component mode mistuning (CMM) method [17]. Using the CoRiD method along with the CB-CMS-CMM, they developed an efficient ROM for nonlinear dynamics of blisks with ring dampers and blade frequency mistuning.
The above-mentioned methods took advantage of a specific feature of ring dampers: they affect the response amplitude of the bladed disk with negligible effects on the system resonance frequencies.

Joannin et al. [39] used the concept of complex nonlinear modes to develop a ROM for mistuned bladed disks subjected to dry friction damping at blade roots. They obtained a compact ROM after performing three consecutive steps to reduce linear, nonlinear and interface DOFs. In this case, the friction contact (i.e. the blade root) was inside the bladed disk sector and this feature is at the basis of the nonlinear substructuring strategy proposed by the authors.

Unfortunately, in the presence of some of the vastly used friction damping sources, such as blade shrouds and underplatform dampers, the above-mentioned approaches are not satisfactory, since the friction contacts occur at the interfaces between adjacent sectors and strongly affect both the response amplitude and the resonance frequencies.

In [40], Mitra et al. developed the so-called Adaptive Microslip Projections (AMPs) to obtain a ROM for shrouded bladed disks, without discriminating between contact and non-contact DOFs. In this case, the reduction basis includes normal modes of multiple linear systems, characterized by different boundary conditions at contact interfaces.

In contrast to linear mistuned bladed disks, also fewer experimental studies have been devoted to nonlinear mistuned bladed disks with friction contacts. This might be due to the inherent complexity of performing such measurements (especially the nonlinear forced response measurements) which necessitates a carefully designed experimental set-up.

The adopted modeling techniques (for predicting the nonlinear forced response levels) in some few available studies [41–43] is typically based on cyclic symmetry assumptions and neglecting the effects of mistuning. In such strategies, the only possible comparison is between the numerical tuned response and the envelope of the experimental maximum response.

Although neglecting the effect of mistuning can be conditionally successful [42, 43], its limitations and validity conditions are not known a priori. Accurate prediction of nonlinear forced response levels of mistuned bladed disks with friction interfaces is quite challenging due to the strong nonlinearities induced at contact surfaces and also rich dynamics of the underlying linear mistuned system itself. This highlights the need for a detailed experimental campaign.

1.3 Objectives and Outline

As it was highlighted in section 1.1, accurate prediction of the forced response levels of bladed disks is a key design tool to access high vibration amplitudes, high stress situations and eventually to estimate fatigue life of the engine components.
In order to get close to realistic operating conditions, nonlinear friction damping (present at contact interfaces) and inevitable presence of the mistuning should be taken into account.

Accordingly, an important milestone of this thesis is the development of reduced order models tailored for nonlinear forced response of mistuned bladed disks with friction contacts.
The proposed models in this thesis work, give insight into efficient and accurate prediction of the nonlinear response levels of mistuned bladed disks with typical configurations of friction joins such as: shrouds, blade-root joints and underplatform dampers.

In the development of the ROMs, the following requirements and features are addressed:

- The ROM must be obtained by performing only sector-level calculations.
- The reduction basis must be invariant of the mistuning pattern. In this way, the reduction is performed only once and the mistuning can be introduced into the final ROM, necessary for statistical analyses.
- It is preferable that the ROM retains physical DOFs associated with contact interfaces for an efficient forced response calculation.

- It is preferable to enhance the accuracy of reduction basis by incorporating modal basis with boundary conditions close to actual kinematics at friction interfaces, especially at microslip (neither fixed nor free).
- It is preferable to implement system-level reductions, to obtain highly compact ROMs and avoid ending up with component assembly and the need of multiple secondary reductions.

Another milestone of the thesis is the experimental and numerical study carried out on an integrally bladed disk with full set of underplatform dampers. In the past few years, undeplatform dampers have attracted considerable attention as a source of dry friction damping.

Accurate prediction of nonlinear forced response levels of mistuned bladed disks with friction dampers is quite challenging due to the strong nonlinearities induced at contact surfaces and also rich dynamics of the underlying linear mistuned system itself. This highlights the need for a detailed experimental campaign. This part of the thesis works aims at providing:

i. An experimental benchmark for nonlinear dynamics of a mistuned bladed disks with UPDs.

ii. A numerical model that can account for features of a mistuned forced response level.

The thesis is organized as following:

- **Chapter 2** presents a component-based-mode reduced order model for nonlinear dynamics of mistuned bladed disks with shroud friction contacts. In the proposed ROM, the blades are reduced using the Craig-Bampton (CB) CMS technique to simply introduce frequency mistuning into the reduced space of the blades. Loaded interface modeshapes of the disk is then used to reduce the disk and the blade-disk interface component. This modal synthesis results in a very compact ROM with no need to perform a secondary reduction, which is a typical requirement after CMS-based reductions. The adopted logic implies that in the presence of friction contacts such as shrouds and underplatform dampers, the friction damping at the blade root joints is negligible and one can model the blade-disk joint as perfectly linearly elastic.

- **Chapter 3** presents a mixed-boundary model reduction technique for nonlinear forced response analysis of mistuned bladed disks with shroud friction contacts. The presented ROM is developed based on the the reduction technique introduced in Chapter. 2. The new approach benefits from the favorable features of the previous ROM and enhances some of its elements by: *(i)* reducing the blades in a more realistic mixed-boundary fashion, *(ii)* modeling the small sector-level frequency mistuning. The latter is especially beneficial when the mistuning is distributed through the sector or is not negligible at blade-disk interface DOFs.

- **Chapter 4** introduces a new reduced order modeling technique based on a Relative Cyclic Component Mode synthesis (RCCMS) approach. The developed ROM is tailored for nonlinear forced response analysis of bladed disks subjected to different sources of friction damping (friction interfaces). RCCMS is a highly compact system-mode-based ROM which only retains relative contact DOFs and a set of generalized coordinates associated with the system in fully stick condition. One of the interesting features of RCCMS is that the reduced space is divided into separate parts, one associated with nonlinear contact DOFs and the other one associated with the underlying linear system. This enables designers and analysts to efficiently employ methods that were initially developed for dynamic analysis of *linear* mistuned bladed disks.

- **Chapter 5** presents experimental and numerical investigation of mistuned forced responses of an integrally bladed disk with full set of underplatform dampers (UPDs). Accordingly, a detailed experimental campaign is conducted on a static test rig called Octopus. This rig is specifically designed to investigate the dynamics of a full-scale integrally bladed disk (blisk) with UPDs in a noncontact manner so that the dynamic response of the system is not modified. This chapter of the thesis provides an experimental benchmark that can be used for nonlinear dynamics of a mistuned bladed disks with UPDs. Moreover, a numerical model that can account for features of a mistuned forced response level.

Chapter 2

Reduced Order Models for Nonlinear Dynamics of Bladed Disks with Shrouds: Fixed-Boundary Component Mode Substitution

2.1 Introduction

In this chapter a component-mode-based reduced order modeling technique is introduced for nonlinear dynamics of mistuned bladed disks with shroud friction contacts. The adopted logic implies that in the presence of friction contacts such as shrouds and underplatform dampers, the friction damping at the blade root joints is negligible and one can model the blade-disk joint as perfectly linearly elastic. Accordingly, eliminating the blade-disk interfaces from the final ROM (without performing any secondary reduction technique) is one of the objectives and features of the method.

In detail, the blades are reduced with the CB-CMS approach, retaining as master DOFs, shroud contact DOFs and interface DOFs between blades and the disk. Then, after performing the so-called primal assembly between the reduced blades and the full disk; at the interface DOFs; the loaded interface modeshapes of the disk are used to approximate the dynamics of the disk and interfaces.

Here, loaded interface modeshapes refer to normal modes of the disk component where blades are statically condensed (loaded) on blade-disk interfaces [44]. The resulting ROM only retains as master DOFs the contact DOFs and, if deemed necessary by the analyst, additional auxiliary DOFs on the blades.

Finally, it is shown that, the CB-CMS reduction matrix of the blades is invariant with respect to the blade frequency mistuning. Accordingly, in the case of small frequency mistuning, a general formulation is derived which enables analysts and designers to obtain the mistuned ROM of the full system based on sector level calculations.

2.2 Reduced Order Modeling Technique

In order to better clarify the mathematical formulation of the reduced order model, the method is firstly applied to a single sector (i.e. disk fundamental sector + 1 blade) and only afterwards it is shown how to extend the sector reduced matrices to the full system and how to introduce blade frequency mistuning into the final reduced system.

2.2.1 Methodology

In the newly developed reduction technique, the fundamental sector of a tuned bladed disk is divided into blade and disk components. First, the CB-CMS reduction is applied to the blade component. Then the modal reduction is performed to project the physical interface and disk DOFs onto the modal coordinates of the disk loaded interface modeshapes. As a preliminary step, the blade and the disk sector DOFs and their corresponding stiffness matrices are partitioned as follows (see Fig. 2.1):

$$
\begin{aligned}
x_B &= \left\{ \begin{array}{c} x_I \\ x_N \\ x_\gamma^b \end{array} \right\}, \quad K_b = \left[\begin{array}{ccc} k_{II}^b & k_{IN}^b & k_{I\gamma}^b \\ k_{NI}^b & k_{NN}^b & 0 \\ k_{\gamma I}^b & 0 & k_{\gamma\gamma}^b \end{array} \right] \\
x_D &= \left\{ \begin{array}{c} x_\gamma^d \\ x_O \end{array} \right\}, \quad K_d = \left[\begin{array}{cc} k_{\gamma\gamma}^d & k_{\gamma O}^d \\ k_{O\gamma}^d & k_{OO}^d \end{array} \right]
\end{aligned}
\tag{2.1}
$$

where x_γ^b and x_γ^d correspond to interface DOFs of the blade and the disk, respectively, x_N represents contact nonlinear DOFs of the blade (e.g. contact nodes at shrouds), x_I represents remaining interior DOFs of the blade and x_O corresponds to other DOFs of the disk except interface DOFs. Note that in more general context, x_N could represent any group of active DOFs that are retained during CB-CMS reduction. Throughout this chapter, all mass matrices are partitioned exactly in the same way as their corresponding stiffness matrices.

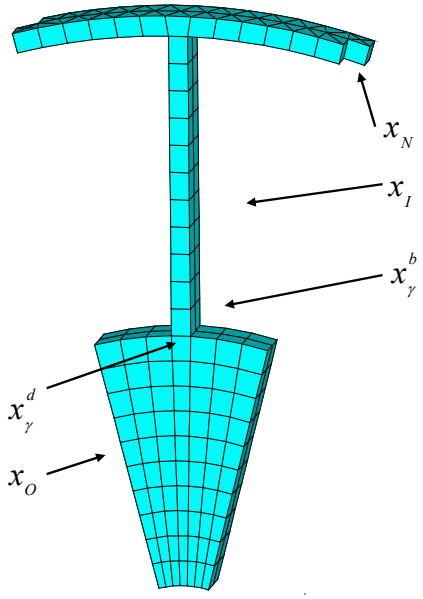

Fig. 2.1 Fundamental sector of a simplified shrouded bladed disk and its partitioned DOFs.

It is worth mentioning that the structural matrices defined in Eq. 2.1 correspond to the linear sector of the bladed disk and the x_N partition denotes DOFs at which friction contact will be modeled during the nonlinear forced response analysis.

2.2.2 Blade Component Reduction

In order to apply CB-CMS on the blade component, blade DOFs are grouped into x_m and x_s vectors to separate master (physical retained) and slave DOFs. Master DOFs include interface DOFs x_γ^b, necessary to enforce CMS primal assembly and nonlinear DOFs x_N, retained for the nonlinear forced response computations. The partitioned blade displacement vector and the corresponding stiffness matrix, take

the following form:

$$x_B = \left\{ \begin{array}{c} x_I \\ \hline x_N \\ x_\gamma^b \end{array} \right\} = \left\{ \begin{array}{c} x_s \\ x_m \end{array} \right\}$$

$$K_b = \left[\begin{array}{cc} k_{ss} & k_{sm} \\ k_{ms} & k_{mm} \end{array} \right] = \left[\begin{array}{c|cc} k_{II}^b & k_{IN}^b & k_{I\gamma}^b \\ \hline k_{NI}^b & k_{NN}^b & 0 \\ k_{\gamma I}^b & 0 & k_{\gamma\gamma}^b \end{array} \right] \tag{2.2}$$

The blade DOFs can now be reduced using the CB-CMS transformation matrix R_{CB}, as follows:

$$\left\{ \begin{array}{c} x_s \\ x_m \end{array} \right\} = R_{CB} \left\{ \begin{array}{c} \eta \\ x_m \end{array} \right\}, \quad R_{CB} = \left[\begin{array}{cc} \Phi_f & \Psi_c \\ 0 & I \end{array} \right] \tag{2.3}$$

where Φ_f are fixed-interface modeshapes of the blade constrained at its master DOFs and $\Psi_c = -k_{ss}^{-1} k_{sm}$ are static constraint modes. Projecting the blade structural matrices onto the CB-CMS coordinates, yields:

$$K_{CB} = R_{CB}^T K_b R_{CB} = \left[\begin{array}{cc} \Lambda_i^b & 0 \\ 0 & K_{cb}^b \end{array} \right]$$

$$M_{CB} = R_{CB}^T M_b R_{CB} = \left[\begin{array}{cc} I & m_{\eta m} \\ m_{m\eta} & M_{cb}^b \end{array} \right] \tag{2.4}$$

where K_{CB} and M_{CB} are blade CB-CMS reduced stiffness and mass matrices, respectively. Different partitions of K_{CB} and M_{CB} are given below:

$$\begin{aligned} K_{cb}^b &= k_{mm} - k_{ms} k_{ss}^{-1} k_{sm} \\ \Lambda_i^b &= \Phi_f^T k_{ss} \Phi_f \\ M_{cb}^b &= m_{mm} + \Psi_c^T m_{ss} \Psi_c + m_{ms} \Psi_c + \Psi_c^T m_{sm} \\ M_{\eta m} &= \Phi_f^T m_{ss} \Psi_c + \Phi_f^T m_{sm} \end{aligned} \tag{2.5}$$

Note that the lower right partition of K_{CB} represents the blade CB-CMS reduced stiffness matrix corresponding to retained physical DOFs (i.e. blade nonlinear and

interface DOFs) and is expanded as follows:

$$K_{cb}^{b} = \begin{bmatrix} k_{cb,NN}^{b} & k_{cb,N\gamma}^{b} \\ k_{cb,\gamma N}^{b} & k_{cb,\gamma\gamma}^{b} \end{bmatrix} = \begin{bmatrix} k_{NN}^{b} - k_{NI}^{b} k_{II}^{b^{-1}} k_{IN}^{b} & -k_{NI}^{b} k_{II}^{b^{-1}} k_{I\gamma}^{b} \\ -k_{\gamma I}^{b} k_{II}^{b^{-1}} k_{IN}^{b} & k_{\gamma\gamma}^{b} - k_{\gamma I}^{b} k_{II}^{b^{-1}} k_{I\gamma}^{b} \end{bmatrix} \tag{2.6}$$

Different partitions of M_{CB} are presented in Appendix B.1.

2.2.3 Interface and Disk Reduction

The proposed modal reduction operates on the disk DOFs plus the interface DOFs retained during the blade CB-CMS reduction, by projecting them to a set of generalized coordinates. Loaded interface modeshapes of the disk are obtained by statically condensing the blade interior DOFs on blade-disk interface DOFs x_{γ}^{b} and then solving the eigenvalue problem of the loaded disk system. Static condensation of interior blade DOFs on interface DOFs can be obtained by:

$$x_B = \left\{ \begin{array}{c} x_I \\ \hline x_N \\ x_{\gamma}^{b} \end{array} \right\} = \left\{ \begin{array}{c} x_i^{b} \\ x_{\gamma}^{b} \end{array} \right\} = \begin{bmatrix} \psi_c^{b} \\ I \end{bmatrix} x_{\gamma}^{b} = \beta x_{\gamma}^{b} \tag{2.7}$$

where x_i^{b} are interior DOFs of the blade and ψ_c^{b} are static constraint modes, given by:

$$\psi_c^{b} = -k_{ii}^{-1} k_{i\gamma} = -\begin{bmatrix} k_{II}^{b} & k_{IN}^{b} \\ k_{NI}^{b} & k_{NN}^{b} \end{bmatrix}^{-1} \begin{bmatrix} k_{I\gamma}^{b} \\ 0 \end{bmatrix} \tag{2.8}$$

Note that, in contrast to the blade CB-CMS reduction where both x_N and x_{γ}^{b} DOFs are retained as master DOFs, here, the blade DOFs are statically condensed only on interface DOFs x_{γ}^{b} and thus the ψ_c^{b} matrix includes the constraint modes of the cantilevered blade. The Guyan reduced mass and stiffness matrices of the blade can be obtained by:

$$\begin{aligned} k_{Guyan}^{b} &= \psi_c^{bT} K_b \psi_c^{b} = k_{\gamma\gamma}^{b} - k_{\gamma i} k_{ii}^{-1} k_{i\gamma} \\ m_{Guyan}^{b} &= \psi_c^{bT} M_b \psi_c^{b} = m_{\gamma\gamma}^{b} + \psi_c^{bT} M_{ii} \psi_c^{b} + M_{\gamma i} \psi_c^{b} + \psi_c^{bT} M_{i\gamma} \end{aligned} \tag{2.9}$$

As a final step, the mass and stiffness matrices of the loaded disk are obtained:

$$\begin{aligned}\tilde{K} &= \begin{bmatrix} k^d_{\gamma\gamma}+k^b_{Guyan} & k^d_{\gamma O} \\ k^d_{O\gamma} & k^d_{OO} \end{bmatrix} \\ \tilde{M} &= \begin{bmatrix} m^d_{\gamma\gamma}+m^b_{Guyan} & m^d_{\gamma O} \\ m^d_{O\gamma} & m^d_{OO} \end{bmatrix}\end{aligned} \tag{2.10}$$

Solving the following eigenvalue problem:

$$\left(\tilde{K}-\Lambda_{LI}\tilde{M}\right)\tilde{\varphi}=0 \tag{2.11}$$

gives the disk loaded interface modeshapes $\tilde{\varphi}$ and eigenvalues Λ_{LI}. Prior to applying the interface-disk modal reduction, one should perform a CMS assembly to cast the partially reduced blisk structural matrices. Enforcing interface compatibility between the CB-CMS reduced blade and the disk component, yields:

$$\begin{aligned}K_1 &= \begin{bmatrix} \Lambda^b_i & 0 & 0 & 0 \\ 0 & k^b_{cb,NN} & k^b_{cb,N\gamma} & 0 \\ 0 & k^b_{cb,\gamma N} & k^b_{cb,\gamma\gamma}+k^d_{\gamma\gamma} & k^d_{\gamma O} \\ 0 & 0 & k^d_{O\gamma} & k^d_{OO} \end{bmatrix} \\ M_1 &= \begin{bmatrix} I & m_{\eta N} & m_{\eta\gamma} & 0 \\ m_{N\eta} & m^b_{cb,NN} & m^b_{cb,N\gamma} & 0 \\ m_{\gamma\eta} & m^b_{cb,\gamma N} & m^b_{cb,\gamma\gamma}+m^d_{\gamma\gamma} & m^d_{\gamma O} \\ 0 & 0 & m^d_{O\gamma} & m^d_{OO} \end{bmatrix}\end{aligned} \tag{2.12}$$

Now, the further reduction can be achieved by expressing the interface and disk DOFs of the displacement vector in terms of loaded interface modal coordinates:

$$\begin{Bmatrix} \eta \\ x_N \\ \left\{ \begin{matrix} x_\gamma \\ x_O \end{matrix} \right\} \end{Bmatrix} = \begin{bmatrix} I & 0 & 0 \\ 0 & I & 0 \\ 0 & 0 & \tilde{\varphi} \end{bmatrix} \begin{Bmatrix} \eta \\ x_N \\ \tilde{\eta} \end{Bmatrix} = R_{LI} \begin{Bmatrix} \eta \\ x_N \\ \tilde{\eta} \end{Bmatrix} \tag{2.13}$$

where R_{LI} denotes the LI reduction matrix. The final reduced mass and stiffness matrices of the fundamental sector is obtained by implementing the following pro-

jections:

$$\begin{aligned} K_{rom} &= R_{LI}^T K_1 R_{LI} \\ M_{rom} &= R_{LI}^T M_1 R_{LI} \end{aligned} \tag{2.14}$$

Final reduced stiffness matrix and its different partitions take the following form:

$$\begin{aligned} K_{rom} &= \begin{bmatrix} I & 0 & 0 \\ 0 & I & 0 \\ 0 & 0 & \begin{bmatrix} \tilde{\varphi}_\gamma \\ \tilde{\varphi}_O \end{bmatrix} \end{bmatrix}^T \begin{bmatrix} \Lambda_i^b & 0 & 0 & 0 \\ 0 & k_{cb,NN}^b & k_{cb,N\gamma}^b & 0 \\ 0 & k_{cb,\gamma N}^b & k_{cb,\gamma\gamma}^b + k_{\gamma\gamma}^d & k_{\gamma O}^d \\ 0 & 0 & k_{O\gamma}^d & k_{OO}^d \end{bmatrix} \begin{bmatrix} I & 0 & 0 \\ 0 & I & 0 \\ 0 & 0 & \begin{bmatrix} \tilde{\varphi}_\gamma \\ \tilde{\varphi}_O \end{bmatrix} \end{bmatrix} \\ &= \begin{bmatrix} \Lambda_i^b & 0 & 0 \\ 0 & k_{cb,NN}^b & k_{cb,N\gamma}^b \tilde{\varphi}_\gamma \\ 0 & \tilde{\varphi}_\gamma^T k_{cb,\gamma N}^b & [\hat{k}] \end{bmatrix} \end{aligned} \tag{2.15}$$

where

$$\hat{k} = \begin{bmatrix} \tilde{\varphi}_\gamma \\ \tilde{\varphi}_O \end{bmatrix}^T \begin{bmatrix} k_{cb,\gamma\gamma}^b + k_{\gamma\gamma}^d & k_{\gamma O}^d \\ k_{O\gamma}^d & k_{OO}^d \end{bmatrix} \begin{bmatrix} \tilde{\varphi}_\gamma \\ \tilde{\varphi}_O \end{bmatrix}. \tag{2.16}$$

The evolution of the original set of DOFs of the fundamental sector during the reduction is depicted in Fig. 2.2.

$$\begin{Bmatrix} x_I \\ x_N \\ x_\gamma \\ x_O \end{Bmatrix} = \begin{Bmatrix} x_s = x_I \\ x_m = \begin{bmatrix} x_N \\ x_\gamma \end{bmatrix} \\ x_O \end{Bmatrix} \xrightarrow[\text{Blade Component}]{R_{CB}} \begin{Bmatrix} \eta \\ x_m \\ x_O \end{Bmatrix}$$

$$\begin{Bmatrix} \eta \\ x_m \\ x_O \end{Bmatrix} = \begin{Bmatrix} \eta \\ x_m = \begin{bmatrix} x_N \\ x_\gamma \end{bmatrix} \\ x_O \end{Bmatrix} \xrightarrow[\text{Interface-Disk Component}]{R_{LI}} \begin{Bmatrix} \eta \\ x_N \\ \tilde{\eta} \end{Bmatrix}$$

Fig. 2.2 Evolution of DOFs during the reduction.

2.2.4 Full Bladed Disk ROM

Without losing any generality of the presented formulation for the single sector, this reduction approach can be easily extended to the full system. In this case, each partition of matrices in Eq. (2.1) should be replaced by a block diagonal matrix, representing the contribution of all sectors in the structural matrices. Accordingly, the blade and the disk stiffness matrices of the full structure can be expressed as follows:

$$K_B = \begin{bmatrix} I \otimes k^b_{II} & I \otimes k^b_{IN} & I \otimes k^b_{I\gamma} \\ I \otimes k^b_{NI} & I \otimes k^b_{NN} & 0 \\ I \otimes k^b_{\gamma I} & 0 & I \otimes k^b_{\gamma\gamma} \end{bmatrix}$$
$$K_D = \begin{bmatrix} I \otimes k^d_{\gamma\gamma} & I \otimes k^d_{\gamma O} \\ I \otimes k^d_{O\gamma} & \bar{k}^d_{OO} \end{bmatrix} \tag{2.17}$$

where I is an identity matrix of size N (number of blades) and $\otimes$ denotes the Kronecker product. In Eq. (2.17), $\bar{k}^d_{OO}$ is the partition of the full disk component corresponding to x_O DOFs. Note that $\bar{k}^d_{OO}$ is not a pure block diagonal partition, due to the presence of internal interfaces between disk sectors. Since the blades are uncoupled to each other and identical as no mistuning is introduced yet, the CB-CMS transformation matrix of N-blades structure, can be obtained from the single blade transformation matrix, as follows:

$$\bar{R}_{cb} = \begin{bmatrix} I \otimes \Phi_f & I \otimes \Psi_c \\ 0 & I \end{bmatrix} \tag{2.18}$$

The CB-CMS reduced stiffness matrix of the full set of blades, can be described as:

$$\bar{K}_{CB} = \begin{bmatrix} I \otimes \Lambda^b_i & 0 & 0 \\ 0 & I \otimes k^b_{cb,NN} & I \otimes k^b_{cb,N\gamma} \\ 0 & I \otimes k^b_{cb,\gamma N} & I \otimes k^b_{cb,\gamma\gamma} \end{bmatrix} \tag{2.19}$$

Enforcing the interface compatibility over the interface DOFs, yields an assembly composed of CB-CMS reduced blades attached to the full disk at the blade-disk

interfaces. The stiffness matrix of this partially reduced system is expressed as:

$$K_I = \begin{bmatrix} I \otimes \Lambda_i^b & 0 & 0 & 0 \\ 0 & I \otimes k_{cb,NN}^b & I \otimes k_{cb,N\gamma}^b & 0 \\ 0 & I \otimes k_{cb,\gamma N}^b & I \otimes k_{\gamma\gamma}^{rom} & I \otimes k_{\gamma O}^d \\ 0 & 0 & I \otimes k_{O\gamma}^d & \bar{k}_{OO}^d \end{bmatrix} \tag{2.20}$$

where $k_{\gamma\gamma}^{rom} = k_{cb,\gamma\gamma}^b + k_{\gamma\gamma}^d$ denotes the interface stiffness partition, made of the CB-CMS reduced stiffness of the blade interface added to the interface stiffness of the disk component. The K_I matrix must be now further reduced by means of loaded interface modeshapes of the full disk (i.e. $\tilde{\Phi}$). Due to the cyclic symmetry of the system, modeshapes of the full disk can be obtained by expanding modeshapes of the loaded fundamental sector computed with cyclic symmetry boundary conditions [31]. The final reduced stiffness matrix of the tuned bladed disk is:

$$K_{ROM} = \begin{bmatrix} I \otimes \Lambda_i^b & 0 & 0 \\ 0 & I \otimes k_{cb,NN}^b & \left(I \otimes k_{cb,N\gamma}^b\right) \tilde{\Phi}_\gamma \\ 0 & \tilde{\Phi}_\gamma^T \left(I \otimes k_{cb,\gamma N}^b\right) & [\hat{K}] \end{bmatrix} \tag{2.21}$$

with

$$\hat{K} = \begin{bmatrix} \tilde{\Phi}_\gamma \\ \tilde{\Phi}_O \end{bmatrix}^T \begin{bmatrix} \underset{n=1..N}{Bdiag}[k_{\gamma\gamma}^{rom^{(n)}}] & I \otimes k_{\gamma O}^d \\ I \otimes k_{O\gamma}^d & \bar{k}_{OO}^d \end{bmatrix} \begin{bmatrix} \tilde{\Phi}_\gamma \\ \tilde{\Phi}_O \end{bmatrix} \tag{2.22}$$

where $\underset{n=1..N}{Bdiag}[k_{\gamma\gamma}^{rom^{(n)}}] = I \otimes k_{\gamma\gamma}^{rom}$.

Note that, the same discussion and methodology is used to obtain the reduced mass matrix of the full system i.e. M_{ROM} (a detailed description is given in Appendix B.1).

2.2.5 Mistuning Modeling

The presented reduction technique is tailored for small blade mistuning. Accordingly, the disk is treated as a tuned cyclic structure and mistuning is introduced as variations in Young's modulus of blades (blade frequency mistuning). In order to introduce mistuning to the final reduced model; in terms of Young's modulus variation of blades; it is beneficial to recall that based on the Hooke's law for isotropic materials,

the element stiffness matrix k^e which relates nodal forces to nodal displacements, is linearly dependent to Young's modulus as follows:

$$k^e = E \cdot k^{e\prime} \tag{2.23}$$

As described before, the CB-CMS method is used to reduce the blades. Therefore, the effect of blade Young's modulus variation on the CB-CMS reduction matrix R_{cb}, defined by Eq. (2.3), is investigated. It turns out that for a single component of nominal Young's modulus E, the corresponding CB-CMS transformation matrix is invariant of Young's modulus, and the resultant CB-CMS reduced stiffness matrix is linearly dependent to E as follows:

$$K_{CB} = \begin{bmatrix} E \cdot \Lambda_i'^b & 0 \\ 0 & E \cdot \left(k'_{mm} - k'_{ms} k'^{-1}_{ss} k'_{sm}\right) \end{bmatrix} \tag{2.24}$$

In the case of mistuned systems, the random Young's modulus can be defined as:

$$E_n = E \cdot (1 + \delta_n) \tag{2.25}$$

where E_n is the Young's modulus of the nth blade, E is the nominal Young's modulus and δ_n is a non-dimensional mistuning parameter used to perturb E. Accordingly, one may obtain the final reduced form of the mistuned stiffness matrix as follows:

$$K_{ROM} = \begin{bmatrix} \underset{n=1..N}{diag}\,(1+\delta_n) \otimes \Lambda_i^b & 0 & 0 \\ 0 & \underset{n=1..N}{diag}\,(1+\delta_n) \otimes k^b_{cb,NN} & \left(\underset{n=1..N}{diag}\,(1+\delta_n) \otimes k^b_{cb,N\gamma}\right) \tilde{\Phi}_\gamma \\ 0 & \tilde{\Phi}_\gamma^T \left(\underset{n=1..N}{diag}\,(1+\delta_n) \otimes k^b_{cb,\gamma N}\right) & [\hat{K}] \end{bmatrix} \tag{2.26}$$

with

$$\hat{K} = \begin{bmatrix} \tilde{\Phi}_\gamma \\ \tilde{\Phi}_O \end{bmatrix}^T \begin{bmatrix} \underset{n=1..N}{Bdiag}[k^{*rom^{(n)}}_{\gamma\gamma}] & I \otimes k^d_{\gamma O} \\ I \otimes k^d_{O\gamma} & \bar{k}^d_{OO} \end{bmatrix} \begin{bmatrix} \tilde{\Phi}_\gamma \\ \tilde{\Phi}_O \end{bmatrix} \tag{2.27}$$

where

$$\begin{aligned} \underset{n=1..N}{Bdiag}[k^{*rom^{(n)}}_{\gamma\gamma}] &= \underset{n=1..N}{Bdiag}[k^{*b^{(n)}}_{cb,\gamma\gamma}] + \underset{n=1..N}{Bdiag}[k^{d^{(n)}}_{\gamma\gamma}] \\ &= \underset{n=1..N}{diag}\,(1+\delta_n) \otimes k^{b}_{cb,\gamma\gamma} + I \otimes k^{d}_{\gamma\gamma} \end{aligned} \tag{2.28}$$

Note that superscript $(.)^*$; first introduced in Eq. (2.27); will be used to denote a mistuned partition. For ROMs to be useful in stochastic nonlinear analysis, necessary to assess statistically the effect of mistuning on the response level of the blades, direct introduction of mistuning in the final ROM is necessary to prevent multiple reductions, one per each analyzed mistuning pattern. K_{ROM} as formulated in Eq. (2.26), allows for direct introduction of mistuning in all its blocks except for $\hat{K}$, which depends on all random variables δ_n and needs to be recomputed for each mistuning pattern. In order to overcome this issue, one option is to assume that the blade mistuning has a negligible effect on this partition and $\hat{K}$ remains constant regardless of the mistuning pattern. It is worth mentioning that, the interface portion of the blade CB-CMS stiffness matrix (i.e. $k^{*b^{(n)}}_{cb,\gamma\gamma}$) is the only source of mistuning introduced in $\hat{K}$, as a byproduct of CMS assembly. From physical point of view, assuming a constant $\hat{K}$ matrix is equivalent to neglect the effect of mistuning on a portion of constraint modes corresponding to interface DOFs of the blades. The validity of this assumption is discussed in the result section.

Another option is to efficiently compute $\hat{K}$ without neglecting the effect of mistuning on this partition. This alternative solution requires a special treatment. To this end, an exact solution is developed based on sector level computations and modeshapes that have already been computed during the reduction steps. The alternative method is illustrated in the next section.

It is worth mentioning that the interface-disk reduction approach is based on loaded interface modeshapes of the disk. As discussed in section 2.2.3, loaded interface modeshapes are obtained by adding Guyan reduced matrices of the tuned blades to the interface partition of the disk matrices and solving the eigenvalue problem of the loaded disk system. In fact the loaded interface modeshapes obtained in the reduction approach are calculated by statically condensing the tuned blades onto the blade-disk interfaces. However, in the reduction process of a mistuned system, one may consider the effect of blade mistuning on the loaded interface modeshapes of the disk. In this context, mistuned loaded interface modeshapes refer

to those modeshapes that are calculated by condensing the mistuned blades onto the blade-disk interfaces. Note that, neglecting the effect of mistuning on loaded interface modeshapes of the disk could be a valid assumption. Since, the dominant portion of $\tilde{K}$ is composed of the tuned disk stiffness matrix, the added mistuned portion (i.e. Guyan stiffness of mistuned blades $\underset{n=1..N}{Bdiag}[k_{Guyan}^{*b^{(n)}}] = \underset{n=1..N}{diag}\,(1+\delta_n) \otimes k_{Guyan}^{b}$) to the interface DOFs could not considerably change the modeshapes of the full disk. Therefore, it is predictable that neglecting the effects of mistuning only on Guyan stiffness of the blades, provides acceptable accuracy. Recall that, in the context of small frequency modeling, it is shown that mistuned modeshapes can be represented as a linear combination of the tuned modes [27]. The validity of this assumption is discussed later in the result section.

2.2.6 Sector Level Computations (Requisites)

As it is seen in Eq. (2.26) all partitions of K_{ROM} are linearly dependent to mistuning parameters except for its extreme lower right partition $\hat{K}$, which is dependent to all random parameters δ_n. Thus, to take into account the effect of mistuning on this partition, one should compute $\hat{K}$ for each mistuning pattern. This would be cumbersome for statistical analyses. Moreover, all other partitions of K_{ROM} are constructed from a single sector stiffness matrix and cyclic loaded interface modes of the disk. However, in industrial applications, projecting the full disk matrix onto the cyclic loaded interface modeshapes is a formidable task due to its computational costs. Therefore, an alternative way for computation of $\hat{K}$ based on sector level computations is needed. For simplicity of notation the following operator is defined as:

$$blkdg[.] = \underset{n=1..N}{Bdiag}[.] \oplus 0_k = \begin{pmatrix} \underset{n=1..N}{Bdiag}[.] & 0 & \cdots & 0 \\ 0 & \multicolumn{3}{c}{\multirow{3}{*}{$\begin{pmatrix} 0 & \cdots & 0 \\ \vdots & \ddots & \vdots \\ 0 & \cdots & 0 \end{pmatrix}_{k\times k}$}} \\ \vdots & & & \\ 0 & & & \end{pmatrix} \tag{2.29}$$

where 0_k denotes additive identity in k (k by k null matrix) and $\oplus$ denotes direct sum of matrices which is defined in Appendix B.2. This operator will be used to denote, in a compact way, a block diagonal matrix of size equal to the total number of disk DOFs with all entries equal to zero except for the partition corresponding to the

blade-disk interface DOFs. By introducing Eq. (2.29) into the loaded disk stiffness matrix which is composed of the disk stiffness matrix K_D (defined by Eq. (2.17)) and the Guyan-reduced stiffness matrices of the blades added to the blade-disk interfaces, it can be represented in the following compact way:

$$\tilde{K} = \begin{bmatrix} I \otimes k^d_{\gamma\gamma} + \underset{n=1..N}{Bdiag}[k^{b^{(n)}}_{Guyan}] & I \otimes k^d_{\gamma O} \\ I \otimes k^d_{O\gamma} & \bar{k}^d_{OO} \end{bmatrix} = K_D + blkdg[k^b_{Guyan}] \tag{2.30}$$

By substituting Eq. (2.17) into Eq. (2.27) and using the compact notation defined by Eq. (2.29), $\hat{K}$ can be written as:

$$\begin{aligned} \hat{K} &= \tilde{\Phi}^T \begin{bmatrix} \underset{n=1..N}{Bdiag}[k^{*rom^{(n)}}_{\gamma\gamma}] & I \otimes k^d_{\gamma O} \\ I \otimes k^d_{O\gamma} & \bar{k}^d_{OO} \end{bmatrix} \tilde{\Phi} \\ &= \tilde{\Phi}^T \begin{bmatrix} \underset{n=1..N}{Bdiag}[K^{*b^{(n)}}_{cb,\gamma\gamma}] + I \otimes k^d_{\gamma\gamma} & I \otimes k^d_{\gamma O} \\ I \otimes k^d_{O\gamma} & \bar{k}^d_{OO} \end{bmatrix} \tilde{\Phi} \\ &= \tilde{\Phi}^T \left(K_D + blkdg[k^{*b}_{cb,\gamma\gamma}] \right) \tilde{\Phi} \end{aligned} \tag{2.31}$$

As previously stated, $\hat{K}$ is composed of tuned disk stiffness matrix and mistuned CB-CMS stiffness of blade interfaces. By adding and subtracting the Guyan stiffness matrix of the tuned blades to the interface DOFs of the $\hat{K}$ central core and using Eq. (2.30), one may cast $\hat{K}$ as follows:

$$\begin{aligned} \hat{K} &= \tilde{\Phi}^T \left(K_D + blkdg[k^b_{Guyan}] - blkdg[k^b_{Guyan}] + blkdg[k^{*b}_{cb,\gamma\gamma}] \right) \tilde{\Phi} \\ &= \tilde{\Phi}^T \left(\tilde{K} - blkdg[k^b_{Guyan}] + blkdg[k^{*b}_{cb,\gamma\gamma}] \right) \tilde{\Phi} \\ &= diag\left(\Lambda_{LI}\right) - \tilde{\Phi}^T_\gamma \underset{n=1..N}{Bdiag}[k^{b^{(n)}}_{Guyan}] \tilde{\Phi}_\gamma + \tilde{\Phi}^T_\gamma \underset{n=1..N}{Bdiag}[k^{*b^{(n)}}_{cb,\gamma\gamma}] \tilde{\Phi}_\gamma \end{aligned} \tag{2.32}$$

Now, based on the derived formulation, $\hat{K}$ can be computed using sector level calculations. According to Eq. (2.32), $\hat{K}$ is mainly constructed from the terms that are independent to mistuning (i.e. the first two terms of Eq. (2.32)) and are just computed for once. In addition, the mistuning is introduced (i.e. the third term of Eq. (2.32)) by projecting a sparse matrix onto the interface portion of loaded interface modeshapes. All those mentioned above, make the alternative formulation computationally cheap

and suitable for statistical analyses. Note that, no approximation is made in derivation of Eq. 2.32 and it calculates the exact $\hat{K}$ as is defined in Eq. 2.27.

2.3 Numerical Solution

The reduced equations of motion of the system can be written as:

$$M_{rom}\ddot{x}_r(t) + C_{rom}\dot{x}_r(t) + K_{rom}x_r(t) = F_{nl}(x_r(t), \dot{x}_r(t)) + F_{ex}(t) \tag{2.33}$$

where $x_{r(t)}$ is the displacement vector of the final reduced system comprised of nonlinear contact DOFs and CB and LI generalized coordinates. M_{rom}, C_{rom} and K_{rom} are mass, damping and stiffness matrices of the final reduced system, respectively. F_{nl} is the vector of nonlinear contact forces and it depends on relative displacements of contact nodes. F_{ex} is the vector of the external forces applied on the system. Note that, the reduced damping matrix C_{rom} can be computed in a systematic manner using the proposed reduction technique. However, by assuming a proportional damping for the ROM, C_{rom} matrix can be simply constructed from reduced mass and stiffness matrices.

The HBM is used to compute the steady state response of the system under periodic external excitation.
An iterative approach based on an alternating frequency/time (AFT) domain approach [45] is used to solve the nonlinear harmonic balance equations, where the nonlinear contact forces are modeled by means of node-to-node state-of-the-art contact elements ([46]).
The numerical solution is described thoroughly in Appendix A.

2.4 Results and Discussions

2.4.1 FE Model

The considered test case in this study is a simplified turbine bladed disk with 12 blades developed in ANSYS. The single sector model contains 429 elements and

460 nodes and the full model comprises 11429 nodes and 34,287 DOFs in total. The FE model of the academic bladed disk and a single sector model are depicted in Fig. 2.3.

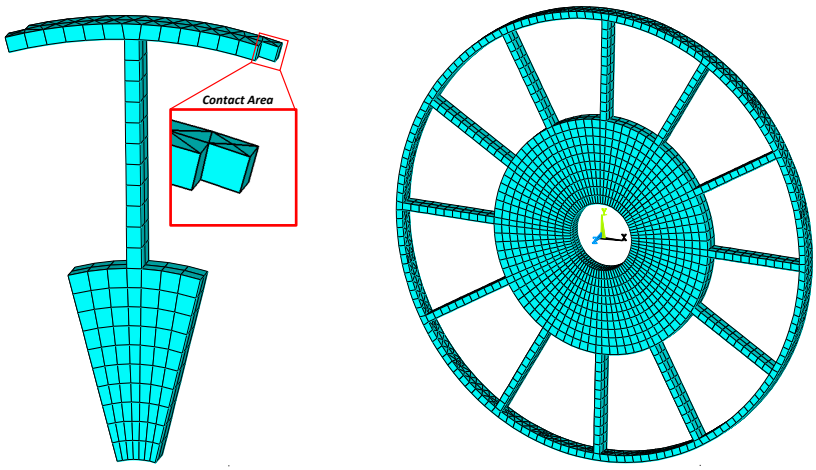

Fig. 2.3 FE model of the academic bladed disk and the single sector model.

The bladed disk is fixed at two circular rows of node lying on the outer faces of the disk. In the fundamental sector, each contact surface at the shroud comprises 4 nonlinear contact nodes and also the blade-disk interface contains 6 nodes. All the linear analyses (e.g. natural frequencies, modeshapes and etc.) are performed on a blisk in fully stick condition, in order to have boundary conditions at shroud interfaces more similar to microslip condition, which are typical operating conditions for shrouds. Fully stick condition is modeled by merging contact node pairs at adjacent shrouds.

Natural frequencies versus the number of nodal diameters (NDs) for the tuned bladed disk in stick condition is depicted in Fig. 2.4.

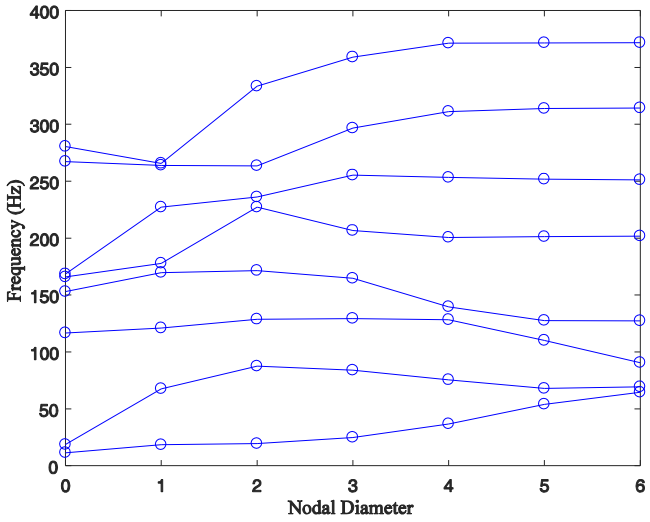

Fig. 2.4 Natural frequency versus nodal diameters for the tuned bladed disk in fully stick condition.

This plot reveals underlying characteristics of system dynamics such as frequency veerings and disk/blade dominated modeshapes. In frequency veering regions blade and disk dominated modeshapes veer from each other by further increasing the ND. Note that, since the adjacent blades are coupled at the shrouds, blade dominated modes are not pure horizontal lines and a slight softening/stiffening behavior is seen for blade mode families. In fact, in some frequency ranges, the vibratory motion of the coupled shrouds (which resemble a ring component attached to the blade tips) has a dominant out of plane component along axial direction. This will introduce an additional compliance to the system. In contrary, increasing the ND in some other ranges, results in a circumferential mode of the coupled shrouds (in tangential direction), which will decrease the system compliance (please see Fig. 2.5). In Fig. 2.4, slanted lines could also be representative of inter-blade couplings which makes it more difficult to distinguish them from disk dominated modes.

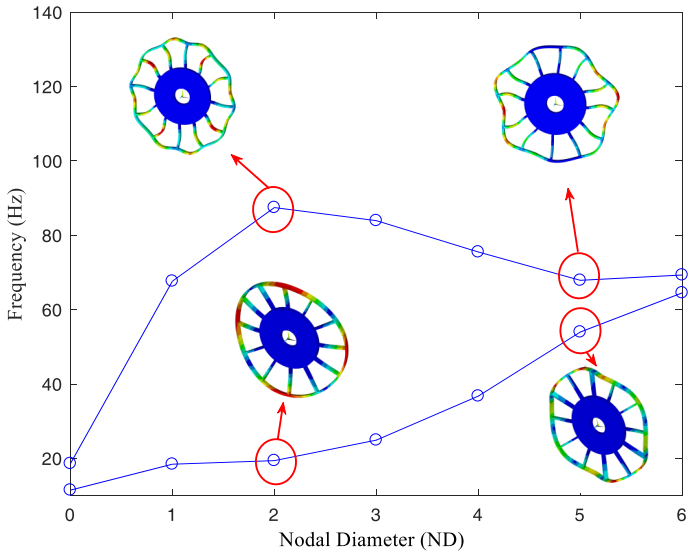

Fig. 2.5 Contour plot of modeshapes at different nodal diameters.

2.4.2 Results for Linear Tuned Bladed Disk

In order to evaluate the accuracy of the proposed reduction technique, eigenvalues of the final reduced system are compared with the exact eigenvalues of the full FE model, obtained in ANSYS. The eigenvalue deviation is defined as $((\lambda_{ROM} - \lambda_{full}))/\lambda_{full}$ where λ_{ROM} denotes eigenvalues of the reduced system and λ_{full} denotes exact eigenvalues of the full model.

Here, the first 100 natural frequencies of the tuned system are compared. Since, the reduction is based on two distinct sets of component modes, the number of retained modes of each set, defines the accuracy of the final ROM. Here, number of retained modes is selected based on the convergence analysis. This is a preliminary step, especially for nonlinear analyses, since, the contribution of higher modes or the presence of modal interaction in the system, are not known a priori.

In addition, "the frequency range of interest" should be taken into account. For instance, near the blade dominated modeshapes, increasing the number of retained loaded interface modeshapes (which are representative of disk dynamics) beyond a certain limit, does not enhance the accuracy of the ROM. In all results, the indicated number of CB modes, refers to the full system and not the retained modes per blade.

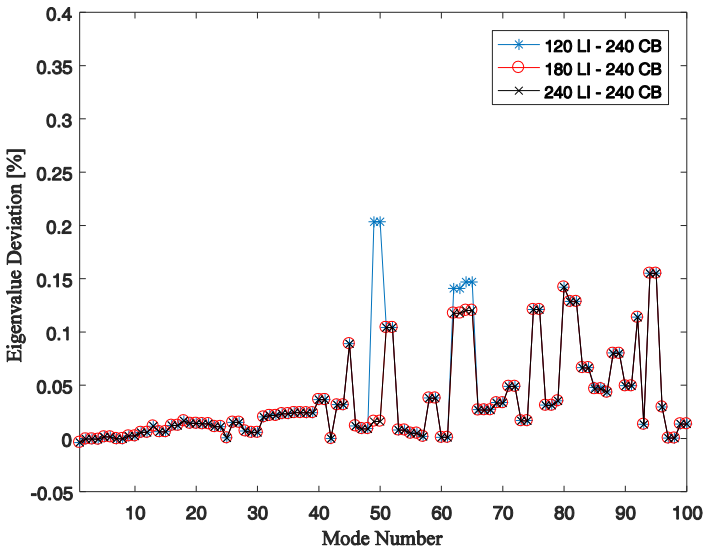

Fig. 2.6 The influence of loaded interface (LI) modeshapes on the eigenvalue deviation between ROM and ANSYS results (tuned blisk in stick).

The effect of retained loaded interface modeshapes in the ROM on the accuracy of the computed eigenvalues is shown in In Fig. 2.6. As it is seen, increasing the number of loaded interface modes in the ROM, increases the accuracy up to a certain level. From a certain level, adding extra modeshapes (corresponding to higher frequencies) does not contribute to the accuracy of the results in the studied range (first 100 modes).

Figure 2.7 shows the influence of the CB modes used in the ROM, on the accuracy of the computed eigenvalues. The number of CB modes used in the ROM can considerably affect the accuracy of the results. It should be noted that the real boundary conditions at the shrouds are different with the CB-CMS boundary conditions where blades are clamped at interface and nonlinear contact nodes. Thus, increasing the number of retained CB modes, will increase the accuracy more significantly. These results, reveal the capability of proposed reduction technique in accurately predicting the natural frequencies of the system.

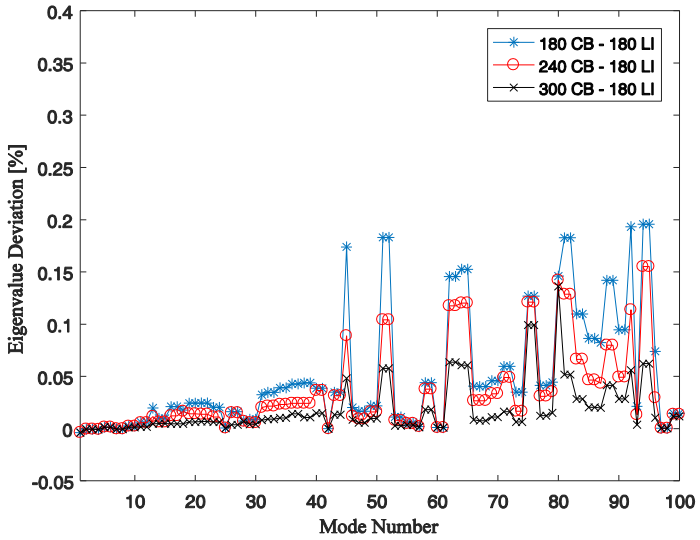

Fig. 2.7 The influence of CB modes on the eigenvalue deviation between ROM and ANSYS results (tuned blisk in stick).

2.4.3 Results for Linear Mistuned Bladed Disk

The performance of the proposed ROM in predicting the eigenvalues of a mistuned blisk is assessed here. The mistuned bladed disk model is obtained by varying the blades Young's modulus (3%) from its nominal value. The random mistuning pattern considered for the test case is listed in Table. 2.1.

Table 2.1 Blade frequency mistuning pattern

Blade number	Mistuning parameter, δ_n
1	0
2	0.0114
3	0.0149
4	-0.0030
5	-0.0250
6	-0.0163
7	0.0248
8	-0.0209
9	0.0195
10	0.0023
11	0.0298
12	-0.0253

The influence of the number of LI and CB modes used in the ROM on the eigenvalue deviations is illustrated in Figs. 2.8 and 2.9, respectively.
As can be observed, similar to the case of tuned blisk, increasing the number of retained modes enhances the results by decreasing the deviation from the exact eigenvalues obtained in ANSYS.

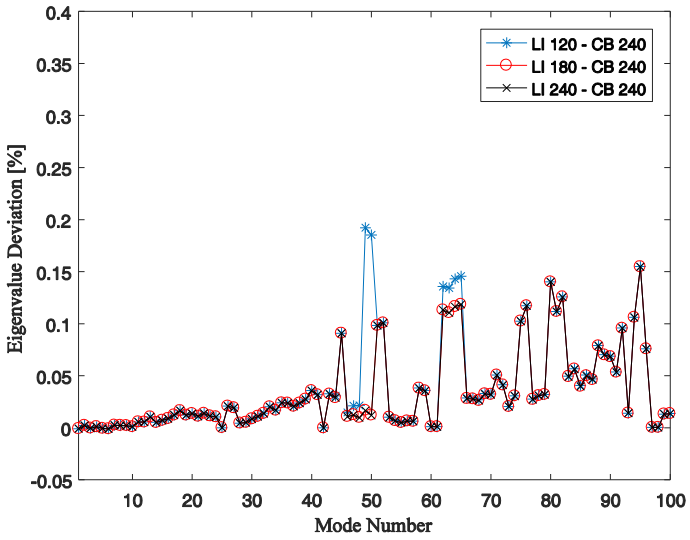

Fig. 2.8 The influence of loaded interface (LI) modeshapes on the eigenvalue deviation between ROM and ANSYS results (mistuned blisk in stick).

Figures 2.8 and 2.9, demonstrate the high accuracy of the reduction approach in predicting the eigenvalues of the mistuned model. Note that sufficient number of LI and CB modes should be retained in the ROM to achieve acceptable accuracy. For instance, the maximum error for predicted eigenvalue of the mistuned system; obtained from a ROM containing 300 CB and 180 loaded interface modes; is about 0.137 %.

2.4.4 Results Based on Mistuned Loaded Interface Modeshapes

The effect of mistuned loaded interface modeshapes on the performance of the ROM is investigated. Figure 2.10 shows the accuracy of two ROMs (based on tuned and mistuned loaded interface modeshapes), in predicting the natural frequencies of the mistuned bladed disk.

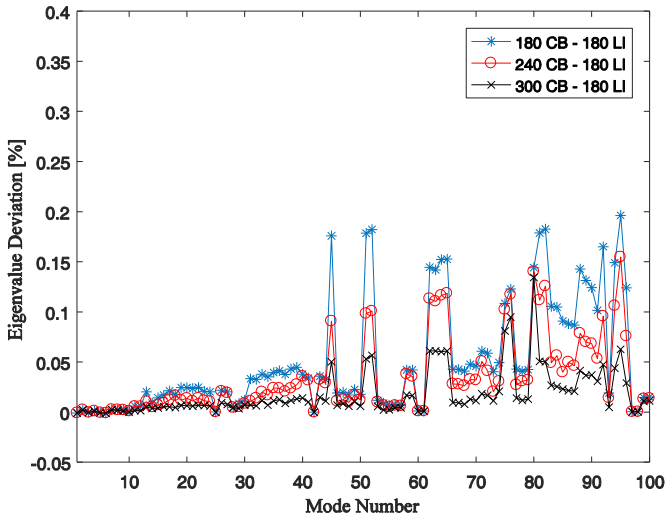

Fig. 2.9 The influence of CB modes on the eigenvalue deviation between ROM and ANSYS results (mistuned blisk in stick).

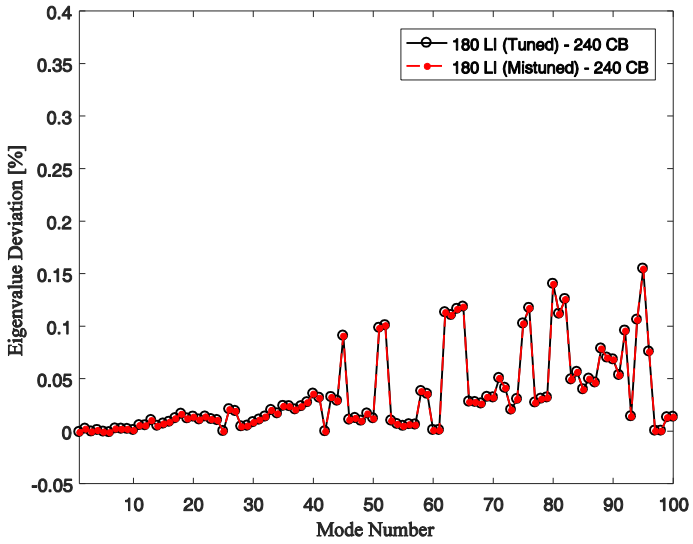

Fig. 2.10 The effect of mistuned loaded interface (LI) mode-shapes on the accuracy of the predicted eigenvalues by the ROM.

As can be seen results coincide well for both ROMs. In other words, considering mistuned loaded interface modeshapes as the reduction basis does not improve the accuracy of the ROM. The demonstrated results are of great importance, especially for statistical analyses, since, changing and computing the reduction basis for each mistuning pattern is not practical. In addition the tuned and mistuned loaded interface

modeshapes are compared with each other using the modal assurance criterion (MAC).

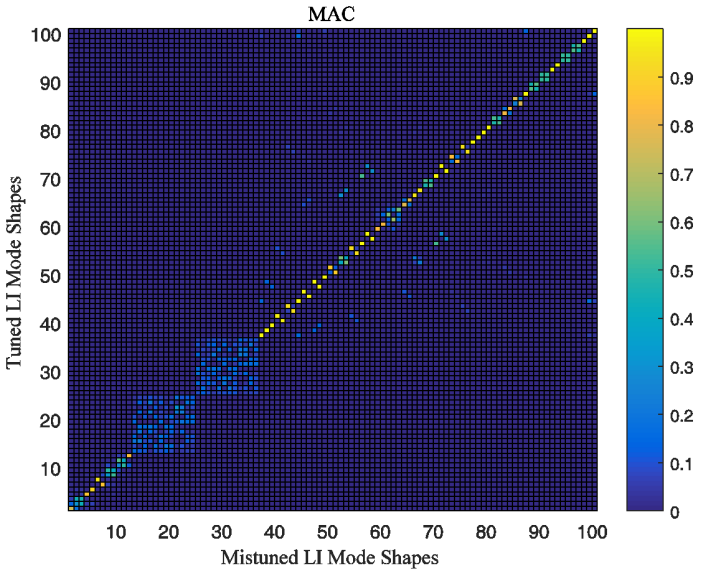

Fig. 2.11 Modal correlation between tuned and mistuned loaded interface (LI) modeshapes.

Figure 2.11 shows a comparison between the tuned and the mistuned loaded interface modeshapes. As it is seen, most part of the MAC diagonal is almost unity indicating that the modeshapes are similar. However, a weak correlation is seen between two dozen modes (i.e. 13-24 and 25-36). Note that the MAC matrix has a block diagonal structure in this range. So, any modeshape chosen from either of these two sets, has modal properties similar to that of modes lying in the same set and is orthogonal to all other modes. For instance, the mistuned loaded interface modeshape number 15 can be represented as a linear combination of tuned loaded interface modeshapes 13 to 24. In this sense, negligible modal property is missed while using tuned loaded interface modeshape.

It is worth mentioning that in the modeling of small frequency mistuning ([27]) it is assumed that the introduced mistuning does not alter the vibration motion type. That is to say, a bending mode remains a bending mode in the presence of mistuning although it will not have a perfect nodal diameter shape.

Another comparison is made between the eigenvectors corresponding to the nonlinear DOFs, obtained from the final ROM. In one of which, mistuned loaded interface modeshapes are used as one of the reduction basis. The diagonal MAC of the

final ROM eigenvectors corresponding to the retained nonlinear DOFs is shown in Fig. 2.12. Note that, modeshapes of ROMs corresponding to Fig. 2.10 are used in computation of the diagonal MAC. As can be seen, modeshape are in an excellent correlation (higher than 0.99) with each other. Thus, the ROMs obtained based on either mistuned or tuned loaded interface modeshapes, give practically identical eigenvectors.

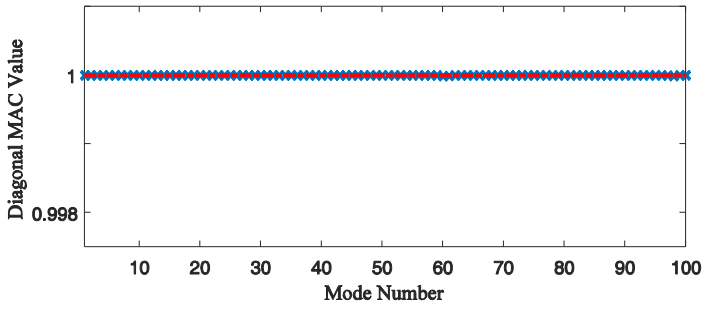

Fig. 2.12 Modal correlation between ROM eigenvectors based on tuned and mistuned loaded interface (LI) modes.

2.4.5 Results Based on Tuned $\hat{K}$ Partition

As discussed in the mistuning modeling section, one assumption to simplify the mistuning introduction into the final reduced stiffness matrix is to neglect the effect of mistuning on the constraint modes corresponding to interface DOFs (i.e. considering a tuned $\hat{K}$ partition in the K_{ROM}). The validity of this assumption is investigated here.

Figure 2.13 shows the difference between exact natural frequencies of a mistuned bladed disk (obtained from full FE in ANSYS) and those obtained from two different ROMs. The red curve shows the results obtained from the ROM with a tuned $\hat{K}$ partition while the black curve represents the ROM results with a mistuned $\hat{K}$ partition. As it is seen, results of the ROM with tuned $\hat{K}$ are in good accordance with results of the ROM with mistuned $\hat{K}$. In fact, due to the minimal contribution of interface DOFs to system dynamics, neglecting the effect of mistuning on them is a valid assumption.

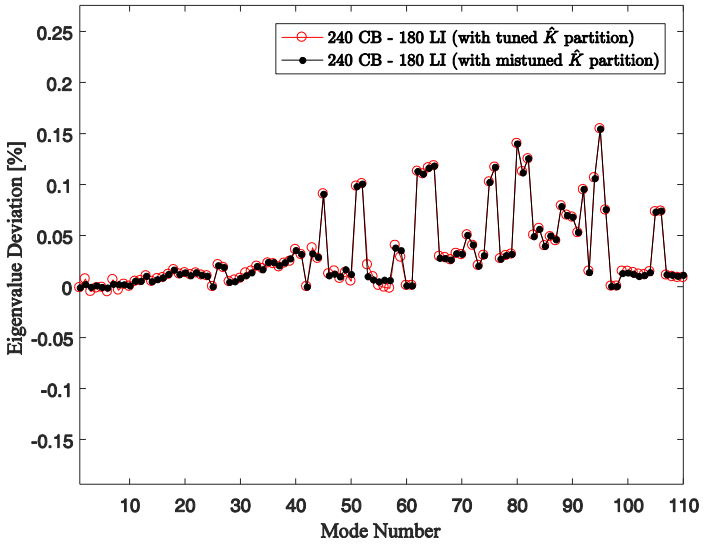

Fig. 2.13 The influence of neglecting the mistuning in $\hat{K}$ partition on the accuracy of predicted eigenvalues by the ROM.

2.4.6 Localized Modeshapes

The presence of mistuning can result in localization of vibration modes. This confines the vibration energy around few number of blades and increases their vibration amplitude, significantly. The capability of the proposed reduction technique in accurately predicting the mode localization is assessed here. To this end, a localized vibration mode, namely 107th mistuned mode with corresponding natural frequency of 372 Hz, is studied. It is worth mentioning that the ROM predicted the mistuned eigenvalue by 0.0096% error.

Figure 2.14 shows a comparison between localized modeshapes obtained by ROM and FE model, for the 107th mistuned modeshape. Only axial component of modal displacements of an identical contact node on each blade, is used to plot the modeshapes. As can be seen, the proposed ROM can accurately model the localized modeshape and its results coincide with exact FE result.

2.4.7 Results for Nonlinear Forced Response Analysis

For the nonlinear forced case, it is assumed that the global tangential and normal contact stiffnesses (i.e. k_{tx}, k_{ty} and k_n, respectively) have same values, and, the global

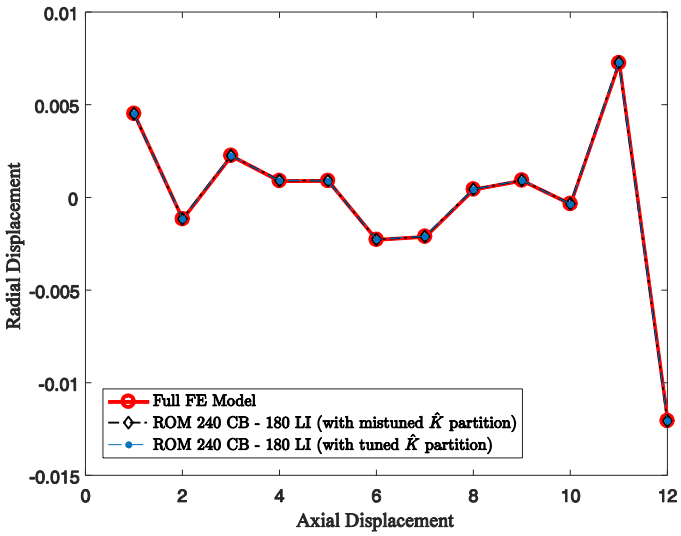

Fig. 2.14 Localized modeshapes obtained from ROM and FE model.

tangential stiffness is uniformly distributed among all local contact nodes. Here, the considered nominal values of the global contact stiffnesses are $k_{tx} = k_{ty} = k_n = 1e4 \quad \mathrm{N}/\mu\mathrm{m}$. The effect of static loads (e.g. centrifugal forces), are modeled by applying a constant normal preload (i.e. N0) on each contact node pair, otherwise a preliminary nonlinear static analysis should be performed to compute the static preloads at contact nodes. Note that the stiffness matrix generally depends on the rotational velocity of the rotor due to stress stiffening and spin softening, however these effects are neglected here.
Periodic external forces are modeled by a traveling wave type excitation of amplitude F0. Note that, two extra master nodes on each blade (located at the blade-shroud tip) are retained as the response and forcing nodes. The amplitude of the periodic response is computed based on a mono-harmonic balance procedure (only including the first harmonic). The tangential component of the periodic solution (calculated at the response node located on blade #1) is used to plot the forced response levels. In all forced cases, a very small viscous damping (with damping ratio $\xi = 0.001$, similar for all modes) is considered to better evaluate the effect of friction damping on the system response. A ROM comprised of 240 CB and 180 loaded interface modes, is used to carry out forced response computations.

The accuracy of the ROMs (one with tuned $\hat{K}$ and the other with mistuned $\hat{K}$) in predicting the nonlinear forced response levels of a mistuned turbine bladed disk

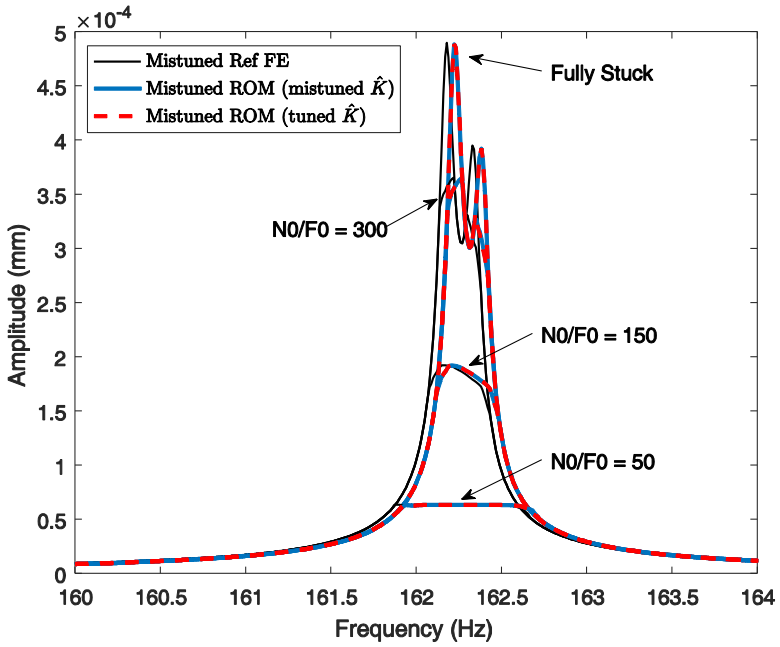

Fig. 2.15 Comparison of nonlinear forced response levels of mistuned ROMs and FE model (EO = 5).

under EO excitation 5 is depicted in Fig. 2.15. As the reference, a CB-CMS reduced FE model; by retaining a large number of CB modes (namely 1200 modes) and retaining the same master DOFs as in the ROMs; is considered. This system is referred to as the Ref FE and in the case of nonlinear forced response analyses, all ROM results are compared with the results of the so-called Ref FE. As it is seen in Fig. 2.15, forced response results of the ROM with tuned $\hat{K}$ is in an excellent accordance with the results of the ROM with mistuned $\hat{K}$ partition. This indicates that the effect of blade frequency mistuning on interface DOFs are negligible. Moreover, the results of both ROMs are in a very good agreement with Ref FE results. The predicted peaks around the resonance are in excellent match with the Ref FE for different values of preload-to-excitation ratio (i.e. N0/F0). A very slight frequency shift (about 0.04 Hz or 0.025% error) is observed in the response levels predicted by ROMs, which is typical of reduced order models. It is evident from the figure, that decreasing the N0/F0 ratio will change the contact state from fully stick condition towards the gross slip. As a result, the increased damping introduced from the shrouds in microslip, decreases the response amplitudes.

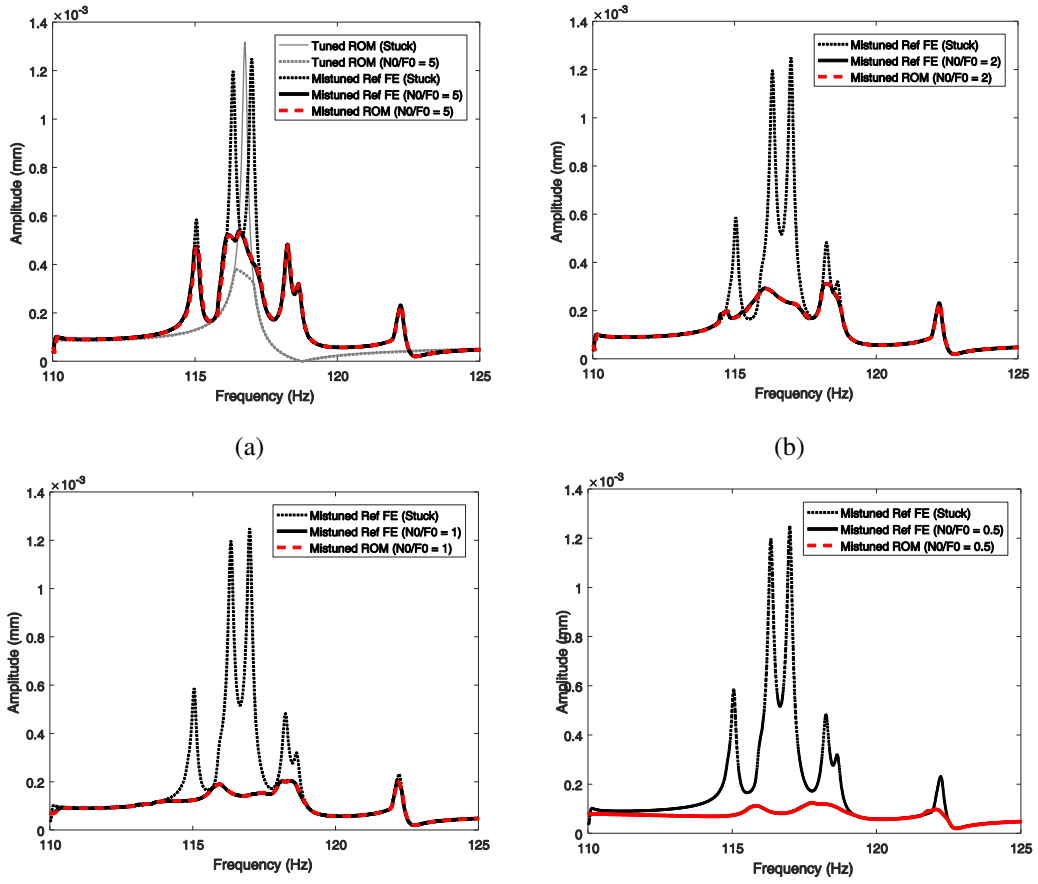

Fig. 2.16 Nonlinear forced response levels of the mistuned ROM versus ref FE. (a) N0/F0 = 5, (b) N0/F0 = 2, (c) N0/F0 = 1, (d) N0/F0 = 0.5.

Nonlinear forced response levels for EO 5 excitation within a high modal density region are shown in Fig. 2.16. Results of the ROM with tuned $\hat{K}$ is presented and compared with Ref FE results. It is expected that the ROM with mistuned $\hat{K}$ partition will give results of the same/higher accuracy. The investigated frequency range is selected near a softening region of Fig. 2.4 and it comprises multiple blade dominated modes. As discussed before (in Fig. 2.4), blades and shrouds within this frequency range experience complex dynamic motions, blades undergo a torsional motion which results in a wavy motion (with a dominant component along axial direction) in the coupled shrouds. In the mistuned system, other ND modeshapes besides ND 5, are also present in the selected range. The accuracy of the ROM in predicting the nonlinear forced response levels is evaluated in this frequency range. As it is seen, the forced response levels predicted by the ROM are in an excellent accordance with

the Ref FE results. In Fig. 2.16a, the response levels of the tuned bladed disk, both in fully stuck and microslip conditions, are shown. It is seen that the response level of the fully stuck tuned system is higher than that of the mistuned one (for this specific considered blade), and that, despite the engine order excitation, multiple peaks are present within the frequency range. Moreover, for the considered blade (namely blade #1) the mistuned nonlinear response level is higher than that of the tuned one. It is an interesting result, that in microslip conditions, the mistuning can increase the nonlinear damped response levels. It should be noted that, the investigated frequency range is far from blade-disk veering regions and in this frequency range, disk does not contribute to the system dynamics, significantly. The effect of preload-to-excitation ratio on the damping performance is evident in Figs. 2.16a to 2.16d. For relatively higher values of N0/F0, it is seen that the contacts are in stick near low amplitude peaks and they behave like linear springs with no damping effects, while near high amplitude peaks, due to the higher relative displacements at contact nodes, the contacts are in microslip and the damping provided by the slip, decreases the periodic response amplitude. Further decreasing of N0/F0 values, increases the slip levels and as a result, the amplitude of the vibration is damped within the full frequency range.

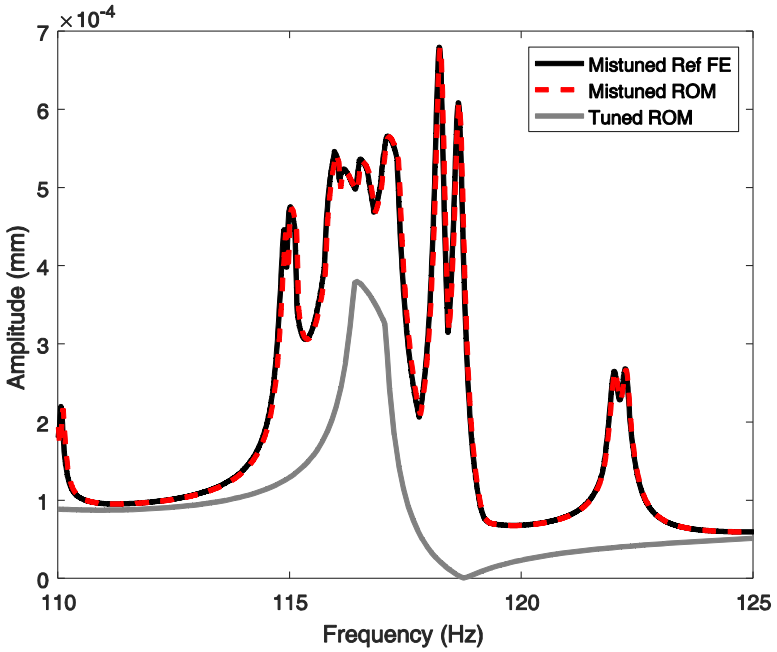

Fig. 2.17 Nonlinear response amplification of the mistuned bladed disk (EO = 5 and N0/F0 = 5).

Figure 2.17 demonstrates the response amplification phenomenon for a mistuned bladed disk in microslip condition. The system is under EO 5 excitation and N0/F0 is equal to 5. It is well known that, for linear systems, mistuning could increase the response levels. Here, the maximum nonlinear response of all blades is computed at each frequency. The depicted nonlinear response curve, is in fact the envelope of the maximum response of all blades. As it is seen the ROM (with tuned $\hat{K}$) results are in excellent accordance with the Ref FE results. It is evident that, even in the presence of friction damping, the damped response of the mistuned system is increased by the amplification factor of 79% (with respect to the maximum response of the tuned system). It can be concluded that, since in the presence of friction damping, mistuning can increase the damped response levels by localizing the response around few number of blades, for an optimum design, the effect of mistuning and friction damping must be modeled simultaneously.

2.5 Conclusion

In this chapter, a new component-mode-based reduced order model was presented for nonlinear dynamics of mistuned turbine bladed disks with shroud friction contacts. The novel reduction technique is based on small mistuning assumption (blade frequency mistuning). As a preliminary step, a single sector composed of one blade and the fundamental sector of the cyclic symmetry disk was considered. Based on the proposed reduction approach, a CB-CMS reduction was applied to the blade component, where shroud contact DOFs and blade-disk interface DOFs were retained as master DOFs, and a modal reduction based on loaded interface modeshapes of the disk applied to the interface and disk components. Finally, it was shown how to extend the single sector results to the full structure.
Based on the developed formulation, the reduced stiffness matrix of the mistuned system is computed by sector level calculations. Both linear analyses and nonlinear forced response results revealed the accuracy of the new reduction technique in predicting the dynamics of the mistuned system especially in high modal density regions. It was revealed that the mistuning can increase the damped response levels. It was shown that the effect of blade frequency mistuning on interface DOFs can be neglected without losing accuracy. This assumption, inevitably, results in a cheaper computational cost for statistical analyses. However, if deemed necessary by the

analyst to take into account the effect of mistuning on interface DOFs, an exact formulation, based on sector level calculations, is provided with minimal computational cost, suitable for statistical analyses.
In this chapter, the method was successfully applied to a mock-up bladed disk with shrouded blades, although the entire process can be applied to bladed disks with underplatform dampers. In that context, master DOFs during the CB-CMS blade reduction should comprise both the blade-disk and the blade-damper interface DOFs.

The research findings of this chapter are published in [47].

Chapter 3

Reduced Order Models for Nonlinear Dynamics of Bladed Disks with Shrouds: Mixed-Boundary Component Mode Substitution

3.1 Introduction

In this chapter a new mixed-boundary model reduction technique is presented for nonlinear forced response analysis of mistuned bladed disks with shroud friction contacts. The presented ROM is constructed based on the main idea of the developed reduction technique in Chapter. 2.

In CMS-based ROMs for systems with localized nonlinearities master DOFs not only include the boundary DOFs that are used for CMS assembly but also contact DOFs at friction interfaces. Consequently, the performance of the final ROM will be tightly dependent on the choice of component normal modes and their assumed boundary conditions at boundary DOFs.

In general, at the so-called constrained boundary DOFs that are shared with other components, fixed boundary condition is a favorable assumption, while, at the so-called active boundary DOFs that are free or interact (without being shared) with

neighboring substructures (as in the case of contact DOFs), assuming a free boundary condition is more realistic as those DOFs are not fixed in the actual dynamics.

In the developed ROM in this chapter, in contrast to conventional fixed- or free-mode Component Mode Synthesis (CMS) techniques, blades are reduced in a mixed-boundary fashion.
Accordingly, blade component normal modes with a more realistic mixed boundary condition (fixed at blade-disk interface and free at shroud contacts) are incorporated into the reduction basis. The new approach benefits from the favorable features of the previous ROM and enhances some of its elements by:

- Reducing the blades in a more realistic mixed-boundary fashion.
- Modeling the small sector-level frequency mistuning.

The latter is especially beneficial when the mistuning is distributed through the sector or is not negligible at blade-disk interface DOFs. As shown in [33], in case of mistuning at the blade-disk interface, possibly due to machining tolerances and mounting errors, ROMs based on blade mistuning may not allow to accurately predict the response levels and sector mistuning is therefore necessary. Moreover, it is known that ROMs based on blade-mistuning only (e.g. CMM [17]), work best in frequency ranges where vibration motion is mostly characterized by blade-dominated modes.
In the proposed ROM, introduction of the mistuning is flexible and can be simply limited to the blade-level if deemed needed by the designer. The final ROM is constructed using one single sector model which makes it suitable for highly refined FE models, typical of industrial applications.
In addition, the reduction basis is invariant of mistuning pattern and computed only once, makes it favorable for statistical analyses.
It should be noted that the presented methodology for modeling the sector-level mistuning is independent of the CMS-based reduction applied to the blades (either fixed, free or mixed) and can be used in constructing the ROM introduced in Chapter 2.

The developed reduction technique in this chapter is applied to a mock-up shrouded blisk. For validation purposes, ROM results were compared with the results of the full-order simulation in ANSYS and a converged CMS-based ROM

(referred to as the baseline ROM). Numerical simulations revealed the excellent accuracy of the developed ROM in predicting the forced response levels of the system.

3.2 Methodology

In this section, first the main idea of the developed reduction technique is described on a typical shrouded bladed disk model (Fig. 3.1). In the remainder, a detailed mathematical description for each reduction step, is provided. In the developed method, the bladed disk is divided into the blades and the full disk component, as depicted in Fig. 3.1a. Nodes lying on blade-disk (crossed circles) and blade-to-blade shroud interfaces (filled circles) are denoted as constrained and active boundary DOFs, respectively. The purpose is to efficiently and accurately reduce the structure such that the retained physical set, only comprises active boundary DOFs.

In the first step, blades are reduced in a mixed-boundary CMS fashion (Fig. 3.1b). To this end, the principle idea of the mixed-boundary reduction technique [48], is utilized and the reduction basis is composed of three mutually orthogonal components:

I. Static constraint modes, corresponding to constrained boundary DOFs.

II. Static residual attachment flexibility modes, corresponding to active boundary DOFs.

III. Mixed-boundary normal modes (fixed at constrained and free at active boundary DOFs).

The reduced set of blades includes constrained boundary DOFs, active boundary DOFs and generalized coordinates associated with mixed-boundary normal modes of the blades.
Note that, either all fixed boundary (e.g. CB-CMS [38]) or all free boundary (e.g. Rubin [49]) CMS techniques have been widely used in dynamic substructuring. Reducing a shrouded blade with those methods will incorporate normal modes of either a doubly clamped blade or a free blade with rigid body motion into the reduction basis. Neither of them is ideal for describing the kinematics of a bladed

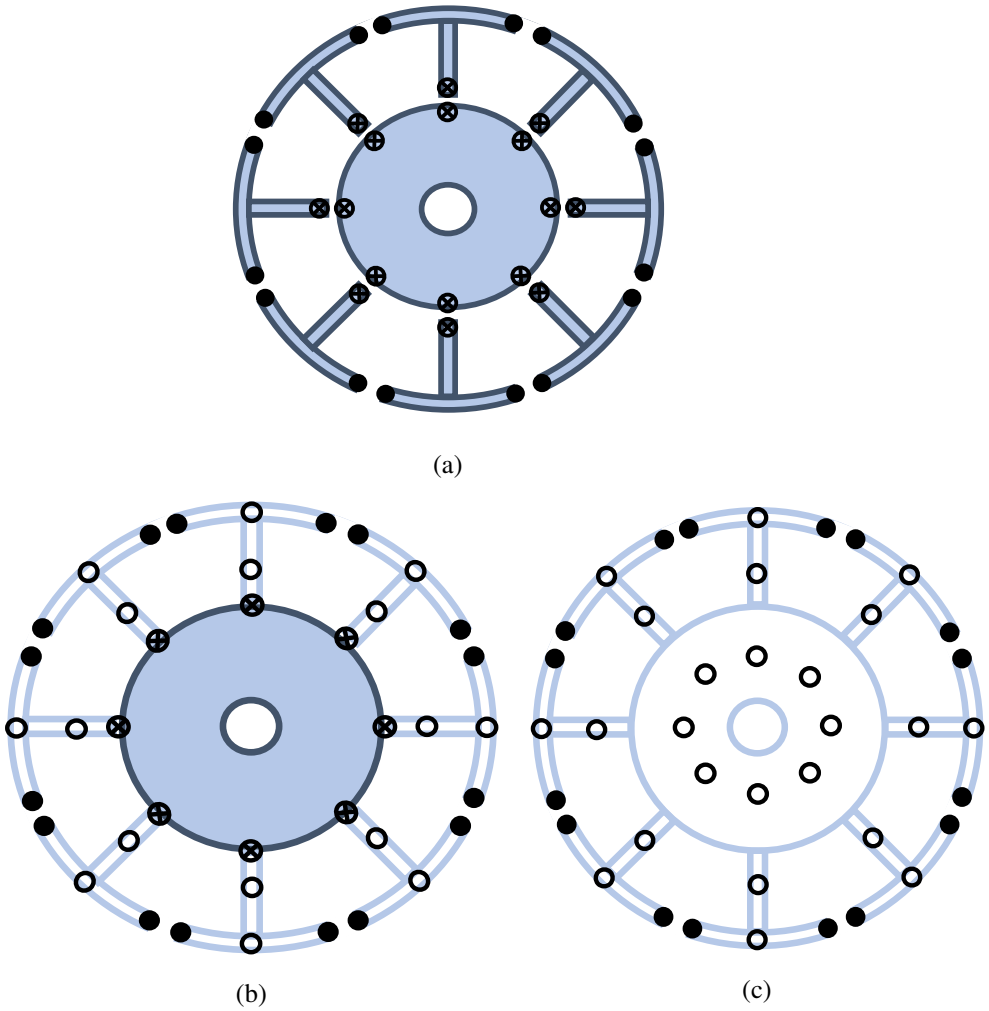

Fig. 3.1 A typical shrouded bladed disk and its reduction based on the developed reduction technique (filled circles: active boundary DOFs; crossed circles: constrained boundary DOFs; open circles: generalized coordinates).

disk with shrouds, since they necessitate retaining a large number of vibration modes in the reduction basis to achieve the desired accuracy.

In the final step of the reduction, a modal synthesis based on tuned loaded interface modeshapes of the disk is performed to reduce the disk component and the redundant blade-disk interface DOFs (Fig. 3.1c). Here, loaded interface modeshapes denote vibration modes of a component in an assembly, where other neighboring structures are statically interconnected to it [44].

Note that in Fig. 3.1 crossed, filled and open circles denote constrained boundary DOFs, active boundary DOFs and generalized coordinates.

The proposed method assumes that, in the presence of friction damping sources, such as, shrouds and underplatform dampers, the energy dissipated by friction at the blade root is negligible and thus the corresponding contact DOFs at the blade-disk interface become redundant.
During the reduction steps, small sector-level frequency mistuning can be efficiently introduced into the ROM. Construction of the mistuned ROM based on sector-level calculations is explained in details in the following sections.

3.2.1 Blade Component – Mixed Boundary Reduction

As explained in section 3.2, the first step in computing the proposed ROM is reduction of the blades. The displacement vector of one single blade and its corresponding structural matrices can be partitioned as follows (see Fig. 3.2):

$$x^b = \begin{Bmatrix} x_a^b \\ x_i^b \\ x_c^b \end{Bmatrix}, \quad k^b = \begin{bmatrix} k_{aa}^b & k_{ai}^b & 0 \\ k_{ia}^b & k_{ii}^b & k_{ic}^b \\ 0 & k_{ci}^b & k_{cc}^b \end{bmatrix}, \quad m^b = \begin{bmatrix} m_{aa}^b & m_{ai}^b & 0 \\ m_{ia}^b & m_{ii}^b & m_{ic}^b \\ 0 & m_{ci}^b & m_{cc}^b \end{bmatrix} \tag{3.1}$$

where the partitioned DOFs are defined as follows:

I. Blade active boundary DOFs x_a^b: that are not shared with adjacent components and are collected to be used in the solution/post-processing steps (e.g. contact DOFs for calculating friction forces, response DOFs for monitoring the response, and etc.).

II. Blade constrained boundary DOFs x_c^b: that are shared between the blade and the disk and couple blades to the disk at blade-disk interfaces.

III. Blade internal DOFs x_i^b: that comprises all other blade DOFs except boundaries.

Based on the utilized mixed-boundary reduction scheme, the displacement vector of one blade, is expressed as [48]:

$$x^b \approx \Psi_{ar} g_a + \Phi_m \eta + \Psi_c x_c^b \tag{3.2}$$

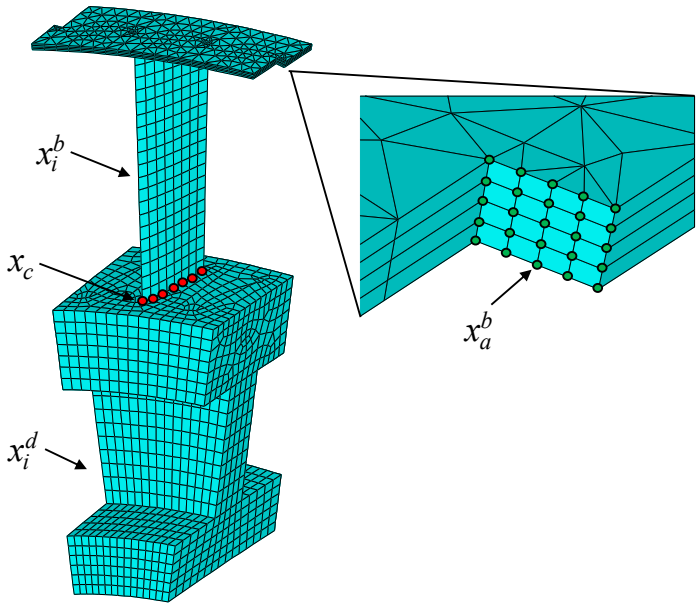

Fig. 3.2 Fundamental sector of a mock-up shrouded blisk and its partitioned DOFs.

where Ψ_{ar} are residual flexibility attachment modes computed at active DOFs x_a^b (with respect to the fixed boundaries); Φ_m are blade cantilever modes (fixed at blade-disk interface and free at active DOFs); and Ψ_{ar} are static constraint modes corresponding to the constrained DOFs x_c^b. Note that here constraint modes are computed by imposing a unitary displacement at each retained constrained boundary DOF while holding the others fixed. Moreover, attachment modes are the static response due to the unit force applied at active boundary DOFs. Excluding the flexibility information already included in the retained mixed-boundary normal modes from the set of attachment modes yields the residual flexibility attachment modes.

In Eq. (3.2), g_a are active boundary forces at active DOFs x_a^b and η are generalized coordinates associated with the mixed-boundary normal modes Φ_m. Equation (3.2) can be written in matrix form as:

$$\begin{Bmatrix} x_a^b \\ x_i^b \\ x_c^b \end{Bmatrix} = \begin{bmatrix} \Psi_{ar} & \Phi_m & \Psi_c \\ 0 & 0 & I \end{bmatrix} \begin{Bmatrix} g_a \\ \eta \\ x_c^b \end{Bmatrix} \tag{3.3}$$

As it is seen in Eq. (3.3), the reduced displacement vector of the blade component includes physical displacements only at constrained DOFs x_c^b. To keep physical displacements at active DOFs (i.e. x_a^b) in the reduced displacement vector, rather than active boundary forces g_a, one may recast the active partition of Eq. (3.3) as follows:

$$g_a = \Psi_{ar,a}^{-1}\left(x_a^b - \Phi_{m,a}\eta - \Psi_{c,a}x_c^b\right) \tag{3.4}$$

Using Eqs. (3.3) and (3.4), blade internal DOFs can be expressed in terms of blade boundary DOFs and generalized coordinates associated with blade cantilever modes, as follows:

$$\begin{aligned} x_i^b = &\left(\Psi_{ar,i}\Psi_{ar,a}^{-1}\right)x_a^b + \left(\Phi_{m,i} - \Psi_{ar,i}\Psi_{ar,a}^{-1}\Phi_{m,a}\right)\eta \\ &+ \left(\Psi_{c,i} - \Psi_{ar,i}\Psi_{ar,a}^{-1}\Psi_{c,a}\right)x_c^b \end{aligned} \tag{3.5}$$

Accordingly, the mixed-boundary transformation matrix of the blade component; that retains physical displacements at active and constrained DOFs; is given by:

$$\left\{\begin{array}{c} x_a^b \\ x_i^b \\ x_c^b \end{array}\right\} = R_{mb}\left\{\begin{array}{c} x_a^b \\ \eta \\ x_c^b \end{array}\right\}, R_{mb} = \left[\begin{array}{ccc} I & 0 & 0 \\ \bar{\Psi}_{ar} & \bar{\Phi}_m & \bar{\Psi}_c \\ 0 & 0 & I \end{array}\right] \tag{3.6}$$

where

$$\begin{aligned} \bar{\Psi}_{ar} &= \Psi_{ar,i}\Psi_{ar,a}^{-1} \\ \bar{\Psi}_c &= \Psi_{c,i} - \Psi_{ar,i}\Psi_{ar,a}^{-1}\Psi_{c,a} \\ \bar{\Phi}_m &= \Phi_{m,i} - \Psi_{ar,i}\Psi_{ar,a}^{-1}\Phi_{m,a} \end{aligned} \tag{3.7}$$

The mixed-boundary transformation matrix R_{mb}, introduced in Eq. (3.6), can be used to reduce the structural matrices of the blade component. For instance, the reduced stiffness matrix of the blade component is given by:

$$\bar{k}^b = R_{mb}^T k^b R_{mb} = \left[\begin{array}{ccc} \bar{k}_{aa}^b & \bar{k}_{a\eta}^b & \bar{k}_{ac}^b \\ \bar{k}_{\eta a}^b & \bar{k}_{\eta\eta}^b & \bar{k}_{\eta c}^b \\ \bar{k}_{ca}^b & \bar{k}_{c\eta}^b & \bar{k}_{cc}^b \end{array}\right] \tag{3.8}$$

Note that, the reduced mass matrix of the blade is computed and partitioned in the same way. Due to the cyclic symmetry of the bladed disks, structural matrices of the blades are identical. Therefore, single blade matrices can be directly used to assemble the reduced matrices of the full set of tuned blades. The vector of the generalized coordinates and the corresponding structural matrices of the reduced blades take the following form:

$$\mathbf{x}^b_{\text{rom}} = \begin{Bmatrix} \mathbf{x}_a \\ \eta \\ \mathbf{x}^b_c \end{Bmatrix}, \quad K^b_{\text{rom}} = \begin{bmatrix} I_N \otimes \bar{k}^b_{aa} & I_N \otimes \bar{k}^b_{a\eta} & I_N \otimes \bar{k}^b_{ac} \\ I_N \otimes \bar{k}^b_{\eta a} & I_N \otimes \bar{k}^b_{\eta\eta} & I_N \otimes \bar{k}^b_{\eta c} \\ I_N \otimes \bar{k}^b_{ca} & I_N \otimes \bar{k}^b_{c\eta} & I_N \otimes \bar{k}^b_{cc} \end{bmatrix}$$
$$M^b_{\text{rom}} = \begin{bmatrix} I_N \otimes \bar{m}^b_{aa} & I_N \otimes \bar{m}^b_{a\eta} & I_N \otimes \bar{m}^b_{ac} \\ I_N \otimes \bar{m}^b_{\eta a} & I_N \otimes \bar{m}^b_{\eta\eta} & I_N \otimes \bar{m}^b_{\eta c} \\ I_N \otimes \bar{m}^b_{ca} & I_N \otimes \bar{m}^b_{c\eta} & I_N \otimes \bar{m}^b_{cc} \end{bmatrix} \tag{3.9}$$

where $\otimes$ denotes the Kronecker product and I_N is the identity matrix of size N (number of blades). Note that, by keeping the DOFs of the same type together, the vector of the generalized coordinates of the blades (i.e. $\mathbf{x}^b_{\text{rom}}$) is divided into $\mathbf{x}_a$, η and $\mathbf{x}^b_c$ partitions which denote active boundary DOFs, mixed-boundary generalized coordinates and constrained boundary DOFs of the blades. The superscript b is removed from the notation of active boundary DOFs of the blades, given the fact that this partition has no counterpart on the disk component and is readily distinguishable.

3.2.2 Loaded Disk Component – Component Mode Substitution

In order to perform the final step of the reduction, one first needs to compute the loaded interface modeshapes of the tuned disk. Here loaded interface modes refer to vibration normal modes of the disk in which blades are statically condensed on the blade-disk interfaces (i.e. constrained DOFs).
This modal synthesis was introduced as the component mode substitution by Benfield and Hruda [44]. These modeshapes can be efficiently computed using cyclic symmetry properties and sector-level calculations.

The cyclic sector model of the loaded disk can be obtained by adding the so-called Guyan reduced mass and stiffness matrices of the blade to the disk sector (at constrained DOFs) and by applying cyclic symmetry constraints at disk interfaces [31].

Once the loaded interface modeshapes of the disk are computed, a modal reduction can be performed on the CMS-assembly of reduced blades and the full disk (Fig. 3.1b). This reduction is performed on the disk partition of the CMS-assembly and will reduce the full disk and the redundant blade-disk interfaces (i.e. constrained DOFs) (Fig. 3.1c). The displacement vector of the full disk component and its corresponding structural matrices is partitioned as follows:

$$x^d = \left\{ \begin{array}{c} x_c^d \\ x_i^d \end{array} \right\}, \quad K^d = \left[\begin{array}{cc} I_N \otimes k_{cc}^d & I_N \otimes k_{ci}^d \\ I_N \otimes k_{ic}^d & k_{ii}^d \end{array} \right],$$
$$M^d = \left[\begin{array}{cc} I_N \otimes m_{cc}^d & I_N \otimes m_{ci}^d \\ I_N \otimes m_{ic}^d & m_{ii}^d \end{array} \right] \tag{3.10}$$

In the partitioned disk stiffness matrix, k_{cc}^d denotes the stiffness matrix corresponding to the constrained DOFs of a *disk sector*; $I_N \otimes k_{cc}^d$ is a block diagonal partition corresponding to the constrained DOFs of the *full disk*; and k_{ii}^d denotes the stiffness partition corresponding to the disk internal DOFs and is block circulant due to the disk-disk interface couplings. The partitioned mass matrix has also the same shape. Enforcing the interface compatibility between the reduced blades and the full disk (at constrained boundary DOFs), yields the displacement vector and the corresponding stiffness matrix of the CMS-assembly:

$$\mathbf{X}^{\text{asm}} = \left\{ \begin{array}{c} \mathbf{x}_a \\ \eta \\ \mathbf{x}_c^{\text{asm}} \\ x_i^d \end{array} \right\},$$
$$K^{\text{asm}} = \left[\begin{array}{cccc} I_N \otimes \bar{k}_{aa}^b & I_N \otimes \bar{k}_{a\eta}^b & I_N \otimes \bar{k}_{ac}^b & 0 \\ I_N \otimes \bar{k}_{\eta a}^b & I_N \otimes \bar{k}_{\eta\eta}^b & I_N \otimes \bar{k}_{\eta c}^b & 0 \\ I_N \otimes \bar{k}_{ca}^b & I_N \otimes \bar{k}_{c\eta}^b & I_N \otimes k_{cc}^{asm} & I_N \otimes k_{ci}^d \\ 0 & 0 & I_N \otimes k_{ic}^d & k_{ii}^d \end{array} \right] \tag{3.11}$$

where $I_N \otimes k_{cc}^{asm} = I_N \otimes \bar{k}_{cc}^b + I_N \otimes k_{cc}^d$ is the coupling partition in the assembly, where the mixed-boundary reduced stiffness of the blade constrained DOFs x_c^b, are loaded on the disk interface DOFs x_c^d. In the displacement vector of the CMS assembly (in Eq. (3.11)), $\mathbf{x}_c^{\text{asm}}$ denotes displacements of the constrained DOFs. The mass matrix of the CMS-assembly is constructed in the same fashion and has the same shape. By

assuming that in the presence of shroud contacts the friction damping at blade root is negligible, one only needs to retain active boundary DOFs $\mathbf{x}_a$ in the final ROM. Accordingly, the final reduction can now be performed on the CMS-assembly by expressing the displacements of the disk partition in terms of loaded interface modal coordinates, as follows:

$$\mathbf{X}^{\text{asm}} = \left\{ \begin{array}{c} \mathbf{x}_a \\ \eta \\ \hline \mathbf{x}_c^{\text{asm}} \\ x_i^d \end{array} \right\} = \left[\begin{array}{cc|c} I & 0 & 0 \\ 0 & I & 0 \\ \hline 0 & 0 & \tilde{\Phi} \end{array} \right] \left\{ \begin{array}{c} \mathbf{x}_a \\ \eta \\ \tilde{\eta} \end{array} \right\} = R_{LI}\mathbf{x}_{\text{rom}} \tag{3.12}$$

where $\tilde{\Phi}$ are loaded interface modeshapes of the disk; $\tilde{\eta}$ are generalized coordinates corresponding to $\tilde{\Phi}$; R_{LI} is the loaded interface transformation matrix; and $\mathbf{x}_{\text{rom}}$ denotes the vector of generalized coordinates of the final ROM.

The ROM of the bladed disk can be obtained by projecting the CMS-assembly onto the R_{LI} modal basis. Accordingly, final reduced stiffness and mass matrices can be expressed as:

$$\begin{aligned} K_{rom} &= R_{LI}^T K^{asm} R_{LI} = \left[\begin{array}{ccc} I_N \otimes \bar{k}_{aa}^b & I_N \otimes \bar{k}_{a\eta}^b & \left(I_N \otimes \bar{k}_{ac}^b\right)\tilde{\Phi}_c \\ I_N \otimes \bar{k}_{\eta a}^b & I_N \otimes \bar{k}_{\eta\eta}^b & \left(I_N \otimes \bar{k}_{\eta c}^b\right)\tilde{\Phi}_c \\ \tilde{\Phi}_c^T\left(I_N \otimes \bar{k}_{ca}^b\right) & \tilde{\Phi}_c^T\left(I_N \otimes \bar{k}_{c\eta}^b\right) & [\hat{K}] \end{array} \right], \\ M_{rom} &= R_{LI}^T M^{asm} R_{LI} \end{aligned} \tag{3.13}$$

where $\tilde{\Phi}_c$ are a partition of loaded interface modeshapes corresponding to constrained DOFs. In Eq. (3.13), the lower right partition of K_{rom} denotes the disk partition of the CMS-assembly projected onto $\tilde{\Phi}$ modal basis:

$$\hat{K} = \tilde{\Phi}^T \left[\begin{array}{cc} I_N \otimes k_{cc}^{asm} & I_N \otimes k_{ci}^d \\ I_N \otimes k_{ic}^d & k_{ii}^d \end{array} \right] \tilde{\Phi} \tag{3.14}$$

Computation of the $\hat{K}$ using the projection shown in Eq. (3.14), demands the full disk matrix and is a formidable task. However, it can be simply split into multiple sector-level calculations as follows:

$$\hat{K} = \sum_{n=1..N} \tilde{\Phi}_n^T \tilde{K}_0 \tilde{\Phi}_n \tag{3.15}$$

where $\hat{K}_0$ denotes the stiffness matrix of the disk partition in the fundamental sector of the CMS-assembly and $\tilde{\Phi}_n$ are cyclic loaded interface modeshapes of the nth sector of the disk component.

An alternative method for efficient calculation of $\hat{K}$ was introduced in section 2.2.6. Accordingly, adding and subtracting the Guyan stiffness matrix of the blades to the interface partition of $\hat{K}$, yields:

$$\hat{K} = diag\,(\Lambda_{LI}) - \sum_{n=1..N} \tilde{\Phi}_{n,c}^T k_{Guyan}^b \tilde{\Phi}_{n,c} + \sum_{n=1..N} \tilde{\Phi}_{n,c}^T \bar{k}_{cc} \tilde{\Phi}_{n,c} \tag{3.16}$$

where Λ_{LI} are squared natural frequencies of the loaded disk system; $\tilde{\Phi}_{n,c}$ are a portion of cyclic loaded interface modeshapes of the nth sector of the disk corresponding to constrained DOFs; and k_{Guyan}^b is the Guyan reduced stiffness matrix of a nominal blade in which blade DOFs are condensed on its constrained DOFs. Note that, $\hat{K}$ is a $p \times p$ matrix and p is the number of retained loaded interface modes.

Both k_{Guyan}^b and Λ_{LI} are readily available from the computation of loaded interface modes $\tilde{\Phi}$ and no extra pre-calculation is needed to obtain $\hat{K}$ by Eq. (3.16). The $\hat{K}$ partition of the ROM stiffness matrix can be computed by either Eq. (3.15) or (3.16), although in Eq. (3.16) the size of projections drops dramatically (i.e. to the blade-disk interface of one sector).

As a concluding remark, the ingredients for the final ROM, constructed by using Eqs. (3.13) and (3.16) and single sector calculations, are here summarized:

I. Mixed-boundary reduced matrices of 1 blade (Eq. (3.8)).

II. Loaded interface modeshapes $\tilde{\Phi}$ and natural frequencies Λ_{LI} of the disk (cyclic symmetry).

III. Guyan reduced matrices of 1 blade (readily available from step II.).

3.2.3 Introduction of the Mistuning

Up to this point, the developed ROM is only suitable for tuned bladed disks. It is well known that the nominally identical components of bladed disks are slightly different from one to another one [16] it is assumed that the mistuning is small and is efficiently modeled as a random perturbation of the Young's modulus of each

sector. Such capability is especially important when the mistuning is not negligible at blade-disk interface DOFs [33]. The blade frequency mistuning which is the most common form of mistuning in bladed disks, is also addressed at the end of this section. More in detail, being δ_n the nondimensional mistuning parameter of the nth sector, the Young's modulus of the nth sector is written as:

$$E_n = E \cdot (1 + \delta_n) \tag{3.17}$$

where E is the Young's modulus of the tuned sector.

The mixed-boundary transformation matrix R_{mb} (introduced in Eq. (3.8)) is invariant of Young's modulus. Accordingly, the R_{mb} of one nominal blade is sufficient to reduce mistuned blades with different Young's moduli. As a result, the reduced stiffness matrix of the nth mistuned blade is linearly scaled by its Young's modulus (i.e. E_n) and the mistuning parameter can be directly injected into the blade partitions of the ROM stiffness matrix. To obtain the mistuned disk stiffness matrix, the principle assumption of SNM theory [27], is employed here. It is assumed that in the presence of small frequency mistuning, mistuned loaded interface modes, can be represented as a linear combination of the tuned loaded interface modes. Accordingly, each sector of the mistuned disk is projected onto its cyclic loaded interface modeshapes. Finally, the reduced stiffness matrix of the mistuned ROM can be obtained by:

$$K_{rom}^{mist} = \begin{bmatrix} \underset{n=1..N}{diag}\,(1+\delta_n) \otimes \bar{k}_{aa} & \underset{n=1..N}{diag}\,(1+\delta_n) \otimes \bar{k}_{a\eta} & \left(\underset{n=1..N}{diag}\,(1+\delta_n) \otimes \bar{k}_{ac}\right)\tilde{\Phi}_\gamma \\ \underset{n=1..N}{diag}\,(1+\delta_n) \otimes \bar{k}_{\eta a} & \underset{n=1..N}{diag}\,(1+\delta_n) \otimes \bar{k}_{\eta\eta} & \left(\underset{n=1..N}{diag}\,(1+\delta_n) \otimes \bar{k}_{\eta c}\right)\tilde{\Phi}_\gamma \\ \tilde{\Phi}_\gamma^T\left(\underset{n=1..N}{diag}\,(1+\delta_n) \otimes \bar{k}_{ca}\right) & \tilde{\Phi}_\gamma^T\left(\underset{n=1..N}{diag}\,(1+\delta_n) \otimes \bar{k}_{c\eta}\right) & \left[\hat{K}_{mist}\right] \end{bmatrix} \tag{3.18}$$

The lower right partition of mistuned ROM stiffness matrix, denotes the projection of the disk partition of the mistuned CMS-assembly onto the tuned loaded interface modes of the disk, and can be computed sector-wise as follows:

$$\hat{K}_{mist} = \sum_{n=1..N} (1+\delta_n)\tilde{\Phi}_n^T \tilde{K}_0 \tilde{\Phi}_n \tag{3.19}$$

An efficient construction of $\hat{K}_{mist}$ can be achieved based on the alternative method introduced in Eq. (3.16). To do so, only the last term of Eq. (3.8) should be updated:

$$\hat{K}_{mist} = diag\,(\Lambda_{LI}) - \sum_{n=1..N} \tilde{\Phi}_{n,c}^{T} k_{Guyan}^{b} \tilde{\Phi}_{n,c} + \sum_{n=1..N} (1+\delta_n) \tilde{\Phi}_{n,c}^{T} \bar{k}_{cc} \tilde{\Phi}_{n,c} \tag{3.20}$$

Note that, one could only model the effect of blade frequency mistuning by substituting $\hat{K}_{mist}$ in Eq. (3.18) with the tuned $\hat{K}$ from either Eq. (3.15) or (3.16).

3.3 Numerical Solution

The reduced equations of motion of a shrouded bladed disk can be expressed as:

$$M_{rom}\ddot{\mathrm{x}}_{\mathrm{rom}}(t) + C_{rom}\dot{\mathrm{x}}_{\mathrm{rom}}(t) + K_{rom}\mathrm{x}_{\mathrm{rom}}(t) = F_{nl}(\mathrm{x}_{\mathrm{rom}}(t), \dot{\mathrm{x}}_{\mathrm{rom}}(t)) + F_{ex}(t) \tag{3.21}$$

where $\mathrm{x}_{\mathrm{rom}}(t)$ is the vector of DOFs of the reduced bladed disk and it comprises active boundary DOFs of the blades $\mathbf{x}_a$, generalized coordinates η associated with mixed-boundary normal modes, and generalized coordinates $\tilde{\eta}$ corresponding to the loaded interface modes; M_{rom} and K_{rom} are reduced mass and stiffness matrices; C_{rom} denotes the reduced damping matrix and is assumed to be proportional to the reduced stiffness matrix (i.e. $C_{rom} = \beta \cdot K_{rom}$); F_{nl} denotes the state dependent vector of nonlinear contact forces acting on the retained nonlinear contact DOFs; and F_{ex} represents the vector of external periodic excitation and acts on retained forcing DOFs. Note that, nonlinear contact DOFs and response/force DOFs, are grouped together into active boundary DOFs (see Fig. 3.2).

In the simulation, shroud contacting interfaces are modeled using the semi-3D contact elements. The considered contact element is composed of two perpendicular Jenkins contact elements with variable normal loads and is imposed at each contact node pair. It is assumed here that the static equilibrium solutions are not affected by higher harmonic solutions, and thus, are solved separately from dynamic solutions. The solution of the static balance equations will give as an output the normal preload acting over the contact surfaces, used as an input in the dynamic analysis.

The steady state response of the reduced system is computed using the HBM and assuming that the response of the system under a periodic excitation remains periodic.

The pseudo-arclength path following technique was implemented to compute the evolution of nonlinear forced response levels with respect to the excitation frequency.

Note that the continuation scheme demands calculation of the Jacobian matrix at each iteration step, which can become a rigorous task. The computational burden was extremely reduced by implementing the analytical Jacobian as described in [15]. The numerical solution is described thoroughly in Appendix A.

3.4 Results and Discussions

The numerical simulations are performed on the mock-up shrouded blisk shown in Fig. 3.3. The full model is composed of 27 sectors and each sector comprises 6052 DOFs. Shroud contact surfaces (shown in Fig. 3.2) contain 25 contact nodes and the full-wheel model comprises 4050 nonlinear contact DOFs. By using the relative notation, only 2025 nonlinear DOFs were solved in the iterative solver.

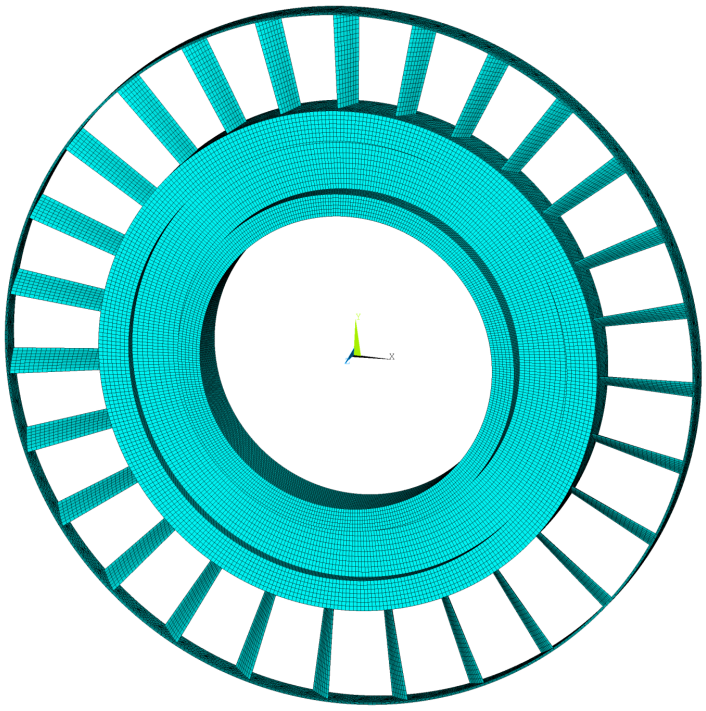

Fig. 3.3 The studied mock-up shrouded blisks.

It is assumed that the blisk is made of the steel with nominal Young's modulus equal to 200 GPa and mass density equal to 7800 kg/m^3. Random Young's moduli

with a uniform distribution and standard deviation of 5% (from the nominal value) were used to model the mistuned shrouded blisk and a uniform normal preload is applied at each shroud contact. The numerical results are presented in the two parts. First, in section 3.4.1 modal analysis results are presented, followed by forced response results in section 3.4.2.

3.4.1 Modal Analysis Results

This section evaluates the performance of the ROM in accurately predicting the natural frequencies and modeshapes of the full mistuned model. To do so, ROM results are compared with the results of the full order model in ANSYS. In the real practice, shroud friction surfaces are mostly subjected to the microslip. Since the stick boundary conditions are more consistent with microslip conditions (compared to free boundaries at shrouds that are more consistent to the gross slip) all the results in the section 3.4.1 are presented for a shrouded blisk with closed contact surfaces. The blisk with closed contacts can be simply modeled by merging the contact node pairs in ANSYS and by clamping the partition of the relative contact DOFs in the ROM.

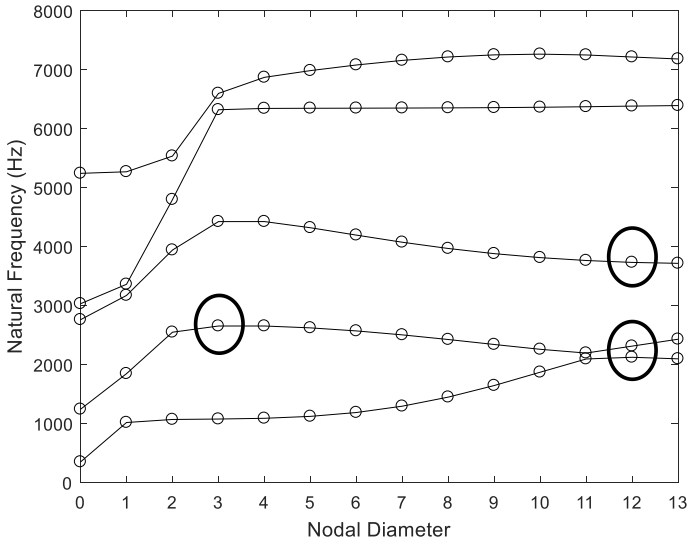

Fig. 3.4 Natural frequencies versus nodal diameter plot for the tuned shrouded blisk with closed contact surfaces.

Figure 3.4 depicts the natural frequency versus nodal diameter plot for the tuned shrouded blisk with closed contact surfaces. In lower families a complex blade-to-

shroud coupling can be seen that is characterized by softening/stiffening behavior. As a result, blade dominated modes are not perfect horizontal lines and blade-disk couplings and veering regions are shifted towards the higher families. This is typical of mock-up shrouded blisks with small number of blades and was also observed in [19, 40]. The specified zones in Fig. 3.4 depict the considered wave number and frequency range of the traveling wave excitations used in section 3.4.2. The performance of the ROM in predicting the natural frequencies of the mistuned shrouded blisk is evaluated in Fig. 3.5. The error metric is defined as the absolute percentage deviation between the natural frequencies predicted by the ROM and the exact natural frequencies computed in ANSYS:

$$e_{\lambda}^{ROM} = \left\| \frac{\lambda^{ROM} - \lambda^{ANSYS}}{\lambda^{ANSYS}} \right\| \times 100 \tag{3.22}$$

For the sake of simplicity, the new developed ROM is denoted by MixBCs in the rest of the paper. The accuracy of the ROM is tightly dependent on its modal basis and the number of retained modes during the reduction. Accordingly, the accuracy of the MixBCs ROM is influenced by both blade component modes (with mixed-boundary conditions) and the loaded interface modes of the disk.

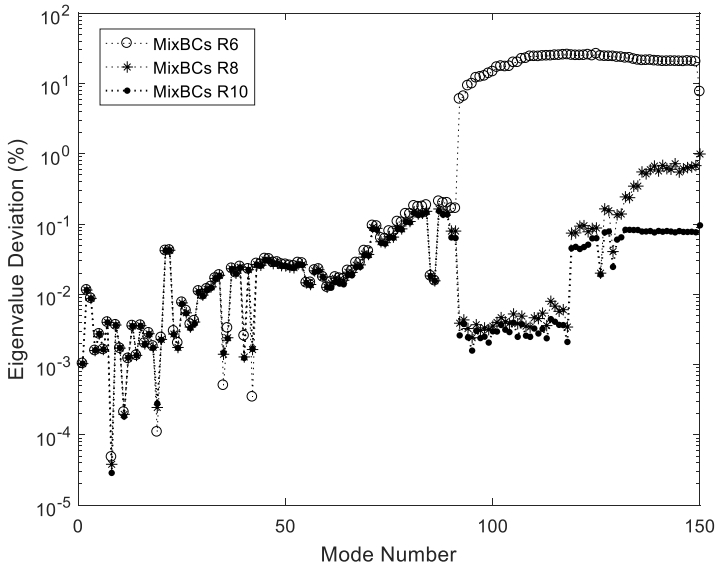

Fig. 3.5 The influence of number of retained (denoted by Rx) blade mixed-boundary modes on the performance of the MixBCs ROM.

A convergence analysis is crucial to guarantee the adequacy of the number of retained modes and the performance of the ROM in the frequency range of interest. Figure 3.5 shows a convergence analysis with regard to the blade mixed-boundary modes in the frequency range of the first five modal families. The number of retained modes per blade are denoted by $\mathbf{R}\boldsymbol{x}$ (where $\boldsymbol{x}$ is a natural number) in Fig. 3.5. It is seen that the ROM shows an excellent accuracy in the frequency range bounded to the frequency range of retained modes and accuracy will drop rapidly for the higher modes.
For instance, by retaining 6 mixed-boundary component modes per blade, the least accurate ROM (i.e. MixBCs R6) can accurately predict the natural frequencies of the first 91 mistuned modes (3 modal families). It is evident that increasing the number of retained modes per blade will significantly improve the accuracy of the ROM for the higher modes.
A similar convergence analysis was performed with respect to loaded interface modes of the disk and is not shown here for the sake of brevity. A converged ROM can be obtained in the frequency range of the first five modal families by retaining 100 loaded disk modes. Note that, all the simulations here (section 3.4) are performed on ROMs containing 100 loaded interface modes.
To better assess the performance of MixBCs ROMs, their accuracy is compared with the ROM obtained in a similar manner except for the blade components that are reduced using the classical CB method. This ROM is referred to as CBCMS ROM. Note that, the only difference between MixBCs and CBCMS ROMs is the type of blade component modes used during the reduction.

Figure 3.6 shows a comparison between the mixed-boundary and fixed-boundary ROMs (i.e. MixBCs vs. CBCMS) in predicting the natural frequencies of the mistuned shrouded blisk with closed contact surfaces. The performance of the ROMs is investigated in a wider frequency range of the first 300 mistuned modes.

It is seen that, the MixBCs ROMs consistently outperformed the CBCMS ROM within their effective frequency range (roughly where the error is below 1%). For instance, the least accurate free-boundary ROM (i.e. MixBCs R6) is much more accurate in predicting the first 91 mistuned natural frequencies than the fixed-boundary ROM (i.e. CBCMS R10) which is obtained by retaining 10 CB modes per blade.
Also the mixed-boundary ROM of the same size (i.e. MixBCs R10) shows a higher accuracy in its effective frequency range (first 190 modes) compared with the CBCMS ROM. Beyond this limit, the introduced error by MixBCs ROM grows faster than

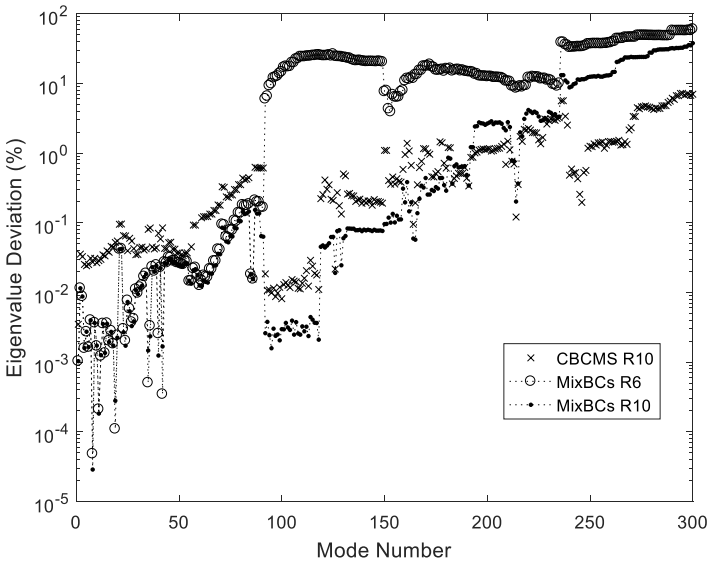

Fig. 3.6 Performance of mixed- and fixed- boundary ROMs in predicting the natural frequencies of the mistuned shrouded blisk.

that of the CBCMS ROM. This is due to the fact that, fixed-boundary modes naturally vibrate at higher frequencies, and thus the introduced error at higher frequencies grows more slowly than that of the free-boundary modes. This can be also verified by visualizing the full system modeshapes at higher frequencies, or more precisely, by computing the modal participation factors at boundary DOFs. To this end, the contour plot of the $142th$ modeshape of the full blisk is depicted in Fig. 3.7. It is evident that assuming fixed-boundaries at shrouds is a reasonably accurate assumption.

It is should be recalled that the performance of different ROMs (i.e. CBCMS and MixBCs) is evaluated in predicting the natural frequencies of a blisk with closed contacts condition, although they were obtained from a blisk with open contacts. To compute the natural frequencies of the blisk with closed contacts, relative displacements between contact DOFs were introduced into the ROM and then were fixed to resemble the closed contact conditions.
For the sake of completeness, in Fig. 3.8 a comparison is make between CBCMS and MixBCs ROMs in predicting the natural frequencies of the mistuned blisk with open shrouds. As it is expected MixBCs outperforms CBCMS and shows a better accuracy especially up to the $162th$ (6*27) mode.

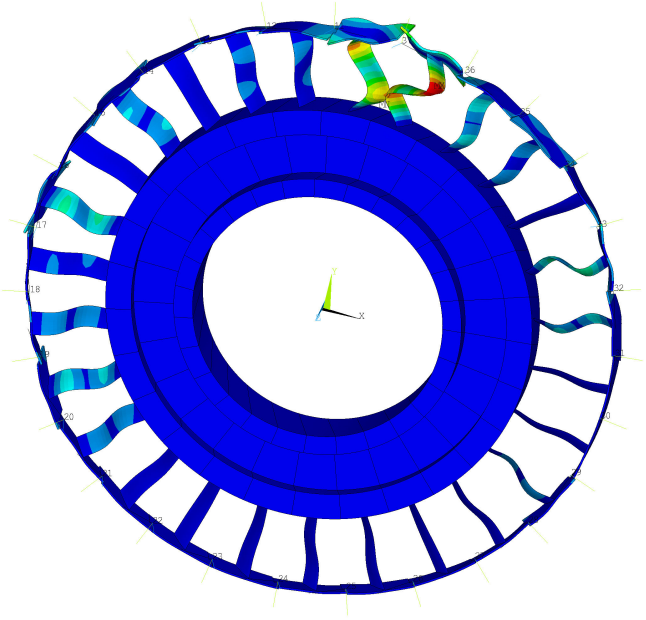

Fig. 3.7 Contour plot of the $142th$ modeshape of the full mistuned shrouded blisk.

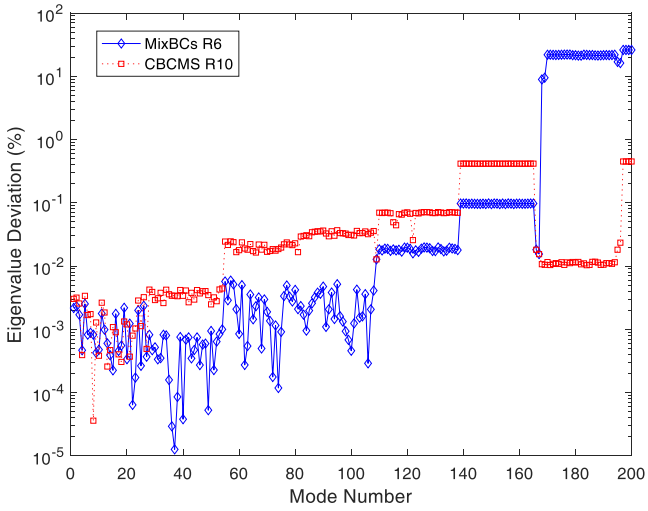

Fig. 3.8 Performance of mixed- and fixed- boundary ROMs in predicting the natural frequencies of the mistuned shrouded blisk with open contacts.

In order to quantify the enhanced accuracy of MixBCs ROMs with respect to the CBCMS ROM, a relative error metric is defined as follows:

$$e^{rel} = \left\| \frac{e_{\lambda}^{CBCMS} - e_{\lambda}^{MixBCs}}{e_{\lambda}^{MixBCs}} \right\| \tag{3.23}$$

Equation (3.23) can be used to measure the difference between errors introduced by different ROMS in predicting the natural frequencies of the mistuned blisk. Figure 3.9 depicts the relative difference between eigenvalue deviations introduced by CBCMS ROM with respect to MixBCs ROMs. It is evident that, the CBCMS ROM introduces considerably larger errors compared to MixBCs ROMs, especially in lower mode families.

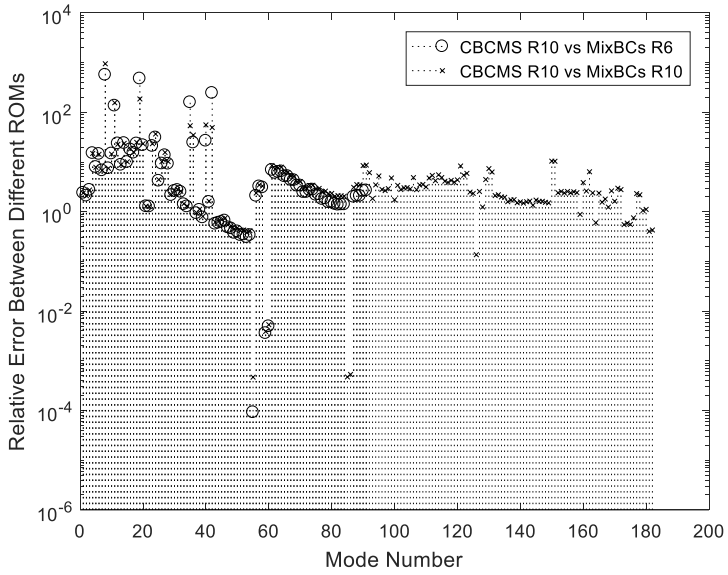

Fig. 3.9 Relative difference between eigenvalue deviations introduced by mixed- and fixed- boundary ROMs.

The performance of the ROM in accurately predicting the modeshapes of the mistuned blisk is of great importance. In fact, forced response levels of the mistuned blisk will be computed using its mistuned modeshapes. To assess the performance of the ROM in predicting the mistuned modeshapes, a metric based on the Modal Assurance Criterion (MAC) is defined as follows:

$$e^{mac} = (1 - diag(MAC)) \times 100 \tag{3.24}$$

The metric defined in Eq. (3.24), demonstrates the percentage deviation of mistuned modeshapes computed by the ROM from the exact modes computed in ANSYS.

The performance of the MixBCs and CBCMS ROMs in modeling the mistuned modeshapes is evaluated in Fig. 3.10. Only the modal displacements at the response

nodes (located at the blade tips, on both leading and trailing edges) were used to compute the MAC values. As it can be seen in Fig. 3.10, the mistuned modeshapes computed by the MixBCs R10 are in an excellent correlation with the modeshapes of the full-order model. The correlation between the MixBCs ROM and the full-order model is above 90% in the selected range (99.87% in average). However, the CBCMS ROM of the same size demonstrates the lack of accuracy (below 90%) at multiple modes.

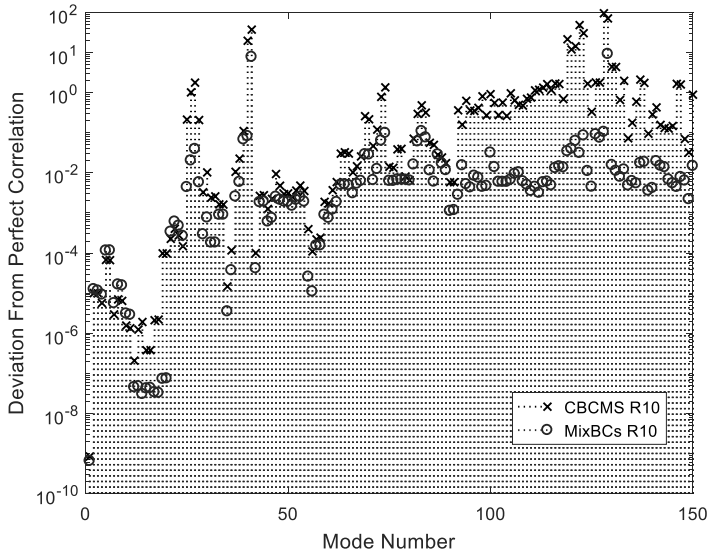

Fig. 3.10 Performance of mixed- and fixed- boundary ROMs in predicting the modeshapes of the mistuned shrouded blisk.

It is evident that the MixBCs ROM can model the modeshapes more accurately in comparison with the CBCMS ROM, at almost every mode in the selected range. In other words, to obtain the similar level of accuracy in the selected frequency range, one might demand a larger fixed-boundary ROM. Figure 3.10 highlights the capability of the MixBCs R10 ROM in accurately predicting the mistuned modeshapes in the presence of localization.

A localized mode, namely the 98^{th} mistuned modes that vibrates at ≈ 6.28 kHz, is selected to assess the ROM. Modeshapes of response nodes (locating at blade tips, on leading edges) are plotted in axial UZ, tangential Uθ, and radial UR directions. As it is seen the predicted mistuned modes is in excellent accordance with full-order model modeshapes, computed by ANSYS.

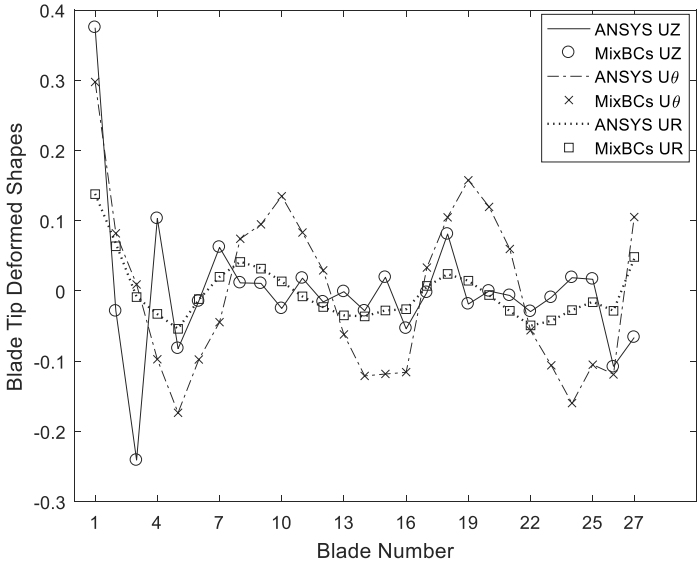

Fig. 3.11 A mistuned modeshape in the presence of vibration localization.

3.4.2 Forced Response Results

In this section the results of forced response analysis are presented. First part is dedicated to the MixBCs ROM and demonstrates its performance in predicting the linear/nonlinear forced responses. In the second part performance of the new proposed MixBCs ROM is compared to that of the classical CBCMS ROM. Forced response levels in either of parts are computed using the same strategy and is described below. Shroud friction surfaces are modeled by imposing a semi-3D contact element at each contact node pair. A homogeneous distribution is considered for both normal preload and the contact stiffness. The contact stiffness is set equal to 1000 N/μm in both normal and tangential directions and a constant friction coefficient of 0.5 is considered. The external excitation is applied on the forcing nodes located at blade tips, in the form of a traveling wave with the amplitude of F0. In details, the dynamics behavior of the mistuned shrouded blisk is investigated around two different resonances depicted in Fig. 3.4, namely under Engine Order (EO) 3 and EO 12 excitations. In order to assess the efficiency of the friction damping in reducing the vibration amplitudes, a very slight stiffness-proportional damping with the coefficient of $\beta = 1.2\text{e-}7$ is used in forced response calculations. It is worth mentioning that the stick condition in this section is modeled slightly different from the so-called closed contact state (obtained by merging the contact node pairs) in

section 3.4.1. Here, stick condition refers to a linear state of the system where contact elements act as fully engaged linear springs (no slip nor separation takes place) when the system undergoes large preload values (engagement is at all DOFs of contact node pairs, i.e. in one normal and two tangential directions of the contact surface). Note that, the chosen values for the contact stiffness are high enough that result in stick natural frequencies with less than 1% deviation from the natural frequencies of the blisk with closed contact surfaces. To validate the nonlinear forced response results, a converged CMS-based ROM is used as the reference. This reference ROM is called Baseline through the rest of the paper and is obtained by applying the Free-Interface substructuring method in ANSYS. The especial linear stick case is validated with both the Baseline and the full-order model simulations in ANSYS. Note that, the linear stick state in ANSYS can be modeled by imposing COMBIN40 spring elements at all contact node pairs. All the forced response calculations are performed on the MixBCs/CBCMS R10 ROM. These ROMs only contain 370 generalized (slave) coordinates (corresponding to 10 mixed/fixed -boundary component modes per blade plus 100 loaded interface modes). In order to reduce the computational time, nonlinear calculations are performed based on the monoharmonic balance approach. It is shown in the literature that monoharmonic simulation can be very accurate especially if the nonlinearity is weak [19]. Note that sufficient number of harmonics is case-dependent and not known a-priori (convergence analysis is inevitible). All response curves depict the tangential component of the solution at a response node located on blade #1, unless otherwise stated.

3.4.2.1 MixBCs ROM Results

Figure 3.12 shows the linear forced response of the mistuned blisk in fully stick condition. The blisk is subjected to an EO 3 excitation under a relatively large preload to excitation ratio. Note that, in the fully stick condition the system behaves linearly and no friction damping is introduced into the system. Since the mistuned modes are not pure nodal diameter modeshapes, multiple resonance peaks are present in the response. The relative error between the ROM and the Baseline is denoted by e_{amp} and is shown at resonance peaks. It is seen that the ROM is in a very good accordance with the full-order simulation in ANSYS. It should be noted that the frequency shift in ROM prediction is about 1 Hz which is negligible in the selected frequency range. Figure 3.13 shows the linear forced response of the mistuned

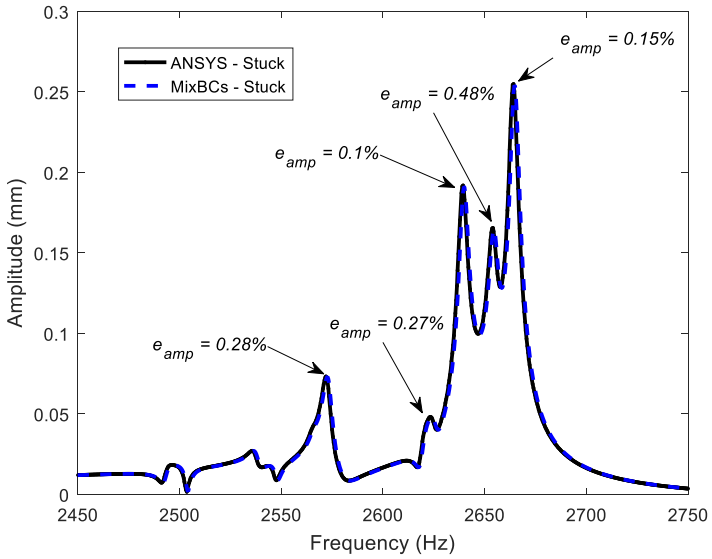

Fig. 3.12 Performance of the ROM in predicting the linear forced response of the mistuned blisk in stick condition under EO 3 excitation. e_{amp} denotes the relative error between the ROM and the Baseline.

blisk in fully stick condition and under EO 12 excitation. Two resonance peaks are evident in the frequency range of the excitation. That is due to the fact that mistuned modes with the dominant 12^{th} harmonic component are few in this range or already hidden under the dominant peaks. It is evident that the ROM result is in an excellent accordance with ANSYS results. Note that, the frequency shift in this case is below 1 Hz.

In order to validate the nonlinear forced response predictions of the ROM, the envelope of the response levels is computed and compared with the Baseline results. Note that, the envelope of the maximum nonlinear response is obtained by computing the maximum nonlinear forced response of the blisk (considering the response of all blades) at each excitation frequency. Figure 3.14 demonstrates the performance of the ROM in accurately predicting the envelope of the maximum nonlinear response of the mistuned blisk under EO 3. It is seen that the ROM predictions are in an excellent accordance with the baseline results. The effect of mistuning on increasing the forced response level is evident in Fig. 3.14. For the blisk in stick condition, the mistuned response level has increased by the amplification factor of 59% with respect to the tuned response level. It is worth mentioning that, in the nonlinear regime, the maximum error is within [0.1 - 0.15]% depending on the loading condition and is

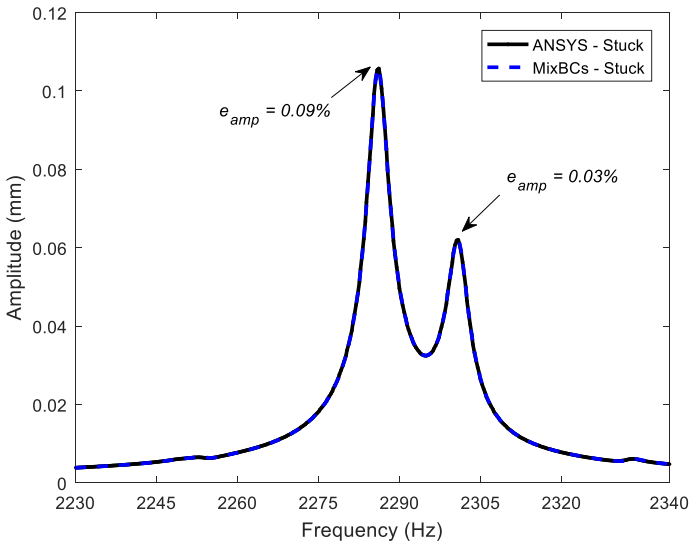

Fig. 3.13 Performance of the ROM in predicting the linear forced response of the mistuned blisk in stuck under EO 12 excitation. e_{amp} denotes the relative error between the ROM and the Baseline.

much smaller than that of the linear stuck case which is about 0.39%. This is due to the fact, the friction damping flattens the steep resonance curves, and reduces the maximum error especially at resonance peaks.

The performance of the ROM in accurately predicting the envelope of the maximum nonlinear response of the mistuned blisk under EO 12 is depicted in Fig. 3.15. The ROM predictions are in an excellent accordance with the Baseline results in this case as well. As it is seen, the effect of mistuning on amplifying the linear response level (about 8%) is not notable. Note that the dynamics of the stuck blisk in this frequency range is characterized by torsion-bending vibrations of blades coupled with dominant vibrations of the shrouds. In this case, the shroud-to-shroud coupling is high enough to allow for a uniform distribution of the vibration energy among all the blades, thus preventing vibration localization. The maximum error in forced response levels is about 0.08% and occurs in fully stick condition near the resonance peak at 2286 Hz.

In order to evaluate the effectiveness of the friction damping, response levels of the ROM are computed under different loading conditions. Figure 3.16 shows the effect of nonlinear friction damping on the response of the mistuned blisk subjected to EO 3 excitation. The simulation is carried out for different preload-to-excitation

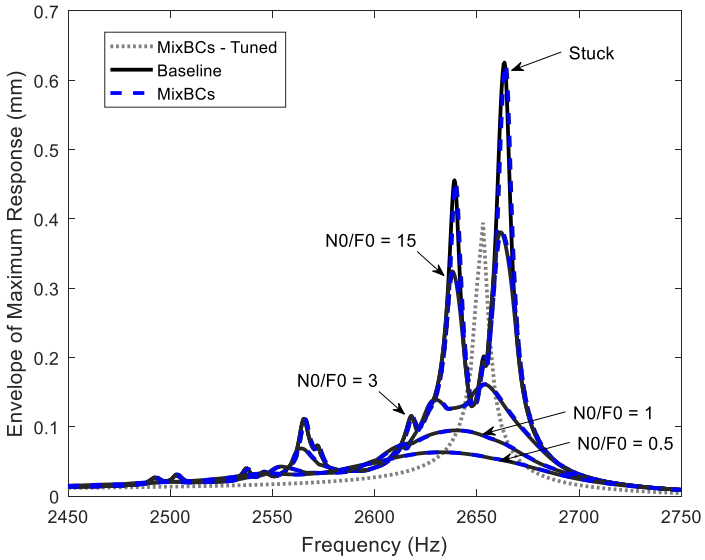

Fig. 3.14 Performance of the ROM in accurately predicting the envelope of the maximum nonlinear response of the mistuned blisk under EO 3.

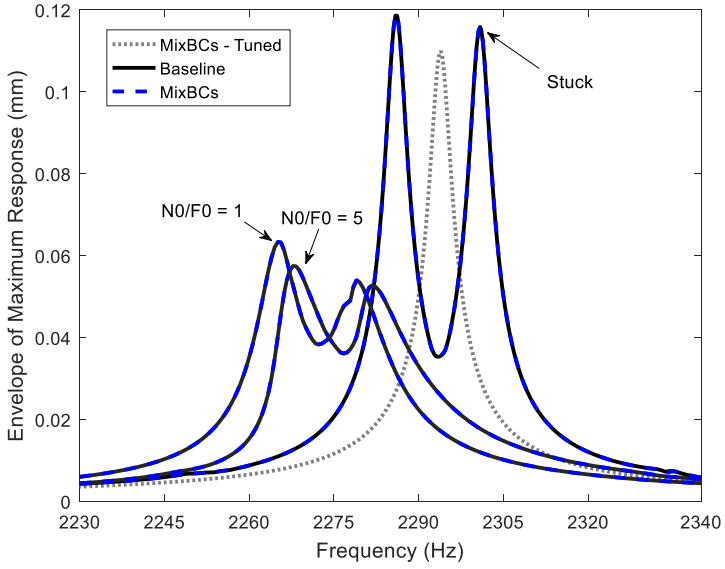

Fig. 3.15 Performance of the ROM in accurately predicting the envelope of the maximum nonlinear response of the mistuned blisk under EO 12.

ratios (i.e. N0/F0), by decreasing the preload value and keeping the excitation amplitude fixed. For high values of the normal preload, the shroud contacts are in stick and the blisk vibrates linearly. Note that no friction damping is introduced

into the system in stick condition. Decreasing the preload values and relaxing the Coulomb limit, develop microslip at shroud friction interfaces. In details, near the resonance peaks with high amplitudes, the relative displacements between contact node pairs are large enough to put the contact into the slip condition and as a result the vibration amplitude starts decreasing by the introduced friction damping. Although, near the peaks with lower amplitudes contacts are still in stick condition with no friction dissipated energy. Further decreasing the N0/F0 values, increases the amount of microslip and the dissipated energy at contact interfaces and ultimately damps the vibration amplitude within the full excitation range. The dependency of the resonance frequencies (shifted towards the left of the frequency axis) and the nonlinear friction damping on vibration amplitudes is evident in Fig. 3.16.

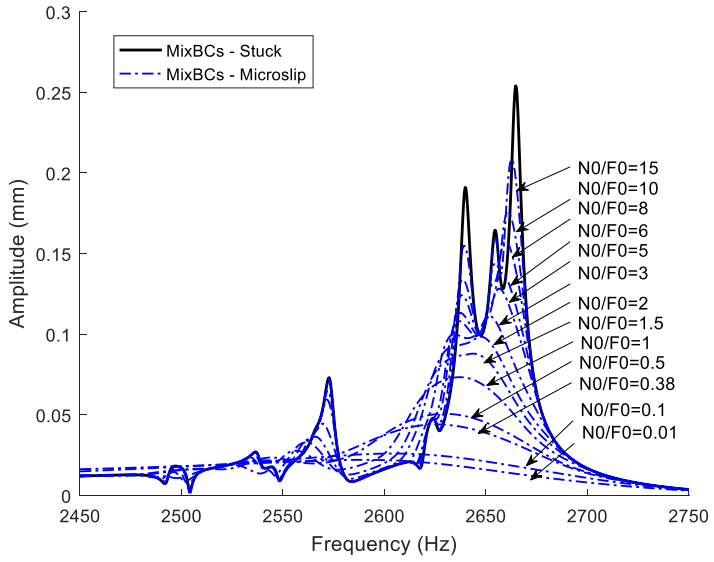

Fig. 3.16 The effect of nonlinear friction damping on forced response levels of the mistuned blisk under EO 3 excitation and different preload-to-forcing conditions.

The effect of nonlinear friction damping on forced response levels of the mistuned blisk under EO 12 excitation and different preload-to-forcing conditions is presented in Fig. 3.17. As it is seen, decreasing the N0/F0 values, initially increases the nonlinear dissipative effects at contact nodes, as the vibration amplitude decreases. Further decreasing the preload value introduces the separation at contact nodes and the efficiency of friction damping drops as the slip decreases at friction interfaces. The increase of separation (i.e. partial contact) at shroud friction interfaces reduces

the blisk stiffness and will ultimately shift the response curve towards the response of the blisk with open contacts.

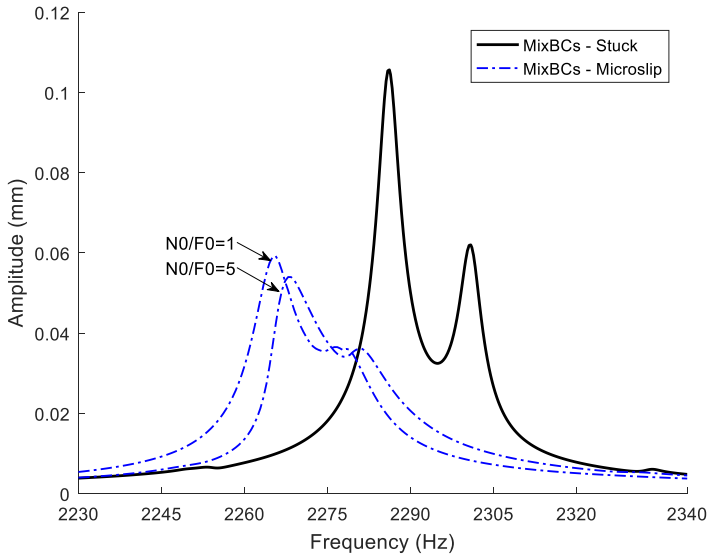

Fig. 3.17 The effect of nonlinear friction damping on forced response levels of the mistuned blisk under EO 12 excitation and different preload-to-forcing conditions.

3.4.2.2 MixBCs vs. CBCMS

As stated earlier, since forced response levels of the mistuned blisk are constructed based on its modal properties, it can be expected that the performance of the ROMs in forced response analysis will vary depending on the frequency range and quality of the predicted modal properties by either of the ROMs.

To better illustrate this, two different frequency ranges around the second and third modal families (shown in Fig. 3.4) are considered for comparison. Figure 3.18 compares the performance of MixBCs and CBCMS ROMs in predicting the envelope of the maximum linear/nonlinear responses of the mistuned blisk under EO 3 excitation and around the second modal family. Forced response levels are dominated by mistuned modes in the range of 2640 to 2665 Hz (namely 51^{st} to 54^{th} mistuned modes in Figs. 3.6 and 3.10). It can be seen that, MixBCs ROM performs slightly better, however, CBCMS ROM can predict both modal properties and forced response levels with comparable accuracy in this frequency range. Figure 3.19 depicts the envelope of the maximum linear/nonlinear responses of the mistuned

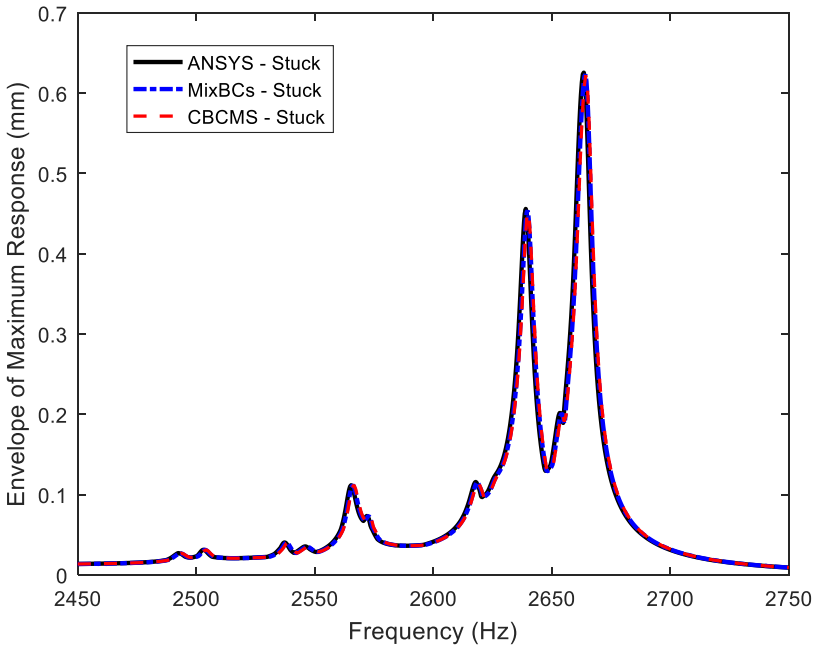

(a)

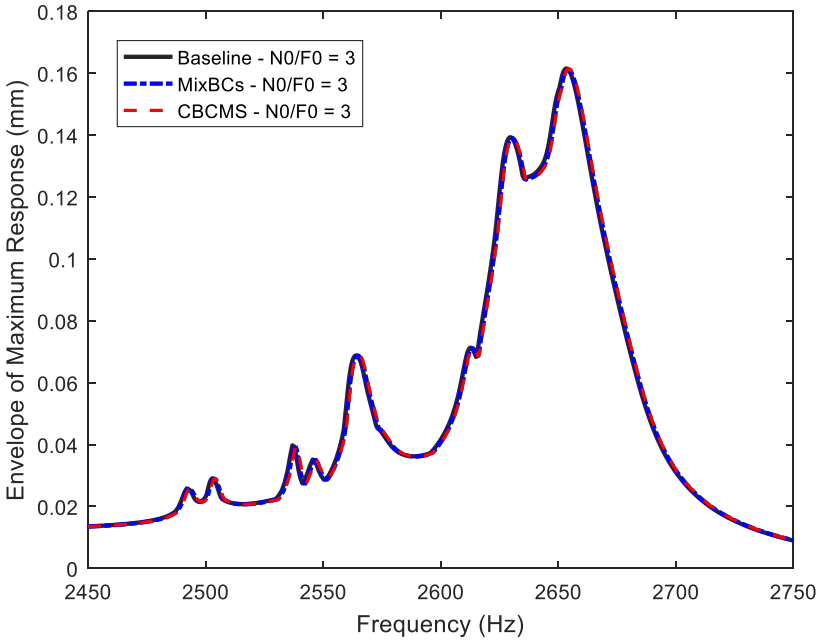

(b)

Fig. 3.18 Performance of the mixed- and fixed- boundary ROMs in predicting the envelope of the maximum response of the mistuned blisk under EO 3 excitation and in (a) fully stick and (b) microslip conditions.

blisk under EO 12 excitation and around the third modal family. Figures 3.6 and 3.10 show that in this frequency range (namely 62^{nd} to 72^{nd} mistuned modes), MixBCs ROM outperforms the CBCMS ROM more noticeably. Consequently, the forced response levels computed by the CBCMS ROM are less accurate compared to that of the MixBCs ROM and this is evident in Fig. 3.19. For instance, the CBCMS ROM introduces about 0.7% error at resonance peak near 3717 Hz for fully stick condition, which is about 9 times bigger than the error introduced by the MixBCs ROM (i.e. 0.077%). In the nonlinear regime, the error introduced by the CBCMS ROM varies between [0.42 – 4.4]% compared to [0.24 – 1.72]% error introduced by the MixBCs ROM.

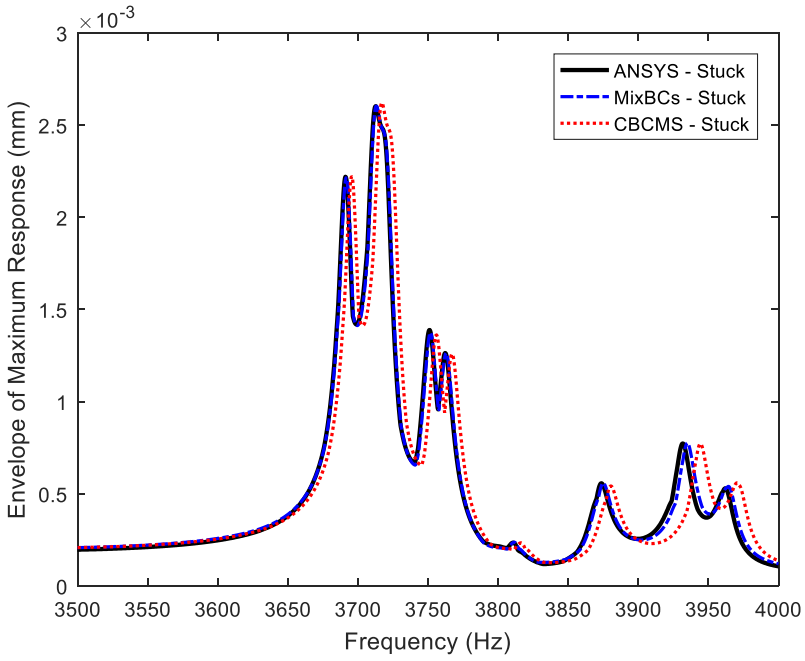

(a)

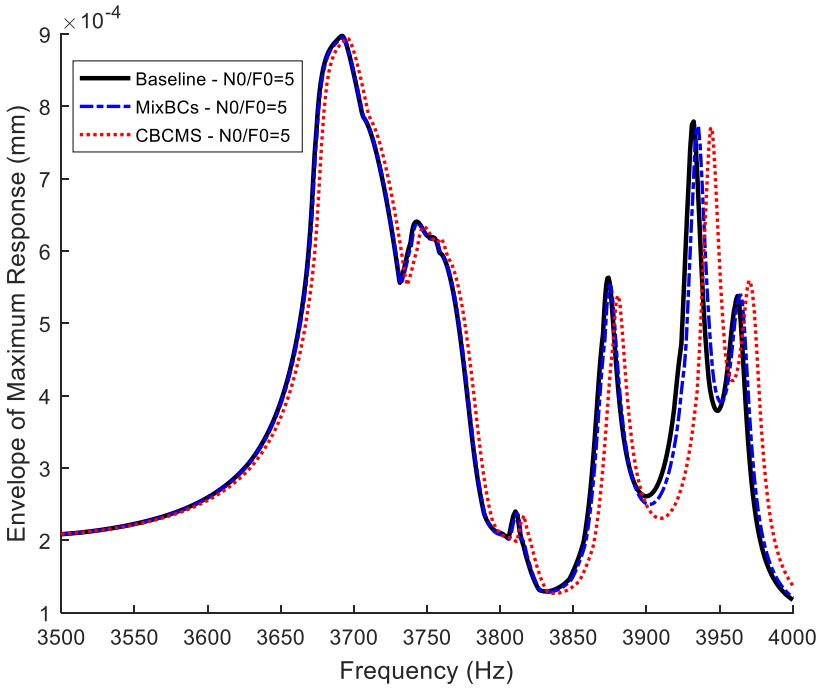

(b)

Fig. 3.19 Performance of the mixed- and fixed- boundary ROMs in predicting the envelope of the maximum response of the mistuned blisk under EO 12 excitation and in (a) fully stick and (b) microslip conditions.

3.5 Conclusion

This chapter, presented a new reduced order model based on a mixed-boundary component mode substitution for nonlinear dynamics of mistuned bladed disks with shroud friction contacts. It benefits from the following features:

- The final mistuned ROM is computed with minimal computational effort and sector-level calculations.
- Blades are reduced in a more realistic mixed-boundary fashion. Accordingly, mixed-boundary component modes of the blades (fixed at blade-disk interface and free at shroud friction contacts) are incorporated into the reduction basis. It was shown that this could remarkably increase the accuracy of the ROM compared with classical fixed-boundary CMS methods.
- Only active boundary DOFs are retained in the Final ROM. Blade-disk interface DOFs were eliminated during the disk reduction by implementing the loaded interface modeshapes of the disk, without performing a secondary reduction scheme.
- Small frequency mistuning is modeled in sector levels.
- The reduction basis is invariant of mistuning and is computed only once which makes the ROM favorable for statistical analyses.

The accuracy of ROM in accurately modeling the mistuned system modal properties and also forced response levels was validated both in ANSYS and the Baseline reference. It was shown that the ROM results are in an excellent accordance with the reference results. In the test case analyzed in this paper, shrouds are modeled as inter-locked working in microslip conditions, being this scenario typical of the earlier part of the blade life. Nevertheless, the mixed-boundary approach looks promising also for modeling the dynamics of bladed disks with (one or more) loose shrouds, being this scenario possible in the later part of the blade life due to the unavoidable fretting wear.

The research findings of this chapter are published in [50].

Chapter 4

Reduced Order Models for Nonlinear Dynamics of Bladed Disk Assemblies with Friction Interfaces: Relative Cyclic Component Mode Synthesis

4.1 Introduction

This chapter introduces a new reduced order modeling technique based on Relative Cyclic Component Mode synthesis (RCCMS). The developed ROM is tailored for nonlinear forced response analysis of bladed disks subjected to different sources of friction damping (friction interfaces).

In its development, the following requirements and features are addressed:

- The ROM must be obtained by performing only sector-level calculations.
- The ROM must include relative displacements between contact surfaces, lying either inside the sector boundaries or located where cyclic symmetry boundaries imposed.
- In the presence of mistuning, the reduction must be performed only once and the small frequency mistuning (either sector-level or blade-level) is directly introduced into the final ROM.

- It is preferable to enhance the accuracy of reduction basis by incorporating modal basis with boundary conditions close to actual kinematics at friction interfaces, especially at microslip (neither fixed nor free).
- It is preferable to implement system-mode-based reductions, to obtain compact ROMs and avoid ending up with component assembly and the need of multiple secondary reductions.
- It is preferable that the ROM retains physical DOFs associated with contact interfaces for an efficient forced response calculation.

The developed ROM is basically consists of two steps:

I. Representing the absolute displacements of the nodes lying on adjacent friction interfaces in terms of relative displacements between the node pairs.

II. Performing the Craig-Bampton Component Mode Synthesis (CB-CMS) on the full-order model already transformed into relative coordinates.

Although, RCCMS is a CMS-based ROM, it can be distinguished from the previously developed ROMs in Chapters 2 and 3 in different ways:

- In contrast to the ROMs in Chapters 2 and 3 that were originally tailored for shrouded bladed disks, RCCMS is suitable for general contact problems.
- The number of unknowns (i.e. nonlinear DOFs) in the reduced space is halved (due to the implementation of relative coordinates).
- Normal modes implemented in the reduction basis are in fact stuck modeshapes of the full system (system-level modes with merged friction interfaces). This results in a highly compact ROM, as only one substructure exists. Moreover, stuck modeshapes are more accurate modal basis for the microslip regime (see section 4.2 for more discussion).

It is worth recalling that, the development of reduced order models in this thesis, initially started by assuming fixed-boundary conditions at the blade interfaces, in Chapter 2. Based on this assumption, normal modes of doubly clamped blades

(i.e. zero displacements at boundary DOFs) were incorporated into the ROM. This assumption was improved in Chapter 3, by incorporating the normal modes of cantilevered blades into the ROM.
In this chapter, this assumption will be further improved by incorporating the normal modes of the full system in stick condition (neither fixed nor free). This objective will be fulfilled by taking the advantage of relative coordinates at interface DOFs and the classical CB-CMS technique.

This chapter is organized as follows: section 4.2 presents the theory and develops ROMs in RCCMS coordinates and sections 4.3.1 and 4.3.2 applies RCCMS to different case studies and evaluate its performance.

4.2 Methodology

This section describes the basic idea of the RCCMS. The RCCMS theory is based on the smart application of relative displacements of friction interfaces and implementation of the CB-CMS reduction technique. The idea of using relative coordinates was first introduced in [51], for forced response analysis of cracked bladed disks. The purpose was to somehow include the vibration modes of the pristine/uncracked blade into the reduction basis. The procedure which was introduced in [51] is described here.

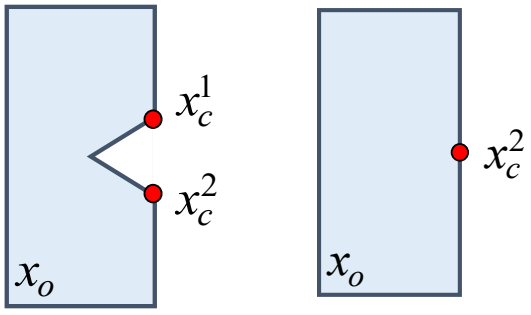

Fig. 4.1 Schematic view of a (a) cracked blade, (b) pristine blade.

Figure 4.1 shows a schematic view of a cracked and a pristine blade. Contact DOFs of crack surfaces of the blade in Fig. 4.1a are denoted by x_c^1 and x_c^2. In the

pristine blade x_c^2 is used to denote the contact DOF although the crack surfaces are merged. Other remaining DOFs of the blades is denoted by x_o.

The stiffness matrix and displacement vector of the cracked blade shown in Fig. 4.1a can be described as follows:

$$\left[\begin{array}{ccc|c} K_{cc}^1 & 0 & K_{co}^1 & x_c^1 \\ 0 & K_{cc}^2 & K_{co}^2 & x_c^2 \\ K_{oc}^1 & K_{oc}^2 & K_{oo} & x_o \end{array}\right] \tag{4.1}$$

By introducing the relative displacements between contact DOFs (i.e. $x_{rel} = x_c^1 - x_c^2$) into the full displacement vector, one may obtain the new displacement vector and stiffness matrix as follows:

$$\begin{aligned} \left\{\begin{array}{c} x_c^1 \\ x_c^2 \\ x_o \end{array}\right\} &= \left[\begin{array}{ccc} I & I & 0 \\ 0 & I & 0 \\ 0 & 0 & I \end{array}\right] \left\{\begin{array}{c} x_{rel} \\ \hline x_c^2 \\ x_o \end{array}\right\} \\ \Rightarrow & \left[\begin{array}{ccc|c} K_{cc}^1 & K_{cc}^1 & K_{co}^1 & x_{rel} \\ K_{cc}^1 & K_{cc}^1 + K_{cc}^2 & K_{co}^1 + K_{co}^2 & x_c^2 \\ K_{oc}^1 & K_{co}^1 + K_{oc}^2 & K_{oo} & x_o \end{array}\right] \end{aligned} \tag{4.2}$$

After introduction of the relative DOFs into the full displacement vector, performing a CB-CMS reduction and retaining x_{rel} as master DOFs gives:

$$\left\{\begin{array}{c} x_{rel} \\ \hline x_c^2 \\ x_o \end{array}\right\} = R_{CB} \left\{\begin{array}{c} x_{rel} \\ \eta \end{array}\right\} \tag{4.3}$$

In this way, authors in [51] were able to include normal modes of the pristine blade into their ROM. Note that, in the context of CB-CMS, fixed interface modes are obtained by clamping the master DOFs. Accordingly, fixing the relative displacements between crack interfaces is equivalent to the following system:

$$\left[\begin{array}{c|cc} 0 & 0 & 0 \\ \hline 0 & K_{cc}^1 + K_{cc}^2 & K_{co}^1 + K_{co}^2 \\ 0 & K_{co}^1 + K_{oc}^2 & K_{oo} \end{array}\right] \left|\begin{array}{c} 0 \\ x_c^2 \\ x_o \end{array}\right. \tag{4.4}$$

which in fact describes the pristine blade shown in Fig. 4.1b.
It is evident that by performing a CB-CMS only afterwards, relative DOFs are included in the full displacements vector, not only half the number of retained contact DOFs but also incorporates fully stick modeshapes (where contact interfaces are merged).
In the RCCMS, the application of relative notation is extended and generalized for nonlinear forced response analysis of mistuned bladed disks with friction interfaces.

In the remainder, section 4.2.1 presents a cyclic multiharmonic RCCMS-based ROM for nonlinear dynamics of tuned bladed disks with friction interfaces located not only inside the sector boundaries (e.g. the blade-root) but also where cyclic symmetry boundaries are imposed (e.g. shroud surfaces).
The tuned ROM is described on a shrouded bladed disk with blade-root joints and the reason is twofold:

i. fill the gap in the literature and utilize relative coordinates when contact DOFs are located at cyclic boundaries.

ii. computational burden of constructing a RCCMS-based mistuned ROM for bladed disks with shroud contacts (this will be elaborated in section section 4.2.2).

Finally, in section 4.2.2, a mistuned ROM is developed in RCCMS coordinates for nonlinear dynamics of mistuned bladed disk with blade-root damping. Different solutions are addressed to construct an efficient ROM invariant of the mistuning pattern, which is necessary for statistical analyses.

4.2.1 Application to Cyclically Symmetric Bladed Disks

The idea of using relative coordinates was applied to a tuned shrouded balded disk in [52]. In that study, the FE model of the fundamental sector was manipulated to define an unconventional cyclic symmetry boundaries such that the shroud contact nodes were lain inside the sector boundaries. However, in real industrial applications such manipulations of the FE model is not favorable and thus a solid formulation and straightforward modeling approach is needed.
The purpose of this section is to remove such limitations by providing a solid and efficient approach. Accordingly, a ROM based on RCCMS is developed for nonlinear

forced response analysis of cyclic bladed disks with multiple friction joints especially at sector boundaries.
The construction of the proposed ROM consists of three steps:

i. First, applying the proper phase conditions at interfaces of the sector model with cyclic symmetry boundary conditions.

ii. Second, representing the absolute displacements of the nodes lying on adjacent friction interfaces in terms of relative displacements between the node pairs.

iii. Finally, performing the CB-CMS on the full-order sector model already transformed into relative cyclic coordinates.

These steps are explained in details in the remainder.

4.2.1.1 Equations of Motion

In this section, the RCCMS is applied to a shrouded bladed disk subjected to nonlinear friction damping at both shrouds and blade root joints (see Fig. 4.2).

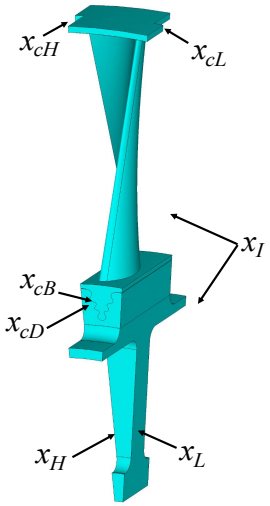

Fig. 4.2 Fundamental sector of the studied shrouded bladed disk and its partitioned DOFs.

It is assumed that the bladed disk is tuned and thus forced response levels of the full system can be computed by using one cyclic sector only. Prior to applying

the RCCMS, it is convenient to partition the displacement vector of the bladed disk fundamental sector as follows :

$$x = \left\{ \begin{array}{c} [x_c] \\ x_I \\ x_L \\ x_H \end{array} \right\}, \quad [x_c] = \left\{ \begin{array}{c} x_{cL} \\ x_{cH} \\ x_{cB} \\ x_{cD} \end{array} \right\} \tag{4.5}$$

where

- x_c denotes the displacement vector of all contact DOFs.
- x_{cL} and x_{cH} denote displacements of shroud contact nodes lying on the low and high shroud interface, respectively.
- x_{cB} and x_{cD} denote displacements of contact nodes at the blade root, lying on the blade and the disk interface, respectively.
- x_L and x_H denote displacements of the nodes lying on the low and high interfaces of the disk sector where cyclic symmetry boundary conditions are to be applied.
- x_I denotes displacements of all other remaining (i.e. internal) nodes of the sector.

Note that, the blade and the disk partitions are uncoupled to each other and the blade-disk coupling will be introduced through nonlinear interactions at the blade root friction interfaces.
It is assumed that the bladed disk is subjected to a periodic wave excitation and its response remains periodic. The steady state vibration response of an isolated sector of the bladed disk can be rep-resented as follows:

$$[-(n\omega)^2 M + in\omega C + K]^{(n)} \bar{x}^{(n)} = \bar{F}_{nl}^{(n)} + \bar{F}_{ex}^{(n)} \tag{4.6}$$

in the frequency domain, where K, M and C are stiffness, mass and the damping matrices of the isolated sector respectively, $\bar{x}^{(n)}$, $\bar{F}_{ex}^{(n)}$ and $\bar{F}_{nl}^{(n)}$ are complex amplitudes of the response, wave excitation and friction forces of the nth harmonic, respectively. In addition, ω is the frequency of the external wave excitation and can be expressed

by $\omega = eo\Omega$, where eo is the engine order of the excitation and Ω is the angular speed of the rotating bladed disk.

4.2.1.2 Cyclic Symmetry Constraints

In the absence of vibration localizations, forced response of bladed disks with localized nonlinearities (e.g. friction contacts), can be assumed symmetric and can be efficiently computed by imposing proper phase conditions at the low and high disk interfaces of the fundamental sector. Cyclic symmetry constraints can be imposed to the fundamental sector by:

$$\bar{x}^{(n)} = \begin{Bmatrix} \bar{x}_c \\ \bar{x}_I \\ \bar{x}_L \\ \bar{x}_H \end{Bmatrix}^{(n)} = \begin{bmatrix} I & 0 & 0 \\ 0 & I & 0 \\ 0 & 0 & I \\ 0 & 0 & e^{in\varphi} \end{bmatrix} \begin{Bmatrix} \bar{x}_c \\ \bar{x}_I \\ \bar{x}_L \end{Bmatrix}^{(n)} = T_{cs}^{(n)} \bar{q}^{(n)} \tag{4.7}$$

In Eq. (4.7) n denotes the harmonic index and $\varphi = 2\pi eo/N_s$ denotes the inter-blade phase angle where N_s defines the number of sectors. By using the cyclic symmetry transformation matrix defined in Eq. (4.7), the multiharmonic balance equations of the cyclic sector can be obtained as:

$$[-(n\omega)^2\bar{M} + in\omega\bar{C} + \bar{K}]^{(n)}\bar{q}^{(n)} = \bar{f}_{nl}^{(n)} + \bar{f}_{ex}^{(n)} \tag{4.8}$$

where $\bar{M}$, $\bar{C}$ and $\bar{K}$ are complex valued structural matrices obtained by applying the proper cyclic symmetry phase conditions according to the harmonic index [14].

4.2.1.3 Introduction of Relative Coordinates

The next step in RCCMS approach is representing the absolute displacements of contact nodes in terms of relative displacements between the contact node pairs. A schematic view of shroud contact boundaries is depicted in Fig. 4.3.

The relative displacements between the contact nodes at the blade root are referred to as the internal relative DOFs and can be determined by:

$$\bar{x}_{rel,i}^{(n)} = \bar{x}_{cB}^{(n)} - \bar{x}_{cD}^{(n)} \tag{4.9}$$

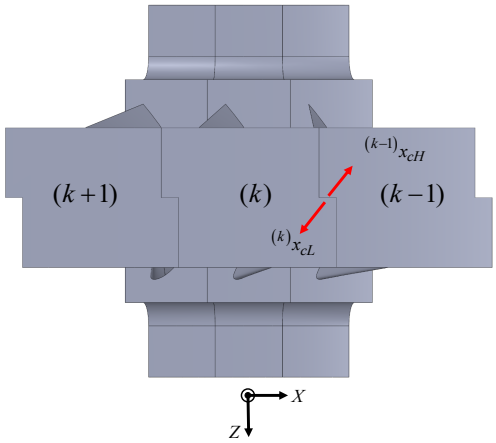

Fig. 4.3 Boundary contact DOFs at adjacent shroud contact surfaces.

In contrast to internal contact nodes at the blade root, shroud contacts are located at the sector boundaries (see Fig. 4.3). As a result, relative displacements between contact nodes lying on adjacent shrouds are referred to as boundary relative displacement. Boundary relative displacements at the low interface of the kth shroud can be expressed as:

$$^{(k)}\bar{x}^{(n)}_{rel,b} = {}^{(k-1)}\bar{x}^{(n)}_{cH} - {}^{(k)}\bar{x}^{(n)}_{cL} \tag{4.10}$$

where $^{(k)}\bar{x}^{(n)}_{cL}$ denotes the low (i.e. right) shroud contact displacements of the kth sector and $^{(k-1)}\bar{x}^{(n)}_{cH}$ denotes high (i.e. left) shroud contact displacements of the $(k-1)$th sector.

The boundary relative displacements defined in Eq. (4.10) can be represented in terms of shroud contact displacements of one sector by employing cyclic symmetry properties as follows:

$$\bar{x}^{(n)}_{rel,b} = e^{-in\varphi}\bar{x}^{(n)}_{cH} - \bar{x}^{(n)}_{cL} \tag{4.11}$$

In Eq. (4.11), the sector index (i.e. (k)) is omitted for the sake of brevity.

Finally, the full displacement vector of the cyclic sector can be represented in relative

coordinates using the following transformation matrix:

$$\bar{q}^{(n)} = \begin{Bmatrix} \bar{x}_{cL} \\ \bar{x}_{cH} \\ \bar{x}_{cB} \\ \bar{x}_{cD} \\ \bar{x}_{I} \\ \bar{x}_{L} \end{Bmatrix}^{(n)} = \left[\begin{array}{cccc|cc} -I & 0 & e^{-in\varphi} & 0 & 0 & 0 \\ 0 & 0 & I & 0 & 0 & 0 \\ 0 & I & 0 & I & 0 & 0 \\ 0 & 0 & 0 & I & 0 & 0 \\ \hline 0 & 0 & 0 & 0 & I & 0 \\ 0 & 0 & 0 & 0 & 0 & I \end{array}\right] \begin{Bmatrix} \bar{x}_{rel,b} \\ \bar{x}_{rel,i} \\ \bar{x}_{cH} \\ \bar{x}_{cD} \\ \bar{x}_{I} \\ \bar{x}_{L} \end{Bmatrix}^{(n)} = T_{rel}^{(n)} \bar{q}_r^{(n)} \tag{4.12}$$

The final relative displacement vector $\bar{q}_r$ (defined in Eq. (4.12)) comprises two distinct groups of DOFs and can be partitioned as follows:

$$\bar{q}_r^{(n)} = \begin{Bmatrix} \bar{x}_N \\ \bar{x}_L \end{Bmatrix}^{(n)}$$

$$\text{with} \quad \bar{x}_N = \begin{Bmatrix} \bar{x}_{rel,b} \\ \bar{x}_{rel,i} \end{Bmatrix} \quad \text{and} \quad \bar{x}_L = \begin{Bmatrix} \bar{x}_{cH} \\ \bar{x}_{cD} \\ \bar{x}_{I} \\ \bar{x}_{L} \end{Bmatrix} \tag{4.13}$$

where $\bar{x}_N$ denotes relative contact DOFs that are used to compute nonlinear friction forces and $\bar{x}_L$ denotes the vector of linear coordinates and contains the DOFs of the cyclic sector with merged friction interfaces (i.e. fully stick condition). Introducing Eq. (4.13) into Eq. (4.8), yields the dynamic balance equations in relative cyclic coordinates, as follows:

$$[-(n\omega)^2 \bar{M}_r + in\omega \bar{C}_r + \bar{K}_r]^{(n)} \begin{Bmatrix} \bar{x}_N \\ \bar{x}_L \end{Bmatrix}^{(n)} = \begin{Bmatrix} \bar{f}_n \\ 0 \end{Bmatrix}^{(n)} + \begin{Bmatrix} 0 \\ \bar{f}_{ex} \end{Bmatrix}^{(n)},$$

$$\text{with} \quad f_n = \begin{Bmatrix} \bar{f}_n^b \\ \bar{f}_n^i \end{Bmatrix} \tag{4.14}$$

where subscript r refers to structural matrices in relative cyclic coordinates.
In Eq. (4.14) $\bar{f}_n$ denotes the amplitude of nth harmonic of the nonlinear friction forces which is composed of boundary friction forces at shrouds (i.e. $\bar{f}_n^b$) and internal friction forces at the blade root (i.e. $\bar{f}_n^i$).

Note that, in the RCCMS reduction technique, moving to relative coordinates is a preliminary step and size reduction comes only afterwards.

4.2.1.4 CB-CMS Reduction

Refined FE models of industrial bladed disks contain numerous DOFs even at the sector level. Thus, computing the forced response levels of the full order model by solving Eq. (4.14) might become prohibitively expensive. To overcome this, the CB-CMS reduction technique is employed to reduce the size of the sector model. The objectives of performing the CB-CMS on equations of motion in relative coordinates, is threefold:

i. First, to retain the relative contact DOFs after the reduction, for nonlinear forced response calculations.

ii. Second, to enhance the accuracy of the reduction basis by employing normal modes with fully stuck boundary conditions.

iii. Third, to achieve a highly reduced ROM by performing a system level reduction.

The CB-CMS reduction method is applied to the cyclic sector in relative coordinates (Eq. (4.14)), by retaining $\bar{x}_N$ as master DOFs and representing $\bar{x}_L$ in terms of modal coordinates corresponding to the fully stick modeshape of the sector. The final reduced displacement vector in RCCMS coordinates can be obtained by:

$$\bar{q}_r^{(n)} = \left\{ \begin{array}{c} \bar{x}_N \\ \bar{x}_L \end{array} \right\}^{(n)} = T_{cb}^{(n)} \bar{q}_{rom}^{(n)} = \left[\begin{array}{cc} I & 0 \\ \Psi & \Omega \end{array} \right]^{(n)} \left\{ \begin{array}{c} \bar{x}_N \\ \bar{\eta} \end{array} \right\}^{(n)} \tag{4.15}$$

where $T_{cb}^{(n)}$ and $\bar{\eta}^{(n)}$ are the CB-CMS transformation matrix and the generalized coordinates of the nth harmonic, respectively. In Eq. (4.14), $\Psi^{(n)}$ denotes relative cyclic constraint modes of the nth harmonic and are obtained by imposing a unitary relative displacement at each retained relative DOF while holding other relative DOFs fixed. Also, $\Phi^{(n)}$ denotes fixed interface cyclic modes of the nth harmonic and are obtained by solving the eigenvalue problem of the linear partition of the cyclic sector.

By introducing Eq. (4.15) into Eq. (4.14), the final reduced dynamic balance equations in RCCMS coordinates, yields:

$$[-(n\omega)^2\bar{M}_{rom}+in\omega\bar{C}_{rom}+\bar{K}_{rom}]^{(n)}\left\{\begin{array}{c}\bar{x}_N\\ \bar{\eta}\end{array}\right\}^{(n)}=\left\{\begin{array}{c}\bar{f}_n\\ 0\end{array}\right\}^{(n)}+\left\{\begin{array}{c}\Psi^H\bar{f}_{ex}\\ \Phi^H\bar{f}_{ex}\end{array}\right\}^{(n)} \tag{4.16}$$

where subscript *rom* refers to the reduced structural matrices in RCCMS coordinates and superscript H denotes the Hermitian transpose.

4.2.1.5 Remarks on Local/Global Coordinate Systems

It should be noted that, the nonlinear contact forces are computed in the local Cartesian coordinate systems of the contact surfaces. Conventional strategies for solving the cyclic dynamic balance equations, demand conversion of contact relative displacements from global cyclic to local contact coordinates and converting back the local friction forces to global cyclic coordinates.
However, a new strategy is introduced here which does need require changing the coordinate systems. The basic idea is to have the relative contact DOFs and their corresponding partition in the cyclic dynamic balance equations written in the local coordinate systems of contact surfaces.
In this way, all the rows and columns of the dynamic balance equations, corresponding to nonlinear DOFs, are already written in local coordinate systems. One only need to show that the cyclic symmetry properties can be also applied to the relative contact displacements written in local Cartesian coordinate systems of contact surfaces.
It is intuitive in the way that, local coordinate systems are attached to the contact surfaces and are rotating in circumferential direction with a phase angle similar to the inter-blade phase angle. In the following, this symmetry property is investigated for one specific shroud contact pair.
The relative displacement of the considered contact node pair in cyclic coordinates are:

$$^{(k)}Q_{rel}(t)=\,^{(k+1)}Q_L(t)-\,^{(k)}Q_H(t) \tag{4.17}$$

in time domain. By employing the cyclic symmetry properties, Eq. (4.17) can be written in terms of cyclic displacements of one sector as:

$$^{(k)}Q_{rel}(t) = {}^{(k)}Q_L(t+\delta t) - {}^{(k)}Q_H(t) \tag{4.18}$$

where δt denotes the time delay between the adjacent sectors. To compute the nonlinear friction forces one needs to convert the cyclic relative displacements into the local Cartesian shroud coordinates. This can be done by using a nominal rotation matrix R, as follows:

$$^{(k)}X_{rel}(t) = R\left[{}^{(k)}Q_{rel}(t)\right] = R\left[{}^{(k)}Q_L(t+\delta t) - {}^{(k)}Q_H(t)\right] \tag{4.19}$$

Equation (4.19) can be further simplified as:

$$^{(k)}X_{rel}(t) = R\left\{R^T\left[{}^{(k)}X_L(t+\delta t)\right] - R^T\left[{}^{(k)}X_H(t)\right]\right\} = {}^{(k)}X_L(t+\delta t) - {}^{(k)}X_H(t) \tag{4.20}$$

which implies that cyclic symmetry properties hold in local Cartesian coordinates. Based on Eq. (4.20), it is convenient to convert the nonlinear partition of the dynamic balance equations into local coordinate systems. In this way, the computed relative displacements and nonlinear forces are readily available in the contact coordinate systems and are injected into the portions of balance equations, written in the same coordinate systems.
In this study, portions of structural matrices corresponding to contact DOFs are simply projected into local contact coordinate systems by using the *nrotat* command in ANSYS.

4.2.2 Application to Mistuned Bladed Disks

As it was stated in section 4.2.1, the idea of using relative coordinates was introduced in [51] and used for linear forced response analysis of a bladed disk with one cracked blade. Staying within the scope (i.e. modeling a bladed disk with a cracked blade), the introduced strategy was adopted and improved in series of studies. For instance in [53], the CMM [17] method was used to model small blade mistuning in the pristine/uncracked structure, in the absence of contact interactions between crack surfaces.

The main focus of these studies was to take into account the effects of mistuning (ranging from small [53], to large [54]) and to develop ROMs for linear forced response of mistuned balded disks with a cracked blade.
Although there are studies in the literature on linear mistuned bladed disks with a cracked blade and they use the idea of relative coordinates, RCCMS adopts the initial idea and introduces a solid formulation that can be used in a more general application, that is nonlinear forced response analysis of mistuned bladed disks with friction interfaces.
It should be noted that, even by including nonlinear damping effect between the crack surfaces of one blade, dealing with a bladed disk with multiple friction interfaces at shrouds, blade root joints and etc. demands a more advanced treatment.
In RCCMS coordinates, the final ROM is composed of a statically reduced component corresponding to relative contact DOFs (referred to as nonlinear partition), and a modal reduced component corresponding to the linear system with merged friction interfaces (referred to as linear partition).
This makes the RCCMS unique and very flexible when modeling the mistuning is deemded needed. Since it allows analysts and designers; in a systematic way; to benefit from powerful theories of mistuning modeling of linear system (e.g. SNM [27], CMM [17], IMM [33] and NEWT [28]) for mistuning analysis of nonlinear system with friction interfaces.
In particular, the current study introduces the small frequency mistuning in the sector-level by employing the principle assumption of the SNM theory. This results in a highly reduced ROM by using system-level modes.
In order to reduce the overall computational burden and to build the ROM using one single sector only, the developed mistuned ROM is tailored for bladed disks with friction interfaces inside the sector boundaries and remote from the blade tip motion (e.g. blade-root joints, underplatform dampers, ring dampers), although the general formulation is applicable to bladed disks with different configurations and all kinds of mistuning.
In the remainder, a mistuned ROM is developed for nonlinear dynamics of bladed disks with blade-root friction damping. The reduction basis is invariant of the mistuning pattern which makes it favorable for statistical characterization of the nonlinear response levels.

4.2.2.1 Equations of Motion

The equations of motion of a general bladed disk system can be represented as:

$$M\ddot{x}(t)+C\dot{x}(t)+Kx(t)=F_{nl}(x(t),\dot{x}(t))+F_{ex}(t) \tag{4.21}$$

where

- M and K are system mass and stiffness matrix, respectively.
- C denotes the linear viscous damping and is assumed to be proportional to mass and stiffness (i.e. $C=\alpha M+\beta K$).
- $x(t)$ denotes the displacement vector of the full system.
- F_{nl} represents the vector of nonlinear friction forces and is dependent on relative displacements and velocities at contact nodes.
- F_{ex} denotes the external periodic forces applied on the system.

Figure 4.4 shows the fundamental sector of the studied mock up bladed disk and the defined partition of DOFs. To assess the friction damping at blade roots, the nodes laying on blade-disk interfaces, are denoted as contact nodes (subscripts c). Other remaining DOFs are denoted by subscripts o. Superscripts b and d are used to distinguish between the blade and the disk DOFs. Prior to performing the new reduction steps, it is convenient to first reorder the full displacement vector and the corresponding structural matrices, as follows:

$$x=\begin{Bmatrix} x_c^b \\ x_c^d \\ x_o^b \\ x_o^d \end{Bmatrix}$$

$$K=\begin{bmatrix} K_{cc}^b & 0 & K_{co}^b & 0 \\ 0 & K_{cc}^d & 0 & K_{co}^d \\ K_{oc}^b & 0 & K_{oo}^b & 0 \\ 0 & K_{oc}^d & 0 & K_{oo}^d \end{bmatrix}, \quad M=\begin{bmatrix} M_{cc}^b & 0 & M_{co}^b & 0 \\ 0 & M_{cc}^d & 0 & M_{co}^d \\ M_{oc}^b & 0 & M_{oo}^b & 0 \\ 0 & M_{oc}^d & 0 & M_{oo}^d \end{bmatrix} \tag{4.22}$$

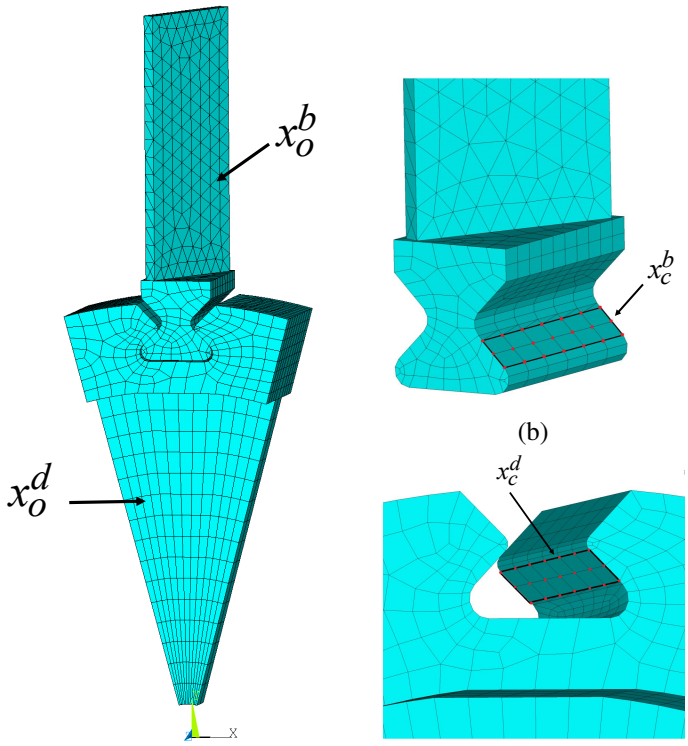

Fig. 4.4 Fundamental sector of the studied bladed disk and its partitioned DOFs.

It should be noted that, Eq. (4.21) represents the partitioned full displacement vector of the system and for instance, x_c^b denotes the contact DOFs of all blades. As evident from Fig. 4.4, the partitions corresponding to blade DOFs are block diagonal and the partition corresponding to other DOFs of the disk (i.e. K_{oo}^d and M_{oo}^d) are block circulant, due to the coupling between the interfaces of disk sectors.

4.2.2.2 Introduction of Relative Coordinates

The first step in RCCMS, as stated in section 4.2.1, is to represent the absolute displacements of contact nodes in terms of the relative displacements between contact node pairs. The relative displacements between contact nodes can be determined by:

$$x_{rel} = x_c^b - x_c^d \tag{4.23}$$

Note that, x_{rel} denotes relative displacements in local coordinate systems of contact surfaces. Accordingly, the full displacement vector can be expressed in relative coordinates by using Eq. (4.23) and introducing the following transformation:

$$\begin{Bmatrix} x_c^b \\ x_c^d \\ x_o^b \\ x_o^d \end{Bmatrix} = \begin{bmatrix} I & I & 0 & 0 \\ 0 & I & 0 & 0 \\ 0 & 0 & I & 0 \\ 0 & 0 & 0 & I \end{bmatrix} \begin{Bmatrix} x_{rel} \\ x_c^d \\ x_o^b \\ x_o^d \end{Bmatrix} = [T]\{x_r\} \tag{4.24}$$

It is evident that, the displacement vector in relative coordinates (i.e. x_r in Eq. (4.24)), can be divided into two distinct groups, namely nonlinear and linear DOFs, as follows:

$$x_r = \begin{Bmatrix} [x_{rel}] = x_N \\ \begin{bmatrix} x_c^d \\ x_o^b \\ x_o^d \end{bmatrix} = x_L \end{Bmatrix} = \begin{Bmatrix} x_N \\ x_L \end{Bmatrix} \tag{4.25}$$

In Eq. (4.25), x_N is the vector of nonlinear coordinates and only contains relative displacements of contact nodes which is used to calculate nonlinear friction forces. On the other hand, x_L is the vector of linear coordinates and contains DOFs of the linear system with no friction interfaces. In fact, x_L denotes a linear system in fully stuck condition (i.e. merged contact nodes).
Introducing Eq. (4.24) into Eq. (4.21), yields the transformed equations of motion in relative coordinates:

$$M_r \begin{Bmatrix} \ddot{x}_N \\ \ddot{x}_L \end{Bmatrix} + C_r \begin{Bmatrix} \dot{x}_N \\ \dot{x}_L \end{Bmatrix} + K_r \begin{Bmatrix} x_N \\ x_L \end{Bmatrix} = \begin{Bmatrix} f_{nl} \\ 0 \end{Bmatrix} + \begin{Bmatrix} 0 \\ f_{ex} \end{Bmatrix} \tag{4.26}$$

where

$$K_r = T^T K T = \left[\begin{array}{c|ccc} K_{cc}^b & K_{cc}^b & K_{co}^b & 0 \\ \hline K_{cc}^b & K_{cc}^b + K_{cc}^d & K_{co}^b & K_{co}^d \\ K_{oc}^b & K_{oc}^b & K_{oo}^b & 0 \\ 0 & K_{oc}^d & 0 & K_{oo}^d \end{array}\right] = \begin{bmatrix} K_{NN} & K_{NL} \\ K_{LN} & K_{LL} \end{bmatrix}$$

$$M_r = T^T M T, \quad C_r = T^T C T \tag{4.27}$$

In Eq. (4.27), M_r and C_r matrices are partitioned in the same fashion as the stiffness matrix and are not shown here for brevity. F_{nl} is the vector of nonlinear friction forces, acting on nonlinear (relative) partition. F_{ex} is the vector of external force and it is assumed that it applies on linear partition only.
Note that, in RCCMS, moving to relative coordinates is a preliminary step, and size reduction comes only afterwards. The benefits of this transformation will become apparent in the following sections.

4.2.2.3 CB-CMS Reduction

Computing the forced response levels of the full order model by solving Eq. (4.26) is prohibitively expensive. To overcome this, the CB-CMS reduction technique is employed to reduce the size of the full order model. The benefits of performing a CB-CMS reduction on a system already represented in relative coordinates is threefold and is addressed in section 4.2.1.
It should be noted that, in classical CB-CMS techniques, the contact nodes laying on both blade and the disk interfaces are retained as master nodes. This could result in a final ROM with large number of retained nodes (usually a secondary reduction technique should be performed as an extra step [25]).
Moreover, the utilized modeshape have boundary conditions (clamped at interface), different from real kinematics of friction interfaces. Consequently, to reduce the errors arisen from the choice of modal bases, usually more number of modes should be retained in the reduction basis.
The new reduction technique; based on RCCMS; could alleviate many of these difficulties. To do so, x_N (relative DOFs) is retained as master DOFs while x_L is represented by modal coordinates. The final reduced displacement vector in RCCMS coordinates is given by:

$$x_r = \left\{ \begin{array}{c} x_N \\ x_L \end{array} \right\} = \left[\begin{array}{cc} I & 0 \\ \Psi_c & \Phi_f \end{array} \right] \left\{ \begin{array}{c} x_N \\ \eta \end{array} \right\} = R_{cb} x_{rom} \tag{4.28}$$

where R_{cb} is the CB-CMS transformation matrix composed of static constraint modes Ψ_c and fixed interface modeshapes Φ_f.
In the relative context, constraint modes can be obtained by imposing a unitary relative displacement at each retained contact node pair while holding the other node

pairs fixed. Moreover, fixed interface modeshapes are normal modes of a bladed disk system with zero relative displacement at contact node pairs, which are in fact the vibration modes of a fully stuck system.
At this step, both Φ_f and Ψ_c can be computed using the cyclic symmetry properties of the system.
The equations of motion of the final reduced system in RCCMS coordinates can be represented as:

$$M_{rom}\left\{\begin{array}{c}\ddot{x}_N\\ \ddot{\eta}\end{array}\right\}+C_{rom}\left\{\begin{array}{c}\dot{x}_N\\ \dot{\eta}\end{array}\right\}+K_{rom}\left\{\begin{array}{c}x_N\\ \eta\end{array}\right\}=F_{nl}+F_{ex} \tag{4.29}$$

where

$$\begin{aligned}K_{rom}&=R_{cb}^T K_r R_{cb}=\left[\begin{array}{cc}K_{Guyan}&0\\0&\Lambda_i\end{array}\right]\\ M_{rom}&=R_{cb}^T M_r R_{cb}=\left[\begin{array}{cc}M_{Guyan}&M_{N\eta}\\M_{\eta N}&I\end{array}\right]\\ F_{ex}&=\left\{\begin{array}{c}F_{ex}^n\\F_{ex}^l\end{array}\right\}=\left\{\begin{array}{c}\Psi_c^T f_{ex}\\\Phi_f^T f_{ex}\end{array}\right\},\quad F_{nl}=\left\{\begin{array}{c}f_{nl}\\0\end{array}\right\}\end{aligned} \tag{4.30}$$

Different partitions of final reduced mass and stiffness matrices are given below:

$$\begin{aligned}\Lambda_i&=\Phi_f^T K_{LL}\Phi_f\\ K_{Guyan}&=K_{NN}-K_{NL}K_{LL}^{-1}K_{LN}\\ M_{Guyan}&=M_{NN}+\Psi_c^T M_{LN}+M_{NL}\Psi_c+\Psi_c^T M_{LL}\Psi_c\\ M_{N\eta}&=M_{NL}\Phi_f+\Psi_c^T M_{LL}\Phi_f\end{aligned} \tag{4.31}$$

4.2.2.4 Mistuning

Since the proposed reduction technique is a CMS-based approach, in general, it is suitable for both small and large mistuning problems. However, the focus of this study is on small frequency mistuning (either blade or sector level).

A general reduced stiffness matrix of a mistuned system can be written as:

$$K_{rom}^{mist} = \begin{bmatrix} \Psi_{mist}^T K_r^{mist} \Psi_{mist} & \Psi_{mist}^T K_r^{mist} \Phi_{mist} \\ \Phi_{mist}^T K_r^{mist} \Psi_{mist} & \Phi_{mist}^T K_r^{mist} \Phi_{mist} \end{bmatrix} = \begin{bmatrix} K_{Guyan}^{mist} & 0 \\ 0 & \Lambda_i^{mist} \end{bmatrix} \tag{4.32}$$

where $\Psi_{mist} = \begin{bmatrix} I & \Psi_c^{mist} \end{bmatrix}^T$ defines mistuned static constraint modes.

So far, no assumption has been made on the mistuning and the general formulation of Eq. (4.32) is applicable to all types of mistuning (considering tht the same logic is applicable to mass matrix as well). However, the focus here will be on small frequency mistuning and the general formulation of Eq. (4.32) will be further simplified to fulfill the following requirements: 1. sectorl-level computations 2. reduction basis invariant of the mistuning pattern (necessary for statistical analyses).

In the RCCMS coordinates, the final ROM is composed of two distinct partitions:

1. Statically reduced component corresponding to relative displacements between contact node pairs (retained for nonlinear forced response calculations); called the nonlinear partition.

2. Modal reduced component corresponding to the fully stuck system (with merged friction interfaces); called the linear partition.

This will split the introduction of mistuning into a classical linear mistuning problem (for the linear partition) and the mistuning problem of the static component (for the nonlinear partition). In practice, these two components are dealt with, independently.
This makes the RCCMS unique and very flexible for mistuning modeling. Since, powerful classical theories (e.g. SNM, CMM, and etc.), are readily applicable for the reduction of the so-called linear partition.
Here, the principle assumption of SNM theory is employed, to make the ROM suitable for statistical analyses and also to obtain a highly compact ROM by using system-level modes.
Accordingly, it is assumed that modeshapes of the mistuned system can be represented as a linear combination of the tuned system modes (in the presence of small

mistuning). This assumption yields:

$$K_{rom}^{mist} = \begin{bmatrix} K_{Guyan}^{mist} & 0 \\ 0 & \Phi^T K_r^{mist} \Phi \end{bmatrix} \tag{4.33}$$

where Φ are cyclic tuned modeshapes of the linear system in fully stuck conditions. It should be noted that, even implementing tuned modeshapes in Eq. (4.33), the linear and nonlinear partitions/DOFs of the system are still statically uncoupled.

In practice, the lower right partition of the mistuned ROM stiffness matrix (Eq. (4.33)), is calculated by sector-level calculations. One may only need sector-level tuned modeshapes that are computed by imposing cyclic symmetry boundary conditions at disk interfaces.
By defining a non-dimensional mistuning parameter δ, as small deviations of nominal Young's modulus of the fundamental sector, the final stiffness matrix of the mistuned ROM can be determined by:

$$K_{rom}^{mist} = \begin{bmatrix} K_{Guyan}^{mist} & 0 \\ 0 & \sum\limits_{n=1..N} (1+\delta_n) \Phi_n^T K^0 \Phi_n \end{bmatrix} \tag{4.34}$$

where K^0 is the tuned stiffness matrix of a single sector and Φ_n are tuned sector-level modeshapes of nth sector DOFs.
The next step in mistuning modeling, which is needed whenever contact node pairs are retained for nonlinear forced response analysis, would be the computation of the mistuned nonlinear partition.

According to Eq. (4.34), this can be ideally achieved by computing the:

$$K_{Guyan}^{mist} = \Psi_{mist}^T K_r^{mist} \Psi_{mist} = K_{NN}^{mist} - K_{NL}^{mist} \left(K_{LL}^{mist}\right)^{-1} K_{LN}^{mist} \tag{4.35}$$

which in general may become a formidable task. Since, the computation of the system-level static modes demands the inversion of the stiffness matrix of the fully stuck system.
Thus, the objective is to develop cost-efficient approaches to compute the mistuned nonlinear partition of the RCCMS stiffness matrix that can yield a trad-off between the solution accuracy and the computational efficiency.

Accordingly, to alleviate the computational burden, two solutions are proposed to estimate the full-order mistuned relative constraint modes, based on sector-level calculations:

i. *Isolated static modes*: that assumes mistuned static modes are confined to the sector-level.

ii. *Cyclic static modes*: that assumes the effect of frequency mistuning on the statically condensed partition is small, and thus the so-called nonlinear partition can be approximated by its tuned counterpart.

It should be noted that, a relative constraint mode is the static responses due to a unitary relative displacement applied on a retained contact DOF while other contact DOFs are held fixed.

Considering that the blade-disk coupling is located at the blade-root joints and also the overall contribution of the disk stiffness (note that this configuration of bladed disks is very common, especially at compressor stages), the strain imposed by the unitary displacement will be mostly confined in the neighborhood of the blade-disk interface and within the sector level.
Accordingly, one may assume that relative static modes are confined to sector-levels and are isolated as if the sector interfaces were clamped. This assumption is referred to as *isolated static modes*. This assumption isolates the static response of each sector. In other words, it is assumed that the imposed unitary displacement at retained contact DOFs of a given sector results in a nonzero static response only in the sector-level and zero static response in other sectors.
By introducing the *isolated static modes* assumption into Eq. (4.34), the final stiffness matrix of the mistuned ROM is constructed as follows:

$$K_{rom}^{mist} \approx \begin{bmatrix} \underset{n=1..N}{Bdiag}\left[(1+\delta_n)K_{Guyan}^{0}\right] & 0 \\ 0 & \sum\limits_{n=1..N}(1+\delta_n)\Phi_n^T K^0 \Phi_n \end{bmatrix} \tag{4.36}$$

where *Bdiag* denotes a block diagonal matrix and K_{Guyan}^{0} is the Guyan stiffness matrix of the tuned fundamental sector with fixed interfaces. Note that, in Eq. (4.36), mistuning is directly introduced into the decoupled statically reduced sectors. The

same logic can be applied to the mass matrix and yields:

$$M_{rom} \approx \begin{bmatrix} I_N \otimes M^0_{Guyan} & \sum\limits_{n=1..N} \Psi^T_{f,n} M^0 \Phi_n \\ \sum\limits_{n=1..N} \Phi^T_n M^0 \Psi_{f,n} & I \end{bmatrix} \tag{4.37}$$

where M^0 denotes the nominal mass matrix of the fundamental sector, M^0_{Guyan} denotes the Guyan reduced mass matrix of the fundamental sector and $\Psi_{f,n} = \begin{bmatrix} I & \Psi_c \end{bmatrix}^T_n$ denotes the static constraint modes of the nth *clamped* sector of the bladed disk. Note that, since the static problem is decoupled and shrunk into sector-levels, in practice one sector is sufficient to construct $\Psi_{f,n}$.

It should be noted that, in many industrial applications, the disk component is stiffer than other components. In this case, it can be expected that, the relative constraint modes are restricted to the sector level and are not distributed along the full wheel, considerably. This assumption is assessed in section 4.3.2.

The stiffness matrix of the mistuned ROM (i.e. Eq. (4.34)) can be also constructed based on the alternative assumption of *cyclic static modes*.

Since, nonlinear DOFs are located at the blade-disk interface, the static response (due to a unitary relative displacement at nonlinear DOFs) is mainly localized at the blade-disk interface level. It can be expected that, near the blade-dominated modes, when disk and interface are not contributing to system dynamics, the effect of mistuning on the static response is negligible and thus using tuned static modes is a reasonable assumption.

Accordingly, relative static constraint modes can be computed using cyclic symmetry properties and the reduction basis (i.e. R_{cb}) introduced in Eq. (4.28) can be used to reduce the stiffness matrix of the mistuned system.

Prior to constructing the stiffness matrix of the mistuned ROM based on the *cyclic static modes* assumption, it is convenient to recast the mistuned stiffness matrix as:

$$K_r^{mist} = K_r + K_r^{\delta} \tag{4.38}$$

where K_r^{δ} denotes the mistuning component of the stiffness matrix. Note that, K_r^{δ} can include either blade or sector frequency mistuning.

Projecting the mistuned stiffness matrix in Eq. (4.38) onto tuned R_{cb} reduction basis, yields:

$$K_{rom}^{mist} \approx \begin{bmatrix} K_{Guyan} + \sum\limits_{n=1..N} \Psi_n^T K_n^\delta \Psi_n & \sum\limits_{n=1..N} \Psi_n^T K_n^\delta \Phi_n \\ \sum\limits_{n=1..N} \Phi_n^T K_n^\delta \Psi_n & \sum\limits_{n=1..N} (1+\delta_n) \Phi_n^T K^0 \Phi_n \end{bmatrix} \tag{4.39}$$

where Ψ_n defines the tuned static constraint modes of the nth cyclic sector.

Recalling that the nonlinear DOFs are located at blade-disk interface, and also the the overall contribution of the disk is not negligible in this configuration, it can be assumed that the static response due to unitary displacements at nonlinear DOFs is not significant, especially at the blade portion. Thus, the stiffness matrix in Eq. (4.39) can be further simplified by neglecting the effect of mistuning components on static terms as follow:

$$K_{rom}^{mist} \approx \begin{bmatrix} K_{Guyan} & 0 \\ 0 & \sum\limits_{n=1..N} (1+\delta_n) \Phi_n^T K^0 \Phi_n \end{bmatrix} \tag{4.40}$$

Note that, the mass stiffness matrix can be simply computed using the cyclic symmetry properties.

The stiffness matrix of the mistuned ROM can be constructed using either Eq. (4.36) or (4.40), and based on sector-level calculations. In addition, the mistuning is directly introduced into the final ROM, which makes the ROM suitable for statistical nonlinear forced response analyses.

4.3 Numerical Results

In the final ROM, node-to-node state-of-the-art contact elements are imposed at all retained contact node pairs to model the friction contacts. Nonlinear friction forces are then calculated based on the contact states and relative displacements at each contact node pair.

The steady state response of the system is computed using the HBM. It is assumed that the response of the system under a periodic excitation is periodic.

The pseudo-arclength path following technique was implemented to compute the evolution of nonlinear forced response levels with respect to the excitation frequency.

Note that the continuation scheme demands calculation of the Jacobian matrix at each iteration step, which can become a rigorous task. The computational burden was extremely reduced by implementing the analytical Jacobian.
The numerical solution is described thoroughly in Appendix A.

4.3.1 Tuned Bladed Disk with Friction Contacts at Shrouds and Blade Roots

To evaluate the performance of the RCCMS-based ROM developed in section 4.2.1 in nonlinear forced response prediction of bladed disks with friction interfaces at sector boundaries, it is applied to the bladed disk shown in Fig. 4.5. The nonlinear friction damping is modeled at both shroud contact surfaces (cyclic symmetry boundaries) and at blade-root joints (inside sector boundaries).

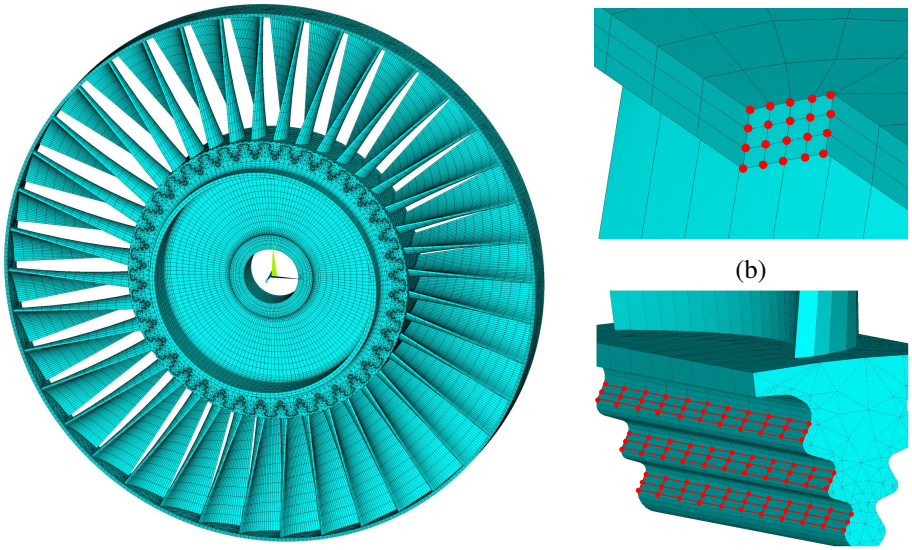

(a) (b) (c)

Fig. 4.5 (a) Full wheel FE model of the mock up bladed disk with friction interfaces at (b) shrouds and (c) blade-root joints.

The mock-up bladed disk is composed of 40 blades, and is made of steel of Young's modulus $E = 200\text{GPa}$, density $\rho = 7800\text{Kg}/\text{m}^3$ and Poisson's ratio $\nu = 0.3$. The fundamental sector model comprises 436 contact nodes in total (20 contact nodes

on each shroud surface and 33 contact nodes on each blade root contact surface) and thus 654 nonlinear relative contact DOFs.
To model the friction contacts, semi-3D contact elements (two perpendicular Jenkins contact elements with variable normal load) are imposed at all retained contact node pairs. The contact stiffness is set equal to 100 $\mathrm{N}/\mu\mathrm{m}$ in both normal and tangential directions and a constant friction coefficient of 0.5 is considered.
The external excitation is applied on the forcing node located at blade tip. It is assumed that the static solutions are not affected by dynamic state of the system. Thus, the static equilibrium state and the corresponding static nonlinear forces are calculated by applying nodal static loads (due to centrifugal forces) to contact node pairs and solving the zeroth order balance equation. Forced response levels are computed based on a monoharmonic balance procedure and by retaining 10 first stuck modeshapes during the construction of the ROM.

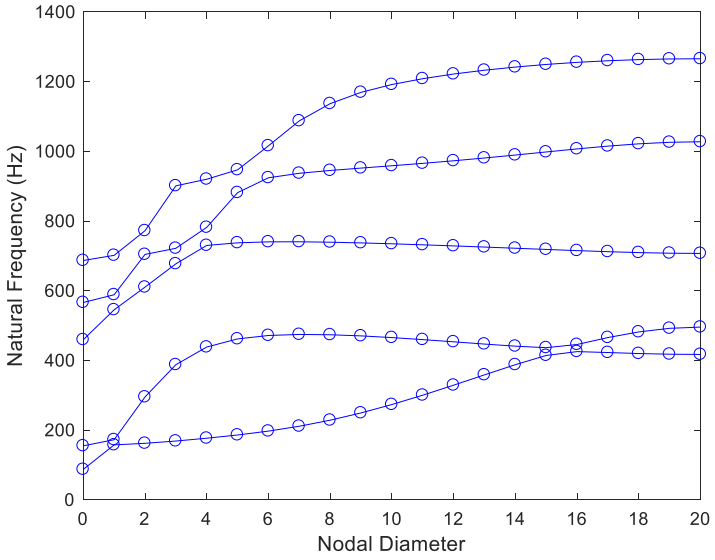

Fig. 4.6 Natural frequencies versus nodal diameters for the tuned bladed disk in fully stick condition.

Figure 4.6 depicts the natural frequencies versus the number of nodal diameters plot for the tuned bladed disk in fully stick condition. All forced response calculations are performed under engine order one excitation (EO 1) and near the first mode of the first family. The tangential component of steady state solutions (calculated for a response node located at the blade tip) are plotted here.

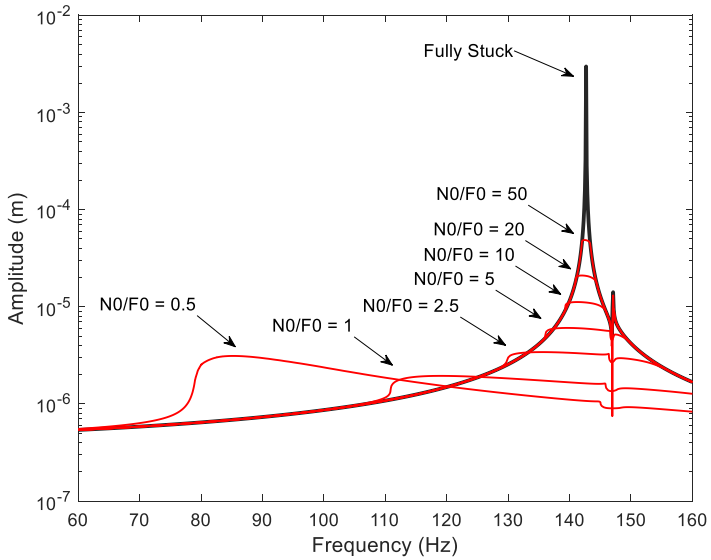

Fig. 4.7 Effect of nonlinear friction damping on forced response levels of the bladed disk under EO 1 excitation.

The effect of nonlinear friction damping on forced response levels of the bladed disk under different preload-to-forcing conditions is presented in Fig. 4.7.
A very slight stiffness-proportional damping was considered to evaluate the performance of the friction damping. As it is seen, decreasing the preload-to-excitation values (i.e. N0/F0), initially increases the nonlinear dissipative effects at contact nodes, as the vibration amplitude decreases.
Further decreasing the preload value introduces the separation at contact nodes and the efficiency of friction damping remarkably drops as the slip decreases at friction interfaces. The increase of separation (i.e. partial contact) at friction interfaces reduces the bladed disk stiffness and will ultimately shift the response curve towards the response of the system with open contacts.

4.3.2 Mistuned Bladed Disk with Friction Contacts at Blade Roots

The developed RCCMS-based mistuned ROM (section 4.2.2) is applied to the bladed disk shown in Fig. 4.8, to evaluate its performance in nonlinear forced response analysis. The mock-up bladed disk is composed of 12 blades and is made of steel. The full-order FE model where the blades are attached to the disk, comprises 42,432 nodes and 127,296 DOFs in total. Each contact surface (see Fig. 4.4) contains 21

contact node pair and the full-order model is composed of 1512 relative contact DOFs.

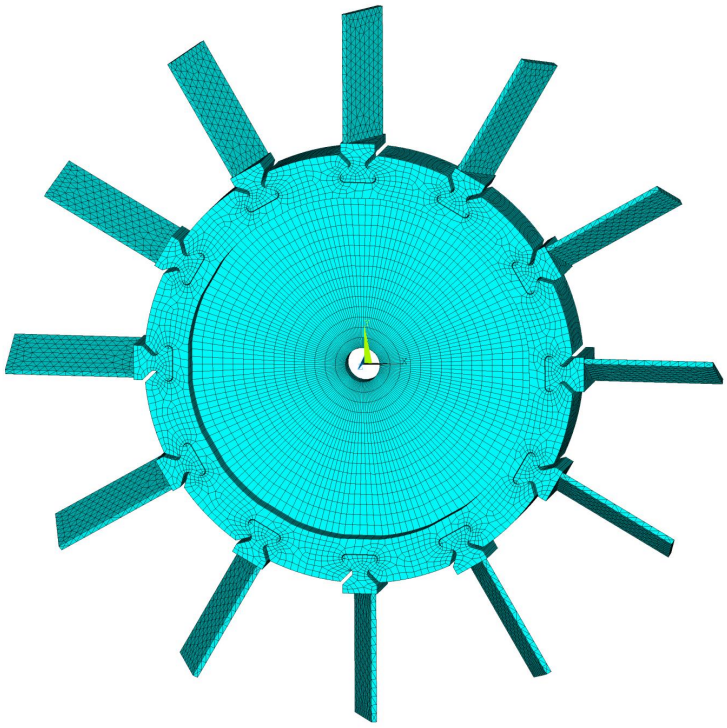

Fig. 4.8 Full wheel FE model of the mock up bladed disk with friction interfaces at blade-root joints.

Accordingly, the nonlinear partition of the ROM consists of 1512 DOFs, and its linear partition is composed of generalized coordinates associated with the R retained system stick modes (total DOFs: $1512 + R$).
Not that, since the ROM is already constructed based on the system-level stick modes, it predicts natural frequencies and modeshapes of the stuck bladed disk with perfect accuracy and the main focus here is the accuracy of the ROM in predicting the forced response levels.
All the forced response calculations are performed on a ROM composed of 300 linear DOFs: i) to have a highly accurate ROM for validation purposes ii) yet very small compared to the nonlinear partition.

The reference model for validating the ROM forced response results, is a CB-CMS reduced model of the full wheel. The mistuned bladed disk model is obtained by defining a random mistuning pattern with uniform distribution and standard deviation of 3%.

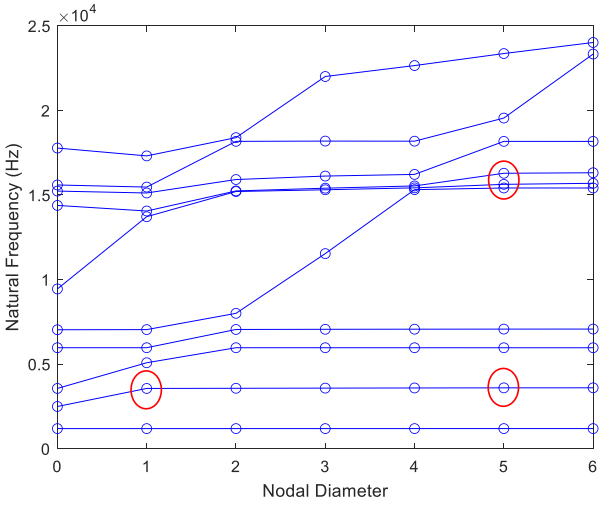

Fig. 4.9 Natural frequencies versus nodal diameters for the tuned bladed disk in fully stick condition.

Natural frequencies versus the number of nodal diameters plot for the tuned bladed disk in fully stick is shown in Fig. 4.9. Red circles show the frequency ranges in which forced response calculation are carried out. The simulation results of the mistuned bladed disk is presented into two subsection based on the construction of the mistuned ROM. In the remainder, the results of the ROM based on *isolated static modes* is presented, followed by the results of the ROM based on *cyclic static modes* assumption.

4.3.2.1 Isolated Static Modes Approach

In simulations in this section, friction contacts are modeled using the semi-3D contact elements (two perpendicular Jenkins contact elements with variable normal load). The contact stiffness is set equal to $k_t = 100\text{N}/\mu\text{m}$, in both normal and tangential directions. This value is defined in a way to have the stuck natural frequencies of the ROM (computed by introducing linear springs of k_t stiffness into the ROM) close to the ANSYS stuck natural frequencies (computed by merging contact node pairs).

All forced response calculations are performed under engine order one excitation (EO 1) of amplitude F0 and around the second modal family. To better evaluate the friction damping, a very slight modal damping (0.1%) was considered for all the modes.

Static loads are modeled by applying a constant normal preload (i.e. N0) on all the retained contact node pairs.
Forced response levels are computed based on a monoharmonic balance procedure. The tangential component of steady state solutions (calculated for a response node located at the tip of nominal blade #1) are plotted here.
The mistuned stiffness matrix is obtained by introducing the secter-level frequency mistuning into the ROM using the Eq. (4.36).

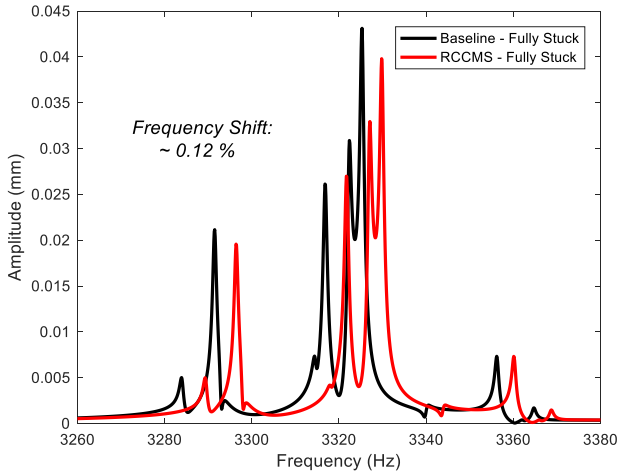

Fig. 4.10 Forced response level of the mistuned bladed disk in fully stuck (EO 1 excitation).

Forced response level of the mistuned bladed disk in fully stuck condition is depicted in Fig. 4.10. As it is seen, RCCMS can mimics the Baseline behavior very good. A frequency shift of about 0.12% is evident in the RCCMS predicted response. This is because of the simplifying assumption made on computation of the relative static modes.
In fact, restricting the relative static modes into the sector level, introduces more stiffness into the ROM. This becomes more evident for the bladed disk with a thinner disk component (like the considered case study) and near lower ND modeshapes.

Figure 4.11 shows nonlinear forced response levels of the mistuned bladed disk in microslip regime. RCCMS shows a good accuracy in predicting the nonlinear behavior of the system. A slight frequency shift is seen for higher values of N0/F0 ratio and near the resonance peaks.
The effect of preload-to-excitation ratio on the damping performance is evident in Figs. 4.11a and 4.11b. Near high amplitude resonance peaks, because of high relative

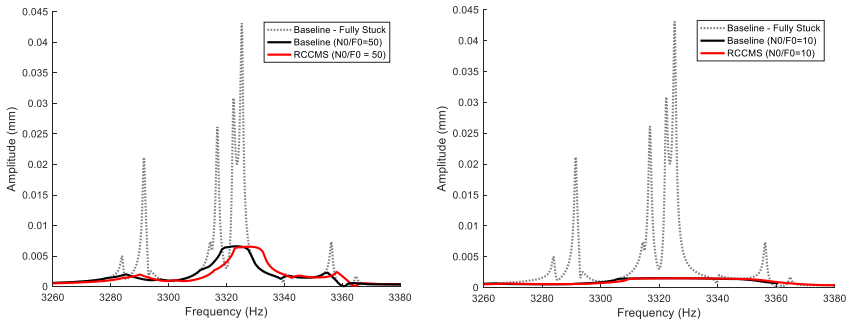

(a) (b)

Fig. 4.11 Nonlinear forced response levels of the mistuned bladed disk in microslip regime (EO 1 excitation).

displacements at contact nodes, contacts are in microslip and the friction damping decreases the response amplitude.
By further decreasing of N0/F0 ratios, contact states will change into gross slip and as a result, the amplitude of the vibration will be damped within the full frequency range.

The studied mock up bladed disk is composed of a rather thin disk component. It is also favorable to evaluate the performance of the RCCMS in predicting the forced response levels of systems with a stiffer disk component. To this end, the Young's modulus of the disk component was artificially doubled to resemble a stiffer disk component.

Figure 4.12 shows the forced response levels of the mistuned bladed disk with an artificially stiffer disk component. The system is under an EO 5 excitation. As it can be seen, RCCMS has predicted forced response levels with an excellent accuracy. In fact, restricting the relative constraint modes to sector levels, becomes a more valid assumption as the disk stiffness increases.

Figure 4.13 shows nonlinear forced response levels of the mistuned bladed disk under EO 5 excitation, for the system with the stiffened disk component. Results reveal the high accuracy of RCCMS in predicting the response of system in microslip. In fact, the simplifying assumption of using sector-level relative constraint modes for computation of RCCMS, will result in highly accurate ROMs for systems with a stiff disk component.

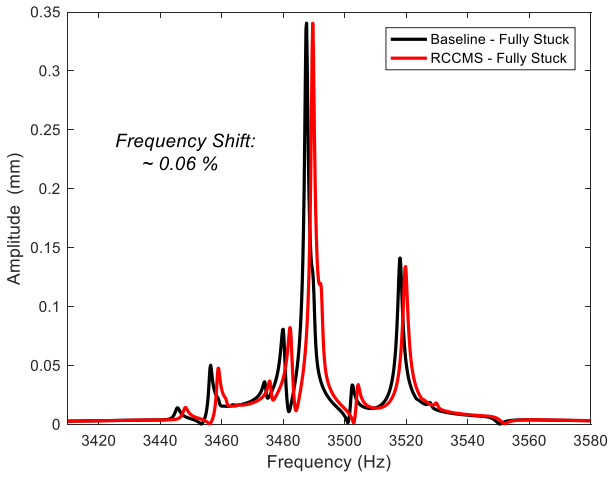

Fig. 4.12 Forced response level of the mistuned bladed disk with an artificially stiffer disk component, in fully stuck (EO 5 excitation).

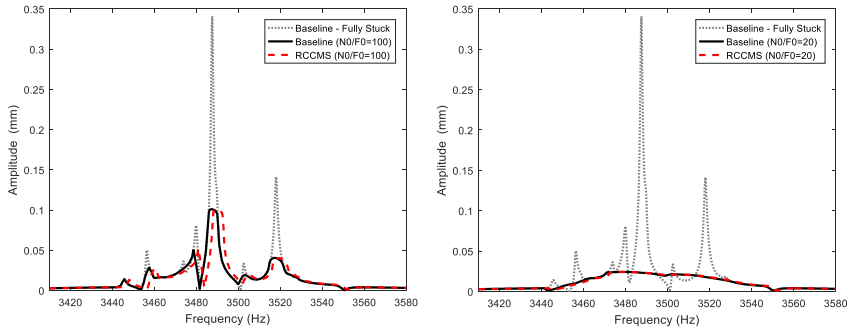

(a) (b)

Fig. 4.13 Nonlinear forced response levels of the mistuned bladed disk with an artificially stiffer disk component in microslip regime (EO 5 excitation).

4.3.2.2 Cyclic Static Modes Approach

In simulations in this section, friction contacts are modeled using the full-3D contact elements with variable normal load [55]. The contact stiffness is remained unchanged (equal to $k_t = 100\text{N}/\mu\text{m}$ in both normal and tangential directions).
Forced response calculations are performed in two different frequency ranges:

i. *low frequency range*: under EO 1 excitation and around the second modal family.

ii. *high frequency range*: under EO 5 excitation and around a densely packed modal families.

To better assess the effect of friction damping, a very slight stiffness-proportional damping with the coefficient of $\beta = 1.5\text{e-}8$ is used in forced response calculations. To model the effect of centrifugal forces, radial static loads (i.e. N0) are applied on forcing nodes at both leading and trailing edges of the blades. Note that here, N0 defines the static load applied on forcing nodes and not the pure normal preload at contact DOFs.

A nonlinear quasi-static analysis is carried out to compute the initial nonlinear static forces and equilibrium positions. To reduce the computational burden, multi-harmonic and coupled static/dynamic HBM simulations are carried out only once to evaluate their effect on forced response levels. The rest of simulations are performed based on a monoharmonic HBM method and by assuming that static equilibrium is not affected by dynamic response.

Forced response levels are presented in terms of the envelope of the maximum response (maximum response of all the blades at every excitation frequency) in tangential direction, calculated at response nodes at blade tips.

In this section, the mistuning is modeled as blade frequency mistuning (using Eq. (4.40)) unless otherwise stated.

Figure 4.14 shows the performance of the RCCMS in predicting the forced response of the mistuned bladed disk in stick condition. The forced response is calculated under EO 1 excitation and around the second modal family. As it is expected, the RCCMS prediction is in excellent accordance with ANSYS result, since the ROM is constructed based on the stick modeshapes. It should be noted that mistuned modeshapes are not pure nodal diameter modes and thus multiple resonance peaks are evident in forced response levels.

The performance of the RCCMS in accurately predicting the forced response levels of the mistuned bladed disk in a high modal density region is depicted in Fig. 4.15. The system in under EO 5 excitation. As it can be seen, RCCMS prediction is in an excellent accordance with ANSYS results. Figure 4.15 reveals that a highly accurate forced response prediction can be achieved using a highly compact ROM in RCCMS coordinates. Note that, the CMS-based baseline ROM contains 500

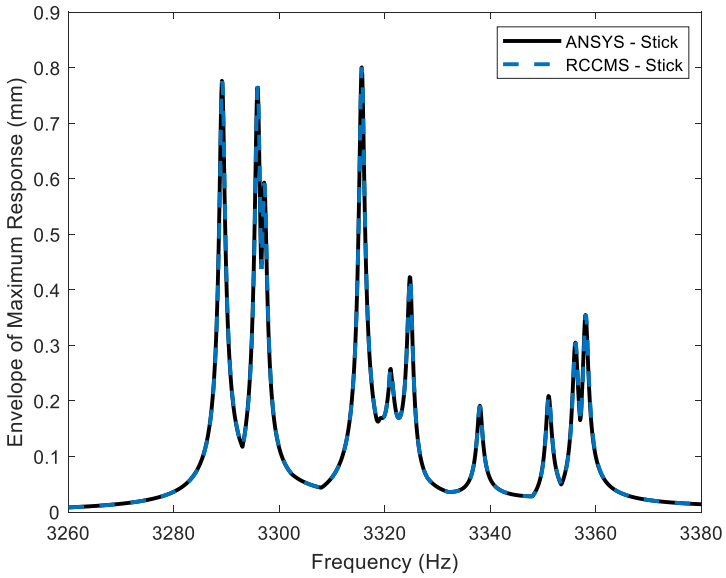

Fig. 4.14 Performance of the RCCMS in predicting the envelope of the maximum linear response of the mistuned bladed disk (with blade-frequency mistuning) under EO 1 excitation.

generalized coordinates only corresponding to the disk component to reach the same accuracy.

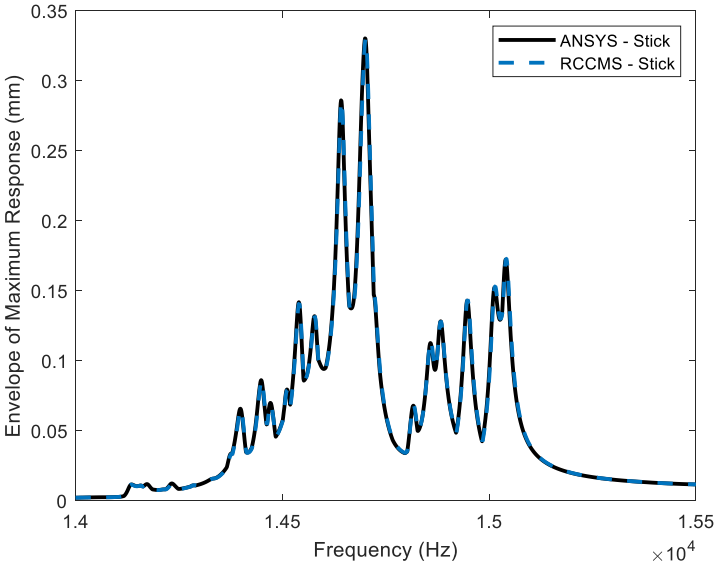

Fig. 4.15 Performance of the RCCMS in predicting the envelope of the maximum linear response of the mistuned bladed disk (with blade-frequency mistuning) under EO 5 excitation.

Figure 4.16 demonstrates the performance of the RCCMS in accurately predicting the envelope of the maximum nonlinear response of the mistuned blisk under EO 1. The predicted nonlinear response levels are in excellent accordance with the baseline results. It is evident that decreasing the preload-to-excitation ratio eventually decreases the vibration amplitude by introducing more friction damping at friction interfaces. The effect of mistuning on increasing the forced response level is depicted for the stick case. It can be seen that the mistuned response level has increased by the amplification factor of 28% with respect to the tuned response level.

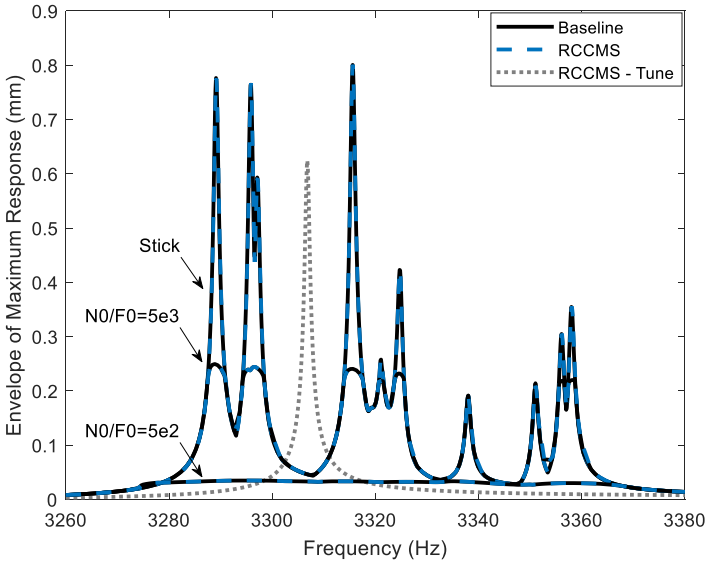

Fig. 4.16 Performance of the RCCMS in predicting the nonlinear response levels of the mistuned bladed disk (with blade-frequency mistuning) under EO 1 excitation.

Table 4.1 Computational costs of computing the nonlinear forced response levels in Fig. 4.16.

ROM	$N0/F0 = 5e3$	$N0/F0 = 5e2$
RCCMS	$0.47h$	$0.3h$
Baseline	$1h$	$0.7h$

The computational costs of computing the nonlinear forced response levels shown in Fig. 4.16 is reported in Table 4.1. Note that, a thorough efficiency evaluation, should take into account the offline costs of computing different ROMs. Another factor that highly affects the computational cost is the number of nonlinear DOFs

in the ROM. It should be noted that, the improvements achieved by the RCCMS ROM in halving the number of nonlinear contact DOFs, cannot be directly seen in Table 4.1. This is due to the fact that, for computing the forced response levels of the baseline ROM, only relative contact DOFs were solved in the iterative solver, although the absolute contact DOFs were retained in the ROM.

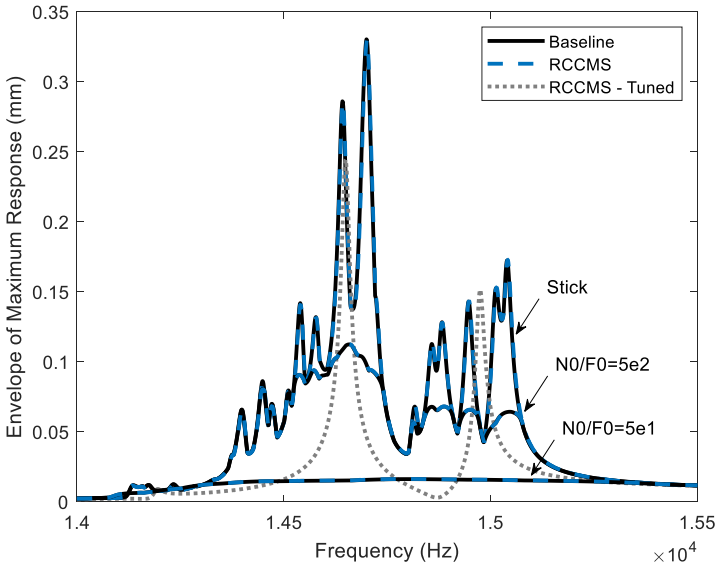

Fig. 4.17 Performance of the RCCMS in predicting the nonlinear response levels of the mistuned bladed disk (with blade-frequency mistuning) under EO 5 excitation.

The performance of the RCCMS in accurately predicting the envelope of the maximum nonlinear response of the mistuned blisk under EO 5 is depicted in Fig. 4.17. The ROM predictions are in an excellent accordance with the baseline results in this case as well. The effect of mistuning on the linear response level in terms of amplification factor is about 35% near the resonance peak at 14700 Hz and 14% near the resonance peak at 15000 Hz.

Table 4.2 Computational costs of computing the nonlinear forced response levels in Fig. 4.17.

ROM	$N0/F0 = 5e2$	$N0/F0 = 5e1$
RCCMS	$2.2h$	$1.4h$
Baseline	$6.2h$	$5.7h$

The computational costs of computing the nonlinear forced response levels shown in Fig. 4.17 is reported in Table 4.1.

One common practice in computing the forced response levels of bladed disks with friction joints is to compute the static preloads acting on contact DOFs in advance by assuming that the static equilibrium is not changed during the vibration. However, it is shown that this approach (the so-called uncoupled static/dynamic approach) can result in poor predictions [56, 57]. The so-called coupled static/dynamic approach in which static and dynamic balance equations are solved simultaneously, is the remedy to obtain accurate results.

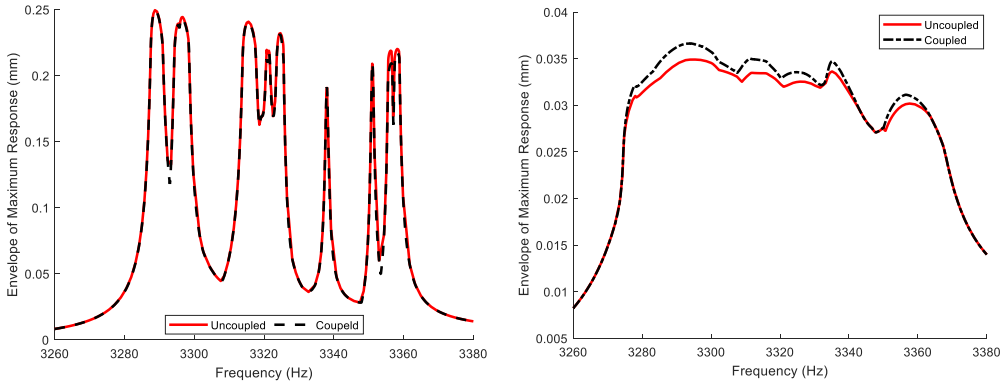

(a) (b)

Fig. 4.18 Nonlinear forced response levels: coupled versus uncoupled static/dynamic HBM. The mistuned bladed disk is under EO 1 excitation and (a) $N0/F0 = 5e3$, (b) $N0/F0 = 5e2$.

The effect of static/dynamic HBM approach on nonlinear forced response levels is examined Fig. 4.18. The mistuned balded disk is undergone EO 1 excitation and two different preload-to-excitation ratios. In Fig. 4.18a and for relatively higher preload values, the uncoupled approach prediction is in accordance with the coupled approach. Given the high preload values, friction contacts are mostly characterized by stick condition and static equilibrium (especially static preload) is not affected by the dynamic solutions. In contrast, in Fig. 4.18b and for relatively lower preload values, friction contacts experience considerable amount of slip. Note that in the coupled approach the Coulomb limit is implemented by taking into account both static and dynamic solutions. As a result, the static equilibrium is modified (relaxed) and overall less slip is introduced by the coupled approach.

The effect of including higher harmonics in HBM on nonlinear forced response levels is investigated in Fig. 4.19. It is evident that the monoharmonic HBM overes-

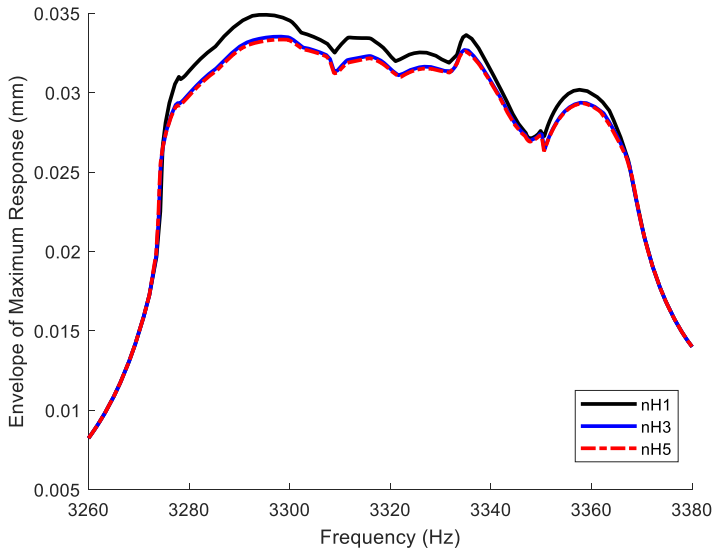

Fig. 4.19 Nonlinear forced response levels for different number of harmonics. The mistuned bladed disk is under EO 1 excitation and N0/F0 = 5e3.

timated the response and including more than 3 harmonics will not have a significant effect on predictions. In the MHBM simulations, the size of the unknowns vector corresponding to the nonlinear DOFs, varies from 3024 to 15120. Recall that, in the uncoupled static/dynamic HBM approach, size of the unknowns vector is equal to $2n_H N$ where n_H and N denote number of harmonics and nonlinear DOFs, respectively.

In the remainder the performance of the RCCMS is evaluated in accurately predicting the forced response levels of the mistuned bladed disk with *sector* frequency mistuning. The mistuned ROM is constructed based on the Eq. (4.40) and using the same mistuning pattern used in section 4.3.2, but present in both blade and disk partitions.

Figure 4.20 shows the envelope of the maximum linear response of the bladed disk with sector frequency mistuning. The bladed disk is in fully stick condition and is subjected to an EO 1 excitation around the second modal family. Overall, the RCCMS prediction is in a very good accordance with ANSYS result, although inclusion of sector frequency mistuning has slightly reduced the accuracy compared to the case of blade mistuning. Note that, the exact definition of the nonlinear partition of the mistuned stiffness matrix (see Eq. (4.32)) demands the inversion of

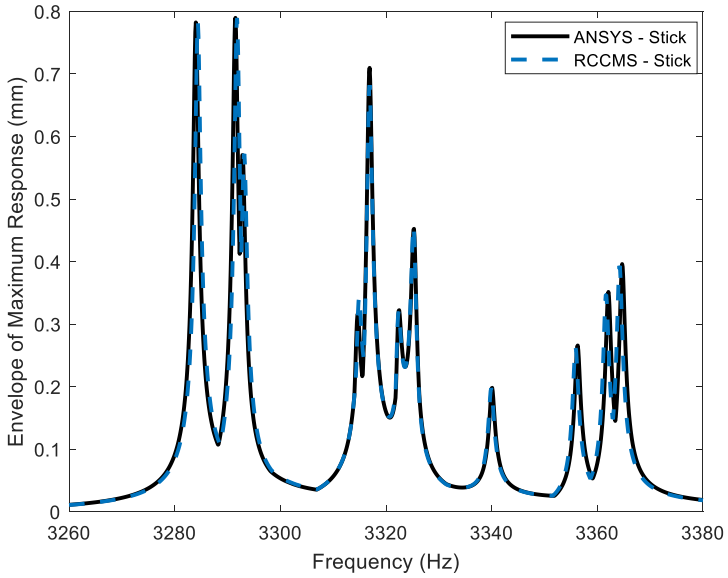

Fig. 4.20 Performance of the RCCMS in predicting the envelope of the maximum linear response of the mistuned bladed disk (with sector-frequency mistuning) under EO 1 excitation.

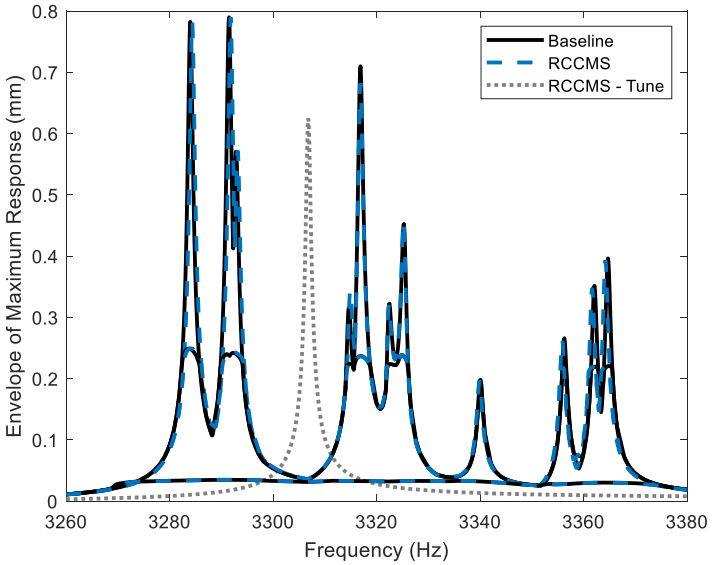

Fig. 4.21 Performance of the RCCMS in predicting the envelope of the maximum nonlinear response of the mistuned bladed disk (with sector-frequency mistuning) under EO 1 excitation.

the full mistuned stiffness matrix.

In the proposed assumption of *cyclic static modes* this partition is approximated

with the tuned Guyan stiffness matrix (see Eq. (4.40)). Thus, it can be expected, this simplifying assumption is more accurate in the case of blade frequency misuning, as only small partitions of the full stiffness matrix (i.e. corresponding to blade components) are varied from their tuned counterparts.

The performance of the RCCMS in predicting the nonlinear response levels of the bladed disk with sector frequency mistuning is depicted in Fig. 4.21. Similar to the linear stick case (i.e. Fig. 4.20) very good accuracy is observed in RCCMS predictions.

It is worth mentioning that, in the nonlinear regime, the overall accuracy is better compared to the linear stuck case. This is because the friction damping flattens the steep resonance curves and reduces the error especially at resonance peaks.

4.4 Conclusion

In this chapter, a new reduction order modeling technique was developed for nonlinear dynamics of bladed disks with (multiple) friction interfaces. The method is called Relative Cyclic Component Mode Synthesis (RCCMS), as it is actually a component-based reduction technique with a reduction basis composed of component modes of the cyclic model represented in relative coordinates of the contact surfaces. RCCMS results in an efficient and highly compact ROM suitable for nonlinear forced response analysis, as it is constructed based on system-level stick modeshapes and only includes relative DOFs between the contact nodes.

For the tuned bladed disks with friction contacts, a cyclic multiharmonic version of the RCCMS was developed which can include stick modeshapes of the system where contact DOFs are located at cyclic boundaries. This ROM was successfully tested on a cyclic bladed disk with friction damping at shroud interfaces and blade-root joints. The RCCMS formulation in general is applicable to all kinds of mistuning and any configuration of bladed disks, however, to reduce the computational burden, it was simplified and tailored for bladed disks with blade-root damping and small frequency mistuning.

The mistuned ROM in RCCMS coordinates benefits from different features, such as:

- Final ROM is obtained by performing sector-level calculations.
- Mistuning is introduced directly into the final ROM at sector-levels (i.e. both blade and disk).
- Physical DOFs corresponding to relative displacements of contact nodes are retained for highly efficient forced response calculations.
- Fully stick modeshapes are implemented in the reduction basis, with boundary conditions more similar to kinematics of friction interfaces.
- Highly compact ROM, due to the implementation of system-level modes, with no need of secondary reduction techniques.

The accuracy of the mistuned ROM in predicting the nonlinear forced response levels was evaluated on a bladed disk with blade-root friction damping. Numerical simulations revealed a good accuracy of the mistuned ROM constructed based on the *isolated static modes* assumption, especially for bladed disks with stiff disk component. An excellent accuracy was observed in the mistuned ROM constructed based on the *cyclic static modes* assumption, especially in the presence of blade frequency mistuning.

The research findings of this chapter are published in [58, 59].

Chapter 5

Experimental and Numerical Investigation of Mistuning Effects on Nonlinear Dynamics of a Bladed Disk with Underplatform Dampers

5.1 Introduction

As it was highlighted in the first chapter of the thesis (see section 1.1), underplatform dampers (UPDs) have attracted considerable attention in the past few years, as a source of dry friction damping in the bladed disks.

In [60–63] the effects of UPDs on nonlinear dynamics of a simplified two bladed structures were studies numerically and experimentally. There are few studies in the literature [41–43, 64], measuring/modeling the effects of UPDs on dynamics of a bladed disks with full set of dampers.

This might be due to the inherent complexity of performing such measurements (especially the nonlinear forced response measurements) which necessitates a carefully designed experimental set-up. The adopted modeling techniques (for predicting the nonlinear forced response levels) in previous studies is typically based on cyclic symmetry assumptions. In such strategies, the only possible comparison is between the numerical tuned response and the envelope of the experimental maximum re-

sponse.
It should be noted that neglecting the effects of mistuning on nonlinear forced response levels of such systems might not be a strong assumption, at least when:

- The response is highly characterized by slip condition. In this situation nonlinear friction damping flattens the response curve and reduces the scatter of the forced response.
- The effect of mistuning on vibration modes is small and small distortion is expected (e.g. at low nodal diameter modes). In this situation tuned vibration modes could predict the envelope of the response in an average sense.

Although neglecting the effect of mistuning can be conditionally successful [42, 43], its limitations and validity conditions are not known a priori. Accurate prediction of nonlinear forced response levels of mistuned bladed disks with friction interfaces is quite challenging due to the strong nonlinearities induced at contact surfaces and also rich dynamics of the underlying linear mistuned system itself. This highlights the need for a detailed experimental campaign.

To this end, a particular test rig, where both the excitation and the response measurement systems are non-contact is used here. In this way, excitation and response measurement systems do not interfere with the dynamics of the bladed disk and, therefore, they do not introduce additional mistuning.

The bladed disk carries UPDs that are in contact with the blade platforms. The produced excitation force on the blades is also large enough to trigger slipping between the UPDs and the platforms. The rig excitation system has, compared with similar test rigs in literature, the two features of being both non-contact and able to produce the same large force amplitude on each blade.

In literature in fact, in [64, 65] the rig produces a traveling wave but with piezo-actuators in contact with the blade. The same happens in [66], where they use shakers. In [67, 68] the rig is equipped with non-contact excitation force but based on acoustic speakers, which give very low excitation force amplitude.
This chapter is organized as follows: section 5.2 presents the campaign results of the mistuned bladed disks and section 5.3 describes the proposed numerical model accounting for mistuning effects.

5.2 Experiments

5.2.1 Motivation

In order to investigate the dynamics of mistuned bladed disk with UPDs a detailed experimental campaign is needed which can reproduce the well-known phenomena originated from nonlinear friction damping and mistuning. The experimental part of this research aims to provide such information. This has a great importance for validation purposes and also for better understanding the impact of key parameters on dynamics of a bladed disk with full set of dampers.

5.2.2 Set-Up Description

The experimental campaign is performed on the static test rig shown in Fig. 5.1a, the so-called Octopus rig. Octopus is purposely designed to investigate the nonlinear dynamics of bladed disks with UPDs or shrouds. The rig is thoroughly described in [69–72] and has been successfully used to evaluate the effects of cylindrical UPDs on the nonlinear forced response of a blisk (i.e. integrally bladed disk) [73].

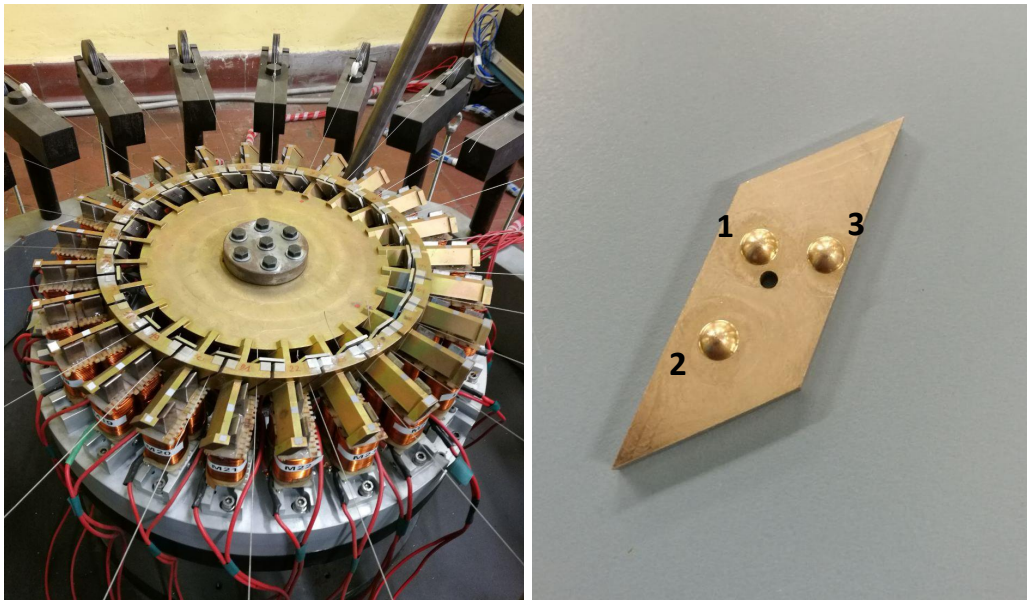

(a) (b)

Fig. 5.1 (a) Octopus test rig. (b) 3-point-contact damper.

Due to the presence of nonlinearities, the control of the excitation force is of primary importance since the force induces local displacements at the contact surfaces, which influence the forced response levels. The Octopus test rig is equipped with a travelling wave excitation system, based on electromagnets, which was designed to have the essential requirements for tests in presence of both mistuning and non-linarites due to friction. These requirements are:

- The absence of contact between blade and exciter.
- The same excitation force on each blade amplitude (with a difference from blade to blade within 2%) modulated with a given time lag which is determined by the engine order index.
- A high excitation force amplitude in order to produce slipping between the friction contacts.
- An accurate measurement of the force amplitude of the rotating force pattern.

The measurement system is a laser scanning vibrometer detecting the response in the out-of-plane (OOP) direction of the blades. The disk is a 24 bladed blisk with well-isolated modal families. A custom-made UPD with a 3-point-contact configuration (sphere-on-flat) was designed to be used in the experiments (Fig. 5.1b). The UPDs are kept in contact with the blade platforms using a static load applied to the center of the mass of the damper using a wire-pully system. The damper is in contact with two blade platforms simultaneously: one on the left-hand-side of the damper and through the spheres 1 and 2, and one on right-hand-side of the damper and through the sphere 3 (Fig. 5.1b).
The objective of the customized design is twofold:

- To highly localize the contact area (in contrast to line contact in wedge/cylindrical dampers). This might be helpful to reduce the uncertainties at contact interfaces.
- To reduce the effect of dampers on system modes of the underlying linear blisk. This might be helpful to assess the effect of dampers on structural mistuning.

5.2.3 Impact Testing

Impact testing was performed by exciting the blisk with an instrumented test hammer at a fixed point on the reference blade foot and the OOP response of all the 24 blade tips is measured using a laser scanning vibrometer. A high frequency resolution (i.e. 0.0195 Hz) was set in the analyzer to capture the frequency split of the mode pairs typical of mistuned blisks. Modal parameters were identified by performing a classical multi-FRF curve fitting technique [74]. An example of the performed modal identification process is shown in Fig. 5.2. Figure shows the measured point mobility FRF at blade 8 and the corresponding reconstructed numerical FRF.

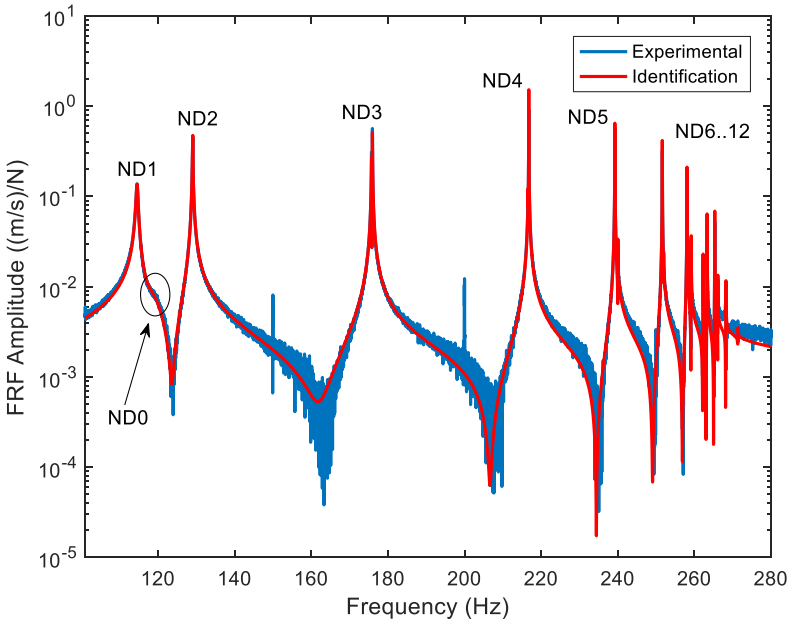

Fig. 5.2 Modal identification of the mistuned blisk without UPDs – point mobility FRF at blade 8.

The identified mistuned natural frequencies and the dominant nodal diameter (ND) modeshape associated with them are reported in Table 5.1. The modal parameters (i.e. mode shapes and natural frequencies) of the 1^{st} modal family are used (see section 5.3.2) to identify the sector mistuning.

Table 5.1 Identified mistuned natural frequencies of the 1^{st} bending family.

Identified Mistuned Natural Frequency (Hz)	Dominant ND Shape	Identified Mistuned Natural Frequency (Hz)	Dominant ND Shape
118.2852	ND0	251.9606	ND6
114.3370	ND1	258.0815	ND7
114.5294	ND1	259.1599	ND7
129.0931	ND2	262.2658	ND8
129.2549	ND2	263.3164	ND8
175.7519	ND3	265.0755	Not Clear
175.9512	ND3	265.3190	Not Clear
216.5900	ND4	266.1091	Not Clear
216.7793	ND4	268.1980	Not Clear
239.2471	ND5	268.2336	Not Clear
240.0025	ND5	269.2743	Not Clear
251.6163	ND6	271.3699	Not Clear

5.2.4 Linear Forced Response Levels

Linear forced response is first measured for the blisk without UPDs for two main reasons:

- To have a reference response to be used to estimate the UPD effect.
- To assess the capability of the modal model, identified by the impact testing, to predict the response of the blisk before UPDs are installed.

Accordingly, forced response measurement have been carried out around the resonance frequencies of the 1st bending family with the dominant ND2 and ND3 components as they are well-isolated and frequency splitting is evident at the corresponding peaks (see Fig. 5.2).

Figure 5.3 shows the frequency response functions of all the blades of the blisk without UPDs. The blisk is subjected to an engine order (EO)2 excitation of amplitude 0.1N. The frequency sweep is performed in the neighborhood of the identified mistuned modeshapes of the blisk showing a dominant ND2 component. The effect of mistuning and the frequency split on FRFs is evident in Fig. 5.3. Note

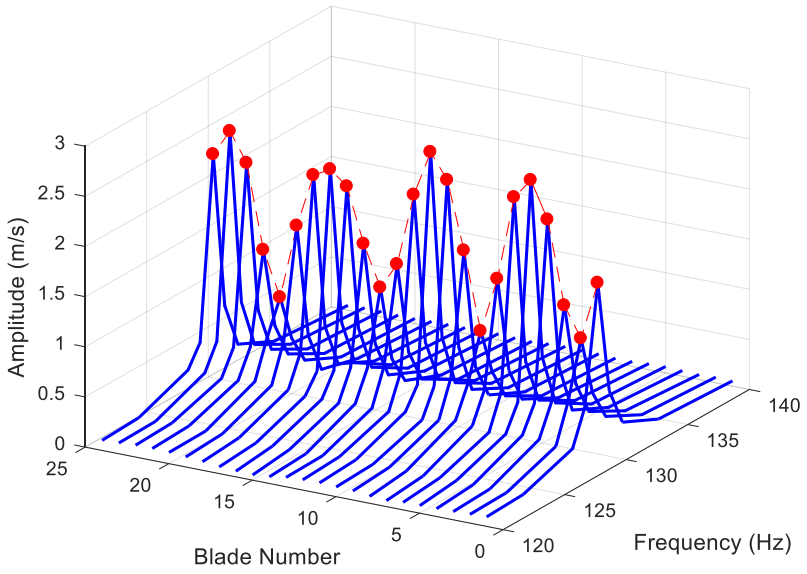

Fig. 5.3 Measured mistuned FRFs of the blisk without UPDs and under EO2 excitation of amplitude 0.1N. Dotted-dashed curve depicts the spatial wave (due to mistuning) at resonance frequency of 129.05Hz.

that, in the ideal tuned case the response of all blades at a given frequency - the so-called Operating Deflection Shape (ODS) - is the same and thus the envelope of the response peaks resembles a straight line. However, the depicted ODS in Fig. 5.3 (i.e. the dotted-dashed curve) is modulated and resembles a spatial wave with 4 maxima. The FRF modulation, typical of bladed disks with small mistuning and due to the frequency splitting of the mode pairs (see [71] for more discussion), was also observed in a rotating blisk using a Blade Tip Timing measurement system [75].

5.2.5 Nonlinear Forced Response Levels

Forced response measurements of the blisk with UPDs and under a traveling wave excitation is given here. This section investigates the effect of nonlinear damping and excitation level on the dynamic response of the mistuned blisk. Moreover, in the presence of dampers, a repeatability check is also performed. The purpose is to ensure a controlled and robust measurement procedure in the presence of UPDs. Note that in all the measurements in the presence of UPDs, a static preload of 9.81N is applied to the dampers using the cables and pulley system shown in Fig. 5.1a.

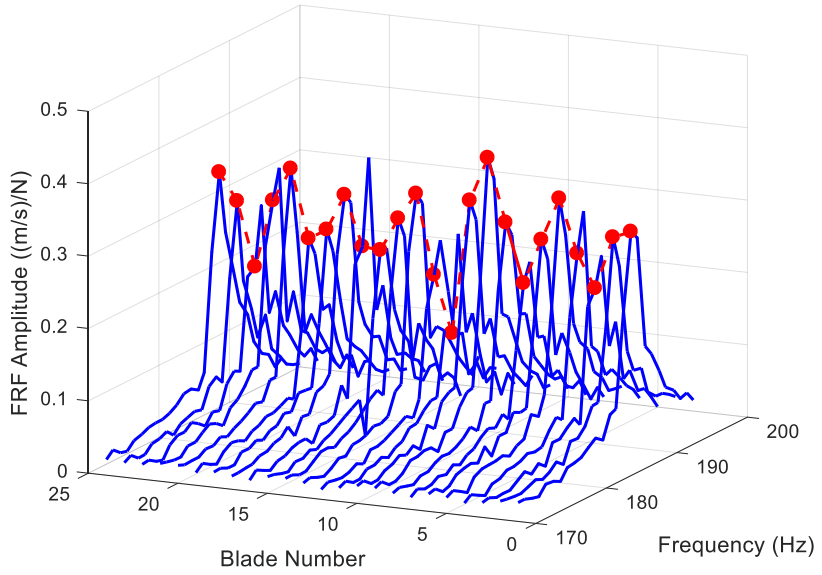

Fig. 5.4 Measured mistuned FRFs of the blisk with UPDs and under EO3 excitation of amplitude 0.1N. Dotted-dashed curve depicts the spatial wave (due to mistuning) at resonance frequency of 186.04Hz.

Figure 5.4 depicts measured mistuned FRFs of the blisk with UPDs and under EO3 excitation of amplitude 0.1N. The frequency sweep is performed in the neighborhood of the identified mistuned modeshapes of the blisk with a dominant ND3 component. A very small excitation level (0.1N) was applied in this set of experiments to resemble a stick-like condition at the friction interfaces. It can be seen that the modulation of FRFs (e.g. Dotted-dashed curve depicts at 186.04 Hz) is more distorted compared with ODS of the blisk with no UPDs, although a ND3 wave (6 maxima) can be recognized. This is due to the fact that the introduced coupling in the system (added by UPDs) has affected the energy distribution among the blades. It should be noted that in the case of ideal stick condition a strong coupling would be present in the system and less localization would be expected. However, due to the nature of the spherical contacts between the dampers and the blade platforms, full-stick conditions cannot be reached in practice and microslip (weaker coupling) will always occur In order to have consistent measurements in the presence of UPDs, each measurement is repeated three times.

The repeatability of the measurements for the blisk with UPDs and under EO3 excitation of amplitude 0.1N is depicted in Fig. 5.5. The mean, the maximum and the minimum of the FRFs of all blades is computed at each repetition and is shown in

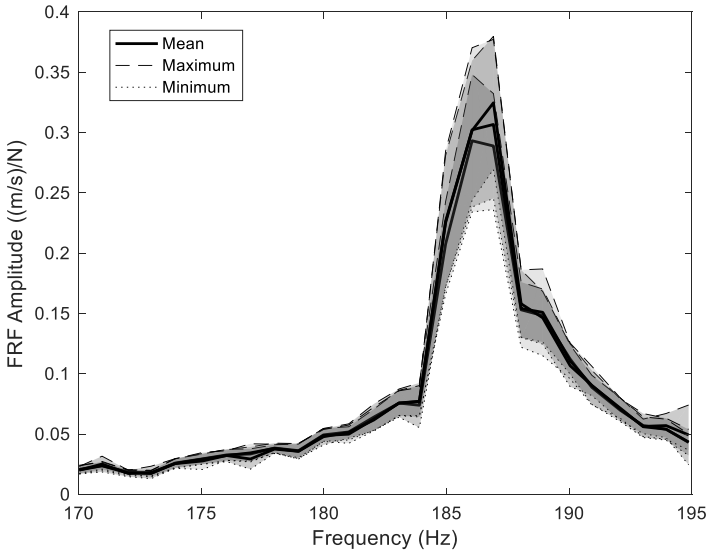

Fig. 5.5 Repeatability of the measured mistuned FRFs of the blisk with UPDs and under EO3 excitation of amplitude 0.1N. Solid, dashed and dotted curves depict the mean, maximum and minimum of the forced response levels at each repetition.

the figure. A very good agreement can be seen between the measurements especially farther from the resonance. The lower repeatability observed near the resonance is due to the variation of friction damping introduced by the UPDs. The effect of excitation level on forced response levels of the blisk with UPDs is shown in Fig. 5.6. The FRFs are measured under EO3 excitation and the forcing value is varied from 0.1N to 1N. Measurements are repeated for three times at each excitation level and mean and envelopes of FRFs are shown in the figure. It is evident that by increasing the excitation level FRF amplitude decreases constantly. In Fig. 5.6b the so-called performance curve (i.e. maximum resonance amplitude versus excitation level) is depicted. It can be seen that, by increasing the excitation level from 0.1N to 1N, the resonance amplitude is only increased 3 times due to the friction damping. Note that increase of excitation amplitude in the system has improved the repeatability of measurements. This behavior is in agreement with the contact model theories and with the experimental findings available in the literature about oscillating friction contacts.

As the vibration amplitude increases, the hysteresis cycle of the tangential contact force fully develops into a parallelogram, whose area (the dissipated energy) is mostly dependent on the friction coefficient, that experiment demonstrates to be a very robust

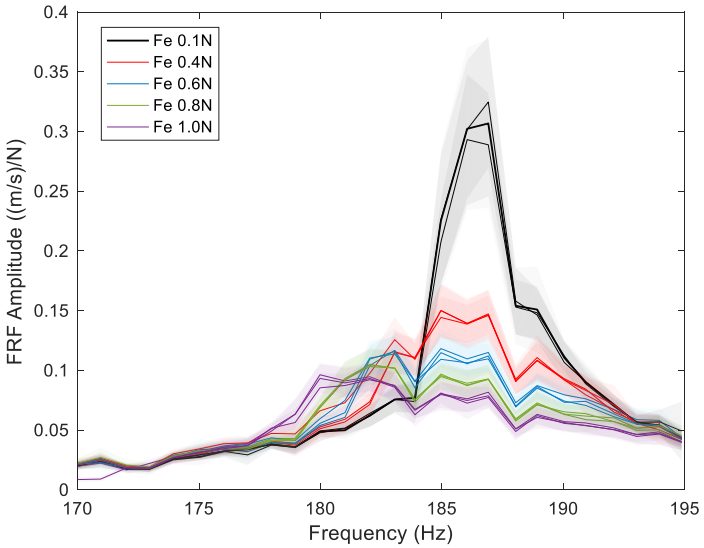

(a)

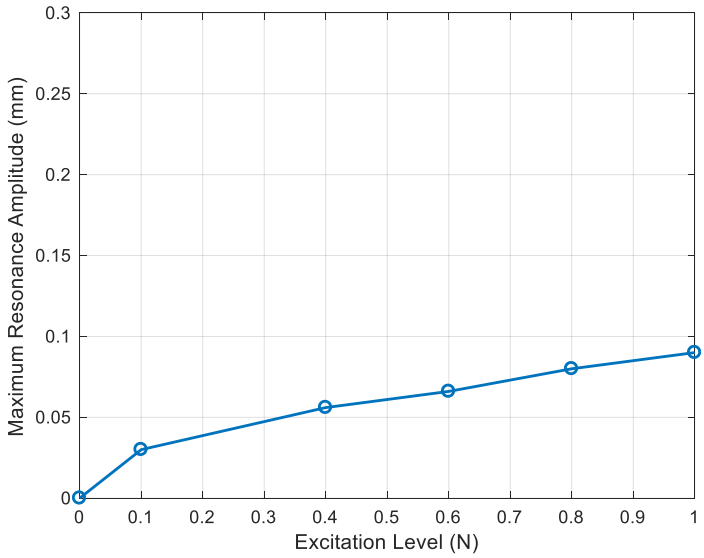

(b)

Fig. 5.6 (a) Effect of excitation level on measured mistuned FRFs of the blisk with UPDs under EO3 excitation. Measurements are repeated for 3 times at each excitation level. Solid lines depict the mean value of the forced response levels. (b) Maximum resonance amplitude versus excitation level (i.e. performance curve) computed using the average response of 3 repetitions.

parameter. On the contrary, as the vibration amplitude decreases, the hysteresis cycle of the tangential contact force tends to assume a more elongated shape, whose area

mostly depends on the tangential contact stiffness and on the microslip portion of the curve, more subjected to uncertainty and variability.

5.3 Modeling

In this section the development of the numerical model of the test rig and its validation is discussed. In the adopted methodology it is assumed that the mistuning introduced by dampers is negligible and hence the mistuning identification process is based on the modeshapes obtained from the hammer test (section 5.2.3) of the blisk without dampers. Note that one of the main purposes of designing a 3-point-contact damper is to localize the contact area and minimize the effect of the damper on system modes (compared with the wedge or cylindrical damper configurations). Being this the scenario at contact interfaces, it can be assumed that the effect of dampers on the mistuning pattern identified from the underlying linear system would be negligible. This assumption is verified later in section 5.3.4.
The adopted modeling procedure is summarized below:

- Construction of a high-fidelity FE model of the tuned blisk.
- Mistuning identification and FE model updating.
- Assessment of the numerical model in predicting the effect of mistuning on dynamics of the blisk.

5.3.1 FE Modeling

The FE model of the tuned blisk and its three first modal families is depicted in Fig. 5.7. Boundary conditions at the disk flange were carefully selected to have natural frequencies of the tuned model in agreement with the identified frequencies from the hammer test.

5.3.2 Mistuning Identification and Model Validation

Since the modal family of interest (i.e. 1^{st} bending) is well isolated from other families (as can be seen in Fig. 5.7b) the Fundamental Mistuning Model Identification

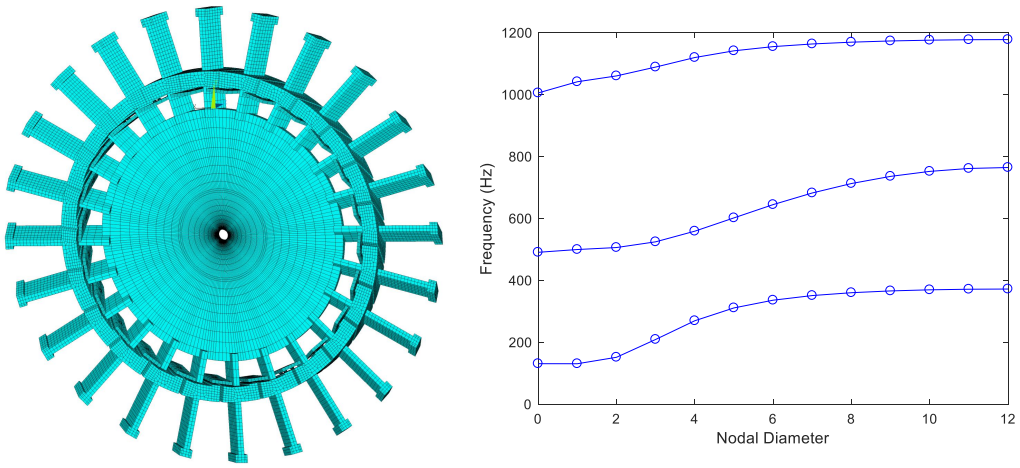

(a) (b)

Fig. 5.7 (a) FE Model of the blisk. (b) Natural frequency vs. nodal diameter plot of the tuned linear blisk (without UPDs).

(FMM ID) is employed to identify the mistuning of the blisk. The method was first introduced in [76] and is tailored for identifying the sector mistuning in integrally bladed disks. The performance of FMM ID in accurately predicting the mistuning pattern of blisks has been shown in many studies (e.g. [77–79]).
The both variants of the FMM ID (i.e. the so-called Basic and Advanced) were implemented and their performance in accurately predicting the identified natural frequencies and modeshapes is evaluated. Note that, the Basic ID uses the tentative tuned frequencies of the system as an input, although the Advanced ID is totally based on the measured data. A better correlation achieved by removing the modes with a considerable disk participation from the input parameters (namely the three first mistuned modes with dominant ND0 and ND1 components). Note that, FMM ID is based on the assumption that the strain energy of the modal family is mainly confined in the blades.
Figure 5.8 shows the identified sector mistuning using the FMM ID. Generally speaking, the mistuning identified by the Basic ID is slightly higher than that of the Advanced ID.

To evaluate the mistuning identification, the tuned FE model was updated with the mistuning patterns and its modal properties were compared with the identified frequencies and modeshapes. Figure 5.9 shows the eigenvalue deviation between the modeled and measured mistuned natural frequencies of the blisk without UPDs. Both

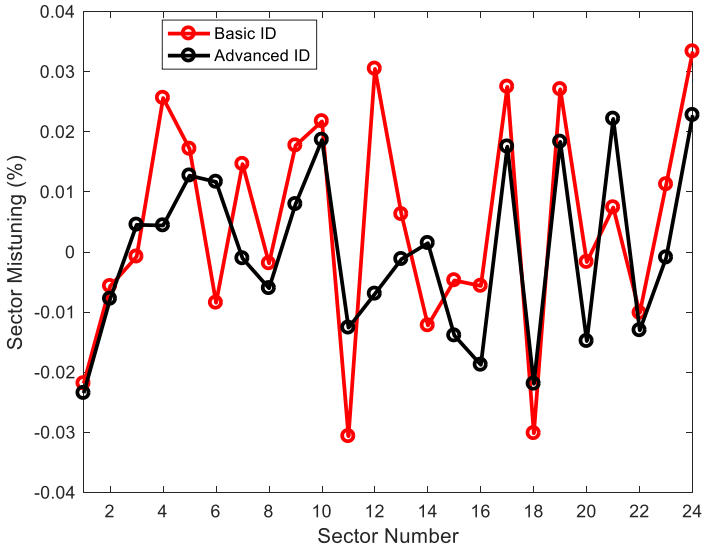

Fig. 5.8 Identified sector mistuning of the blisk without UPDs based on Basic and Advanced FMM ID.

Basic and Advanced IDs show a very good performance in modeling the mistuned natural frequencies, although Advanced ID predictions are generally better.

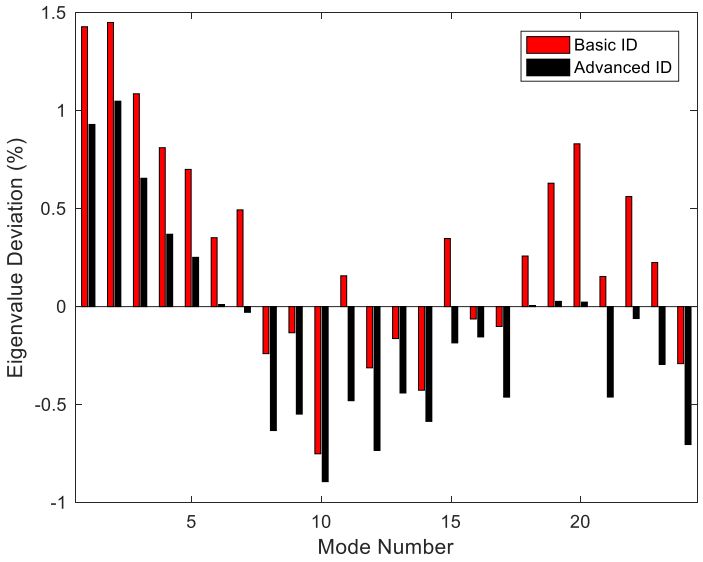

Fig. 5.9 Performance of the mistuned FE models in predicting the measured natural frequencies of the linear blisk without UPDs.

The maximum error (about 1.45%) was introduced by the Basic ID-based model, in predicting a ND1-like disk mode natural frequency. The Advanced ID shows an

excellent performance (error below 0.02%) in predicting the natural frequencies of the 6^{th} and 7^{th} modes with dominant ND3 component. Recall that forced response measurements were performed under a traveling wave excitation with ND3 shape.
To evaluate the numerical modeshapes (computed using the mistuned FE model) the Modal Assurance Criterion (MAC) is employed. Figure 5.10 shows the modal correlation between the experimental and Basic ID-based FE model, modeshapes.

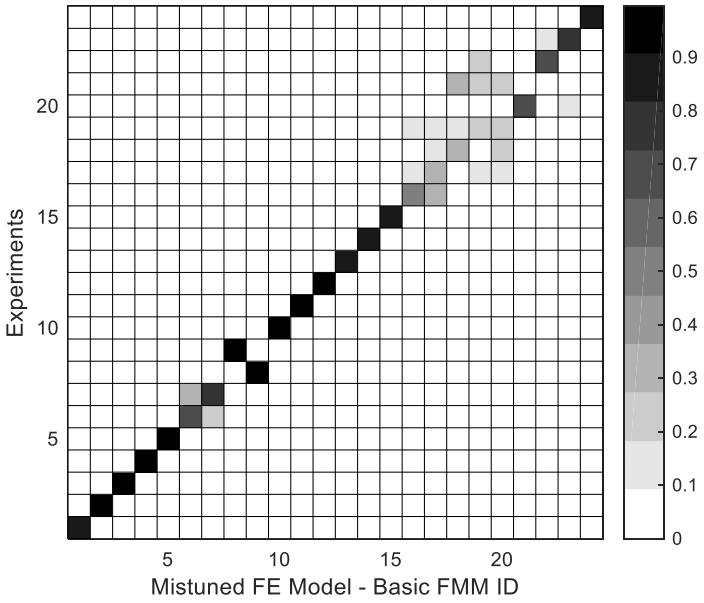

Fig. 5.10 Modal correlation between the experimental and FE model (based on the Basic FMM ID) modeshapes of the blisk without UPDs.

Overall, a good agreement can be seen between the numerical and experimental modes. The correlation decreases for the modes with dominant ND7 to ND9 components. These modes correspond to the high modal density region shown in Fig. 5.2. Note that the main focus of the identification is to get the best correlation near the modes with dominant ND3 components (i.e. 6^{th} and 7^{th} mistuned modes) in-line with the applied EO3 excitation in forced response measurements.
Figure 5.11 shows the modal correlation between the experimental and Advanced ID-based FE model modeshapes. An improved correlation can be seen between the experimental and numerical modeshapes, especially around the modes of interest (i.e. the 6^{th} and 7^{th} mistuned modes with the dominant ND3 component). The Advanced ID-based model will be used in the subsequent numerical simulations as it showed a better performance in predicting the modal properties of the mistuned blisk.

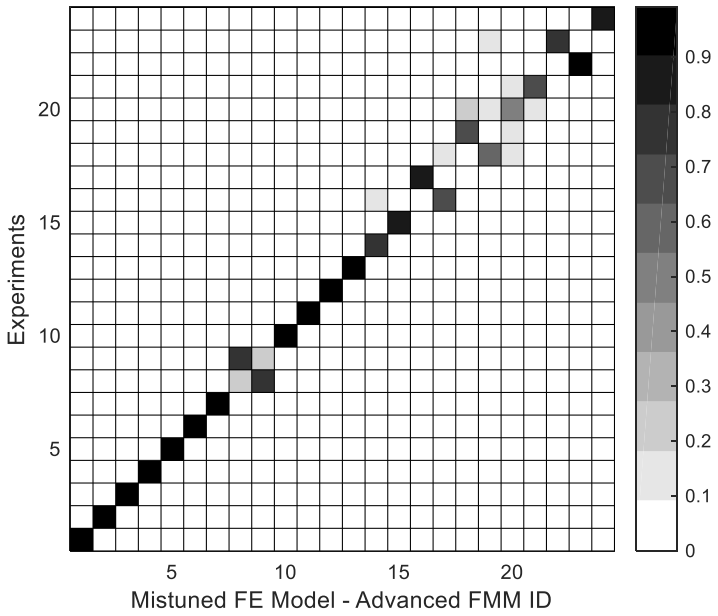

Fig. 5.11 Modal correlation between the experimental and FE model (based on the Advanced FMM ID) modeshapes of the blisk without UPDs.

As it was stated before, one purpose of designing 3-point-contact UPDs was to minimize the effect of dampers on the modeshapes of the blisk. A quantitative comparison is made between the numerical mistuned modeshapes (only 1^{st} family) of the blisk in the presence and the absence of UPDs. The blisk with UPDs is modeled as fully-stuck by merging the contact nodes between the dampers and blade platforms. Note that, the FE mesh of the dampers are not updated with the mistuning pattern as they were not present in identification.

Figure 5.12 shows the modal correlation between the numerical mistuned modeshapes of the blisk in free and fully stick condition. Higher modeshapes with dominant higher ND components are more affected by the presence of damper (the frequency deviation is also higher for these modes), since the inter-blade mechanical coupling provided by the dampers is higher and thus the effect of blade mistuning on the mode shapes changes significantly. On the contrary, the mistuned modes of interest (i.e. 6^{th} and 7^{th} modes) are less distorted by dampers and show about 71% correlation.

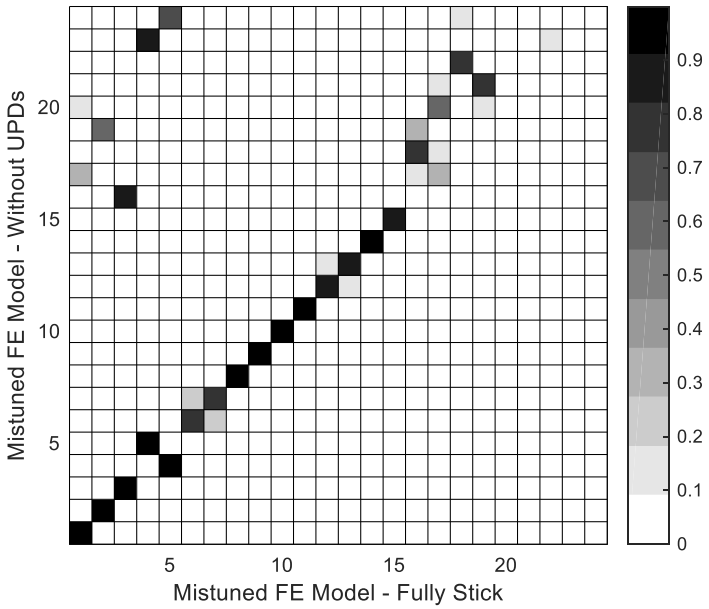

Fig. 5.12 Modal correlation between numerical mistuned mode-shapes of the blisk in free and fully stick condition.

5.3.3 Effect of Mistuning on FRFs in the Absence of UPDs

As it was observed in the experiments (sections 5.2.4 and 5.2.5), mistuning can significantly modulate the forced response levels. For instance, this can be recognized from the scatter of FRFs of the blades in Fig. 5.3. The blisk is under EO2 excitation and the ODS of the response is modulated by a fixed spatial wave whose number of lobes is twice the number of EO. The performance of the mistuned numerical model in predicting the FRF modulation can be used as a measure of acceptable simulation and mistuning identification. To this end, a hybrid numerical model is defined for the computation of the forced response levels as follows:

$$X = \sum_{n=1}^{N} \frac{\phi_n \phi_n^T}{\omega_n^2 - \omega^2 + i2\xi_n \omega_n \omega} F \tag{5.1}$$

where X denotes the displacement vector, ω_n denotes the nth angular natural frequency, ξ_n denotes the nth modal damping ratio, ϕ_n defines the nth vibration mode-shape, F defines the excitation force vector and ω denotes the angular excitation frequency. The advantage of the hybrid model is that both experimental and numerical data can be employed together. Accordingly, in Eq. (5.1) employed vibration

modes are computed based on the mistuned FE model, and damping ratios and resonance frequencies are defined based on the measurements. Linear forced response levels of the experimental measurements shown in Fig. 5.3 are computed here. To this end, 4^{th} and 5^{th} mistuned modes with dominant ND2 components were retained in the hybrid model and an EO2 wave excitation of amplitude 0.1N was defined similar to the experiment conditions.
Figure 5.13 shows the comparison between the numerical and experimental normalized ODSs of the blisk without UPDs at 129.25 (Hz) and under EO2 excitation of amplitude 0.1N. The predicted modulation of the blade FRFs (due to the mistuning) is in a very good agreement with the experiments. This can ensure the effectiveness of the mistuned model in predicting the dynamics of the linear blisk without UPDs.

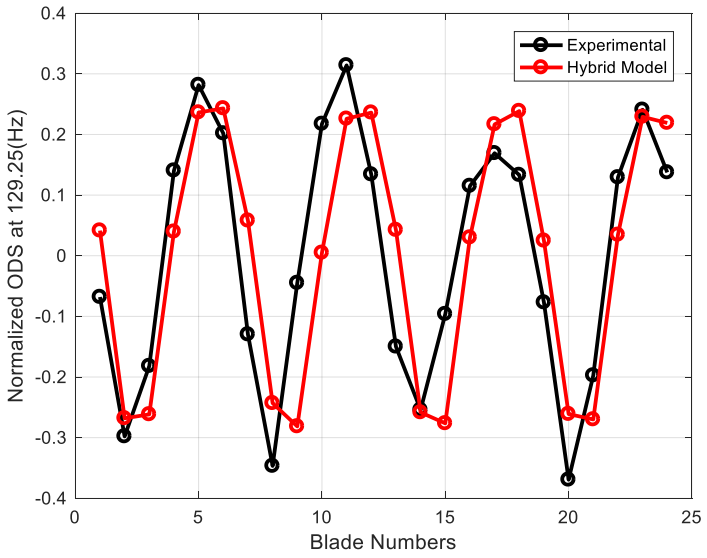

Fig. 5.13 Normalized ODS of the blisk without UPDs at 129.25 (Hz) and under EO2 excitation of amplitude 0.1N.

5.3.4 Effect of Mistuning on FRFs in the Presence of UPDs

In modeling the vibratory response of mistuned bladed disks with UPDs one principal and valid question to be answered is:

– Is the sector frequency mistuning pattern, identified by means of the linear blisk without dampers, still valid when dampers are included in the system?

The importance of the above question is that: if the effect of dampers on the blisk sector mistuning is negligible, one could use the mistuned vibration modes of the underlying linear system in further nonlinear simulations, otherwise, an identification scheme that takes account of the dampers should be selected over the proposed approach. Recall that one purpose of designing a 3-point-contact damper was to minimize the mistuning and uncertainty induced by dampers.
To assess the effect of dampers on the mistuning pattern of the underlying linear blisk, the hybrid model (Eq. (5.1)) is used to predict the modulation of the measured FRFs of the blisk with UPDs.
Note that in the presence of UPDs, especially at higher excitation levels, the proposed linear hybrid model is not capable of predicting forced response levels due to the presence of nonlinear friction damping in the system. Although at lower excitation levels, when the resonance frequency is already stabilized to the fully-stick value, the system behavior is relatively close to the linear stick condition and the induced friction damping might be negligible. This was observed numerically in [3] and [3] where nonlinear dynamics of mistuned bladed disks with shroud friction contacts were studied.
Accordingly forced response levels of the blisk with UPDs are computed for the experimental set-up shown in Fig. 5.5 where the measurement is performed under EO3 excitation of amplitude 0.1N, resembling a stick-like condition. Based on the measured FRFs (Fig. 5.5), it can be expected that this linearization assumption might be more reasonable around the second resonance peak (at 188.04 Hz) as the vibration amplitude and consequently the induced friction damping is lower compared to that of the first peak (at 186.04 Hz).

To compute the linearized FRFs, 6^{th} and 7^{th} modes (i.e. ND3-like modes) of the mistuned FE model in stick condition were employed in the hybrid model and an EO3 wave excitation of amplitude 0.1N was defined similar to the experiment conditions. The application of stick modeshapes in the hybrid model is in accordance with the assumed contact state of the test set-up and is in-line with observations in Fig. 5.12.
Figure 5.14 shows the comparison between the numerical and experimental normalized ODSs of the blisk with UPDs at 186.04 (Hz) and under EO3 excitation of amplitude 0.1N. The measured ODS is depicted in terms of the mean and standard deviation of all three repetitions.
It can be seen that the linearization assumption fails to accurately predict the modu-

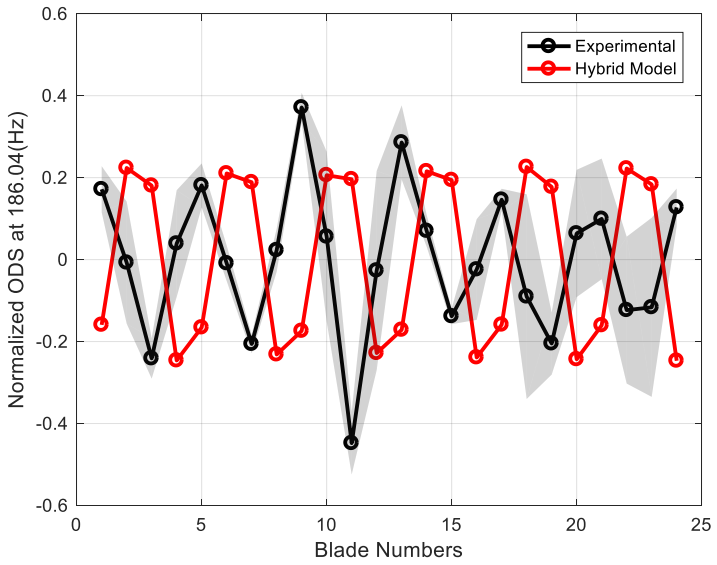

Fig. 5.14 Normalized ODS of the blisk with UPDs at 186.04 (Hz) and under EO3 excitation of amplitude 0.1N.

lation of the mistuned FRFs. This is due to the fact that at this resonance frequency the induced friction damping is not negligible and the nonlinear coupling introduced by the dampers changes the energy distribution among the blades. A slight vibration localization is evident around the 11^{th} blade that might be due to the weak coupling in the presence of microslip. In contrast the linearized model resembles the stick condition (rather strong coupling) and shows a uniform vibration distribution among the blades.

Figure 5.15 shows the comparison between the numerical and experimental normalized ODSs of the blisk with UPDs at 188.04 (Hz) and under EO3 excitation of amplitude 0.1N. The measured ODS is depicted in terms of the mean and standard deviation of all three repetitions. At this resonance frequency the linearized model is able to predict the clocking of the mode shape and the relative phase of the blades with respect to the 1^{st} one (either in-phase or out-of-phase), although underestimating some peaks localized in specific blades.
This is due to the fact that the response ODS at this frequency (around the second peak in Fig. 5.5 vibrates with lower amplitude and neglecting the friction damping is not a very strong assumption in this case.
It was observed that the proposed mistuned model (in which the mistuning was identified from the linear blisk without dampers) can predict the dynamics of the

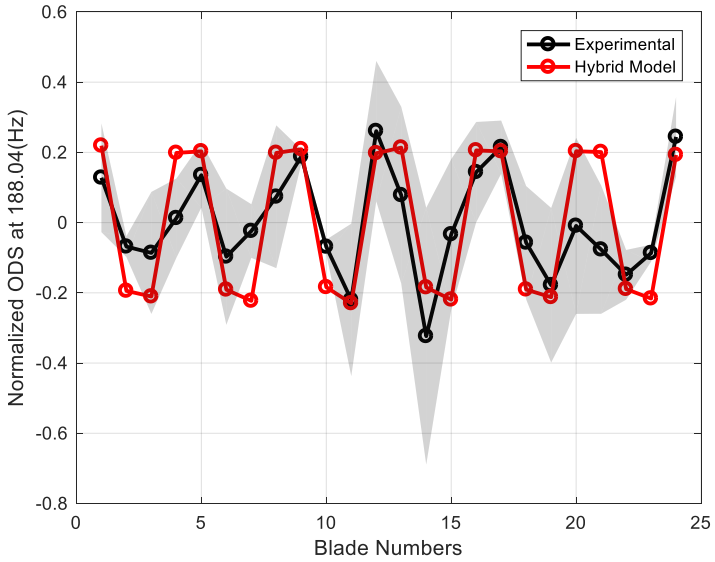

Fig. 5.15 Normalized ODS of the blisk with UPDs at 188.04 (Hz) and under EO3 excitation of amplitude 0.1N.

blisk with UPDs in linearized stick regime. Thus, it can be concluded that adding the dampers does not influence the structural mistuning of the system. This allows to use the computed mistuned modes of the linear system as a reduction basis in advanced nonlinear calculations.

5.4 Conclusion

In this chapter, experimental and numerical characterization of vibratory response of a mistuned blisk (i.e. integrally bladed disk) with UPDs was presented. The 1^{st} bending family of the linear mistuned blisk without UPDs was identified and the frequency splitting of the mode pairs was observed. The measured modal properties were used to identify the structural mistuning of the linear blisk. A careful mistuning identification carried out using the FMM ID and the effectiveness of the identified patterns in modeling the system modal properties was evaluated.

Forced response investigations were performed on the mistuned blisk in the presence and absence of UPDs. A noncontact system for applying a travelling wave excitation and a laser scanning vibrometer for measuring the response at the blade tips was employed to avoid affecting the system response.

The effect of UPDs on dynamic response of the mistuned blisk was investigated. A

very good repeatability observed in measuring the nonlinear forced response levels in the presence of UPDs.
A linearized hybrid model was proposed to model the effect of mistuning on forced response levels. The model successfully predicted the modulation of linear mistuned FRFs due to the mistuning.
The linearized model was also able to predict the modulation of nonlinear mistuned FRFs in stick condition (when nonlinear friction damping is negligible) with a good accuracy.
This shows that adding the dampers did not influence the structural mistuning of the system which is in accordance with the initial objective of designing a 3-point-contact damper. Based on this observation one may use the same mistuning pattern identified from the linear blisk to build a mistuned numerical model for nonlinear dynamics of the mistuned blisk with UPDs.
As one of the objectives of this research is to provide an experimental benchmark for nonlinear dynamics of a mistuned blisk with underplatform dampers, the FE model and raw experimental data will be available to public, one year after the publication of this paper. The benchmark might be helpful for researchers to test and validate numerical models of mistuned bladed disks with friction contacts.

The research findings of this chapter are accepted for publication in the journal Engineering for Gas Turbines and Power.

References

[1] M. Krack, L. Salles, and F. Thouverez, "Vibration Prediction of Bladed Disks Coupled by Friction Joints," *Archives of Computational Methods in Engineering*, 2016.

[2] A. V. Srinivasan, "Flutter and Resonant Vibration Characteristics of Engine Blades," *Journal of Engineering for Gas Turbines and Power*, vol. 119, no. 4, p. 742, 1997.

[3] E. Seinturier, "Forced response computation for bladed disks industrial practices and advanced methods," *LECTURE SERIES-VON KARMAN INSTITUTE FOR FLUID DYNAMICS*, vol. 2, p. 5, 2007.

[4] S. Zucca, C. M. Firrone, and M. M. Gola, "Numerical assessment of friction damping at turbine blade root joints by simultaneous calculation of the static and dynamic contact loads," *Nonlinear Dynamics*, vol. 67, no. 3, pp. 1943–1955, 2012.

[5] D. Charleux, C. Gibert, F. Thouverez, and J. Dupeux, "Numerical and experimental study of friction damping blade attachments of rotating bladed disks," *International Journal of Rotating Machinery*, vol. 2006, pp. 1–13, 2006.

[6] F. Alinejad, D. Botto, M. Gola, and A. Bessone, "Reduction of the design space to optimize blade fir-tree attachments," vol. Volume 7A: Structures and Dynamics, 06 2018. V07AT30A003.

[7] J. Szwedowicz, S. Slowik, A. Mahler, and C. J. Hulme, "Nonlinear Dynamic Analyses of a Gas Turbine Blade for Attainment of Reliable Shroud Coupling," *Volume 4: Turbo Expo 2005*, pp. 553–561, 2005.

[8] J. Szwedowicz, R. Visser, W. Sextro, and P. A. Masserey, "On Nonlinear Forced Vibration of Shrouded Turbine Blades," *Journal of Turbomachinery*, vol. 130, no. 1, p. 011002, 2008.

[9] M. M. Gola and C. Gastaldi, "The Present State of "Solid" under-Platform Damper Mechanics at AERMEC-POLITO," vol. 302, no. 1, p. 12017, 2018.

[10] L. Panning, K. Popp, W. Sextro, F. Gotting, A. Kayser, and I. Wolter, "Asymmetrical underplatform dampers in gas turbine bladings: theory and application," pp. 269–280, 2004.

[11] E. Cigeroglu, N. An, and C.-H. Menq, "Wedge damper modeling and forced response prediction of frictionally constrained blades," pp. 519–528, 2007.

[12] E. Cigeroglu, N. An, and C.-H. Menq, "Forced response prediction of constrained and unconstrained structures coupled through frictional contacts," *Journal of Engineering for Gas Turbines and Power*, vol. 131, no. 2, 2009.

[13] E. Ciğeroğlu and H. N. Özgüven, "Nonlinear vibration analysis of bladed disks with dry friction dampers," *Journal of Sound and Vibration*, vol. 295, no. 3-5, pp. 1028–1043, 2006.

[14] E. P. Petrov, "A Method for Use of Cyclic Symmetry Properties in Analysis of Nonlinear Multiharmonic Vibrations of Bladed Disks," *Journal of Turbomachinery*, vol. 126, no. 1, p. 175, 2004.

[15] C. Siewert, L. Panning, J. Wallaschek, and C. Richter, "Multiharmonic Forced Response Analysis of a Turbine Blading Coupled by Nonlinear Contact Forces," *Journal of Engineering for Gas Turbines and Power*, vol. 132, no. 8, p. 082501, 2010.

[16] M. P. Castanier and C. Pierre, "Modeling and analysis of mistuned bladed disk vibration: current status and emerging directions," *Journal of Propulsion and Power*, vol. 22, no. 2, pp. 384–396, 2006.

[17] S.-H. Lim, R. Bladh, M. P. Castanier, and C. Pierre, "Compact, generalized component mode mistuning representation for modeling bladed disk vibration," *AIAA journal*, vol. 45, no. 9, pp. 2285–2298, 2007.

[18] C. Siewert and H. Stuer, "Forced Response Analysis of Mistuned Turbine Bladings," vol. Volume 6: Structures and Dynamics, Parts A and B, pp. 1145–1156, 06 2010.

[19] M. Mitra, S. Zucca, and B. I. Epureanu, "Effects of Contact Mistuning on Shrouded Blisk Dynamics," vol. Volume 7A: Structures and Dynamics, 06 2016. V07AT32A026.

[20] A. Madden, B. I. Epureanu, and S. Filippi, "Reduced-order modeling approach for blisks with large mass, stiffness, and geometric mistuning," *AIAA journal*, vol. 50, no. 2, pp. 366–374, 2012.

[21] R. Bladh, C. Pierre, M. P. Castanier, and M. J. Kruse, "Dynamic Response Predictions for a Mistuned Industrial Turbomachinery Rotor Using Reduced-Order Modeling," *Journal of Engineering for Gas Turbines and Power*, vol. 124, no. 2, p. 311, 2002.

[22] A. Cardona, T. Coune, A. Lerusse, and M. Geradin, "Multiharmonic method for non-linear vibration analysis," *International Journal for Numerical Methods in Engineering*, vol. 37, no. 9, pp. 1593–1608, 1994.

[23] D. D. Klerk, D. J. Rixen, and S. N. Voormeeren, "General Framework for Dynamic Substructuring: History, Review and Classification of Techniques," *AIAA Journal*, vol. 46, no. 5, pp. 1169–1181, 2008.

[24] J. Yuan, F. Scarpa, G. Allegri, B. Titurus, S. Patsias, and R. Rajasekaran, "Efficient computational techniques for mistuning analysis of bladed discs: A review," *Mechanical Systems and Signal Processing*, vol. 87, pp. 71–90, 2017.

[25] R. Bladh, M. P. Castanier, and C. Pierre, "Component-Mode-Based Reduced Order Modeling Techniques for Mistuned Bladed Disks—Part I: Theoretical Models," *Journal of Engineering for Gas Turbines and Power*, vol. 123, no. 1, p. 89, 2001.

[26] A. Hohl, C. Siewert, L. Panning, and J. Wallaschek, "A substructure based reduced order model for mistuned bladed disks," pp. 899–906, 2009.

[27] M.-T. Yang and J. H. Griffin, "A Reduced-Order Model of Mistuning Using a Subset of Nominal System Modes," *Journal of Engineering for Gas Turbines and Power*, vol. 123, no. 4, p. 893, 2001.

[28] C. Fitzner, B. I. Epureanu, and S. Filippi, "Nodal energy weighted transformation: A mistuning projection and its application to FLADE™turbines," *Mechanical Systems and Signal Processing*, vol. 42, no. 1-2, pp. 167–180, 2014.

[29] M. P. Castanier, Y.-c. Tan, and C. Pierre, "Characteristic Constraint Modes for Component Mode Synthesis," vol. 39, no. 6, 2001.

[30] L. Carassale and M. Maurici, "Interface Reduction in Craig–Bampton Component Mode Synthesis by Orthogonal Polynomial Series," *Journal of Engineering for Gas Turbines and Power*, vol. 140, 12 2017. 052504.

[31] B. J. Olson, S. W. Shaw, C. Pierre, R. G. Parker, and P. J. Davis, "Circulant Matrices and Their Application to Vibration Analysis," vol. 66, no. July 2014, 2016.

[32] D. M. Feiner and J. Griffin, "A fundamental model of mistuning for a single family of modes," *J. Turbomach.*, vol. 124, no. 4, pp. 597–605, 2002.

[33] P. Vargiu, C. M. Firrone, S. Zucca, and M. M. Gola, "A reduced order model based on sector mistuning for the dynamic analysis of mistuned bladed disks," *International Journal of Mechanical Sciences*, vol. 53, no. 8, pp. 639–646, 2011.

[34] M. Mitra and B. I. Epureanu, "Dynamic Modeling and Projection-Based Reduction Methods for Bladed Disks with Nonlinear Frictional and Intermittent Contact Interfaces," *Applied Mechanics Reviews*, vol. 71, no. 5, pp. 1–22, 2019.

[35] W. Tang, S. Baek, and B. I. Epureanu, "Reduced-Order Models for Blisks With Small and Large Mistuning and Friction Dampers," *Journal of Engineering for Gas Turbines and Power*, vol. 139, no. 1, p. 012507, 2016.

[36] W. Tang, B. I. Epureanu, and S. Filippi, "Models for blisks with large blends and small mistuning," *Mechanical Systems and Signal Processing*, vol. 87, no. July 2016, pp. 161–179, 2017.

[37] W. Tang and B. I. Epureanu, "Nonlinear dynamics of mistuned bladed disks with ring dampers," *International Journal of Non-Linear Mechanics*, vol. 97, no. September 2016, pp. 30–40, 2017.

[38] R. Craig and M. Bampton, "Coupling of substructures for dynamic analyses," *AIAA journal*, vol. 6, no. 7, pp. 1313–1319, 1968.

[39] C. Joannin, F. Thouverez, and B. Chouvion, "Reduced-order modelling using nonlinear modes and triple nonlinear modal synthesis," *Computers and Structures*, vol. 203, pp. 18–33, 2018.

[40] M. Mitra, S. Zucca, and B. I. Epureanu, "Adaptive Microslip Projection for Reduction of Frictional and Contact Nonlinearities in Shrouded Blisks," *Journal of Computational and Nonlinear Dynamics*, vol. 11, no. 4, p. 041016, 2016.

[41] S. Zucca, D. Di Maio, and D. J. Ewins, "Measuring the performance of underplatform dampers for turbine blades by rotating laser Doppler vibrometer," *Mechanical Systems and Signal Processing*, vol. 32, pp. 269–281, 2012.

[42] C. Gastaldi, E. Grossi, T. M. Berruti, *et al.*, "On the choice of contact parameters for the forced response calculation of a bladed disk with underplatform dampers," *Journal of the Global Power and Propulsion Society*, vol. 1, p. 5D19RH, 2017.

[43] I. A. Sever, E. P. Petrov, and D. J. Ewins, "Experimental and numerical investigation of rotating bladed disk forced response using underplatform friction dampers," *Journal of Engineering for Gas Turbines and Power*, vol. 130, no. 4, 2008.

[44] W. BENFIELD and R. HRUDA, "Vibration Analysis of Structures by Component Mode Substitution," *AIAA Journal*, vol. 9, no. 7, pp. 1255–1261, 1971.

[45] T. M. Cameron and J. H. Griffin, "An Alternating Frequency/Time Domain Method for Calculating the Steady-State Response of Nonlinear Dynamic Systems," *Journal of Applied Mechanics*, vol. 56, no. 1, p. 149, 1989.

[46] C. M. Firrone and S. Zucca, "Modelling friction contacts in structural dynamics and its application to turbine bladed disks," in *Numerical Analysis-Theory and Application*, InTech, 2011.

[47] S. M. Pourkiaee and S. Zucca, "A Reduced Order Model for Nonlinear Dynamics of Mistuned Bladed Disks With Shroud Friction Contacts," *Journal of Engineering for Gas Turbines and Power*, vol. 141, no. 1, p. 11031, 2019.

[48] A. Majed, E. E. Henkel, and C. Wilson, "Improved method of mixed-boundary component-mode representation for structural dynamic analysis," *Journal of spacecraft and rockets*, vol. 42, no. 5, pp. 825–831, 2005.

[49] S. Rubin, "Improved component-mode representation for structural dynamic analysis," *AIAA journal*, vol. 13, no. 8, pp. 995–1006, 1975.

[50] S. M. Pourkiaee and S. Zucca, "Mixed-boundary component mode substitution for nonlinear dynamics of mistuned shrouded bladed disks," *AIAA Journal*, pp. 1–13, 2019.

[51] V. Kharyton, J.-P. Laine, F. Thouverez, and O. Kucher, "Cracked blade detection from bladed disk forced response," pp. 353–362, 2009.

[52] J. Gross, P. Buhl, U. Weber, X. Schuler, and M. Krack, "Effect of creep on the nonlinear vibration characteristics of blades with interlocked shrouds," *International Journal of Non-Linear Mechanics*, vol. 99, no. May 2017, pp. 240–246, 2018.

[53] O. Marinescu, B. I. Epureanu, and M. Banu, "Reduced order models of mistuned cracked bladed disks," *Journal of Vibration and Acoustics*, vol. 133, no. 5, 2011.

[54] Y. Gan, J. L. Mayer, K. X. D. Souza, and B. I. Epureanu, "A Mode-Accelerated XXr (MAX) method for complex structures with large blends," *Mechanical Systems and Signal Processing*, vol. 93, pp. 1–15, 2017.

[55] M. Afzal, I. Lopez, and L. Kari, "An analytical calculation of the Jacobian matrix for 3D friction contact model applied to turbine blade shroud contact," *Computers and Structures*, vol. 177, pp. 204–217, 2016.

[56] C. M. Firrone, S. Zucca, and M. M. Gola, "The effect of underplatform dampers on the forced response of bladed disks by a coupled static / dynamic harmonic balance method," *International Journal of Non-Linear Mechanics*, vol. 46, no. 2, pp. 363–375, 2011.

[57] S. Zucca and C. Maria, "Nonlinear dynamics of mechanical systems with friction contacts : Coupled static and dynamic Multi-Harmonic Balance Method and multiple solutions," *Journal of Sound and Vibration*, vol. 333, no. 3, pp. 916–926, 2014.

[58] S. Mehrdad Pourkiaee, S. Zucca, and R. Parker, "Relative cyclic component mode synthesis and its application to nonlinear vibration analysis of mistuned bladed disks with friction joints," *Proceedings of ISMA 2018 - International Conference on Noise and Vibration Engineering and USD 2018 - International Conference on Uncertainty in Structural Dynamics*, pp. 1965–1978, 2018. cited By 1.

[59] S. Mehrdad Pourkiaee and S. Zucca, "Nonlinear forced response analysis of bladed disks using a relative cyclic component mode synthesis approach," *Proceedings of the 26th International Congress on Sound and Vibration, ICSV 2019*, 2019. cited By 0.

[60] C. M. Firrone, "Measurement of the kinematics of two underplatform dampers with different geometry and comparison with numerical simulation," *Journal of sound and vibration*, vol. 323, no. 1-2, pp. 313–333, 2009.

[61] D. Botto, C. Gastadi, M. M. Gola, and M. Umer, "An experimental investigation of the dynamics of a blade with two under-platform dampers," *Journal of Engineering for Gas Turbines and Power*, vol. 140, no. 3, 2018.

[62] A. Bessone, F. Toso, and T. Berruti, "Investigation on the dynamic response of blades with asymmetric under platform dampers," 2015.

[63] L. Pesaresi, L. Salles, R. Elliott, A. Jones, J. Green, and C. Schwingshackl, "Numerical and Experimental Investigation of an Underplatform Damper Test Rig," *Applied Mechanics and Materials*, vol. 849, pp. 1–12, 2016.

[64] M. J. Kruse and C. Pierre, "An experimental investigation of vibration localization in bladed disks: part i—free response," 1997.

[65] B. Beirow, F. Figaschewsky, A. Kühhorn, and A. Bornhorn, "Modal analyses of an axial turbine blisk with intentional mistuning," *Journal of Engineering for Gas Turbines and Power*, vol. 140, no. 1, 2018.

[66] U. Strehlau and A. Ku¨ hhorn, "Experimental and numerical investigations of hpc blisks with a focus on travelling waves," vol. 44014, pp. 865–877, 2010.

[67] K. W. Jones and C. J. Cross, "Traveling wave excitation system for bladed disks," *Journal of propulsion and power*, vol. 19, no. 1, pp. 135–141, 2003.

[68] J. A. Judge, S. L. Ceccio, and C. Pierre, "Traveling-wave excitation and optical measurement techniques for non-contacting investigation of bladed disk dynamics," *Shock and Vibration Digest*, vol. 35, no. 3, pp. 183–190, 2003.

[69] C. M. Firrone and T. Berruti, "Non contact measurement system with electromagnets for vibration tests on bladed disks," *Applied Measurement Systems, edited by Zahurul Haq. InTech*, pp. 77–108, 2012.

[70] T. Berruti, "A test rig for the investigation of the dynamic response of a bladed disk with underplatform dampers," *Mechanics Research Communications*, vol. 37, no. 6, pp. 581–583, 2010.

[71] C. Firrone and T. Berruti, "An electromagnetic system for the non-contact excitation of bladed disks," *Experimental mechanics*, vol. 52, no. 5, pp. 447–459, 2012.

[72] C. M. Firrone, T. M. Berruti, and M. M. Gola, "On force control of an engine order–type excitation applied to a bladed disk with underplatform dampers," *Journal of vibration and acoustics*, vol. 135, no. 4, 2013.

[73] T. Berruti, C. M. Firrone, and M. M. Gola, "A test rig for noncontact traveling wave excitation of a bladed disk with underplatform dampers," *Journal of Engineering for Gas Turbines and Power*, vol. 133, no. 3, 2011.

[74] D. J. Ewins, "Modal testing: theory and practice, vol. 15," *Letchworth: Research studies press*, 1984.

[75] G. Battiato, C. M. Firrone, and T. M. Berruti, "Forced response of rotating bladed disks: Blade Tip-Timing measurements," *Mechanical Systems and Signal Processing*, vol. 85, no. July 2016, pp. 912–926, 2017.

[76] D. Feiner and J. Griffin, "Mistuning identification of bladed disks using a fundamental mistuning model—part i: theory," *J. Turbomach.*, vol. 126, no. 1, pp. 150–158, 2004.

[77] D. Feiner and J. Griffin, "Mistuning identification of bladed disks using a fundamental mistuning model—part ii: application," *J. Turbomach.*, vol. 126, no. 1, pp. 159–165, 2004.

[78] D. L. Gillaugh, A. A. Kaszynski, J. M. Brown, J. A. Beck, and J. C. Slater, "Mistuning evaluation comparison via as-manufactured models, traveling wave excitation, and compressor rigs," *Journal of Engineering for Gas Turbines and Power*, vol. 141, no. 6, 2019.

[79] D. L. Gillaugh, A. A. Kaszynski, J. M. Brown, J. A. Beck, and J. C. Slater, "Strain gage ramifications on mistuning in as-manufactured models and experimental testing," *Journal of Engineering for Gas Turbines and Power*, vol. 142, no. 5, 2020.

[80] B. Yang, M. Chu, and C. Menq, "Stick–slip–separation analysis and non-linear stiffness and damping characterization of friction contacts having variable normal load," *Journal of Sound and vibration*, vol. 210, no. 4, pp. 461–481, 1998.

[81] E. Petrov and D. Ewins, "Analytical formulation of friction interface elements for analysis of nonlinear multi-harmonic vibrations of bladed disks," *J. Turbomach.*, vol. 125, no. 2, pp. 364–371, 2003.

[82] C.-H. Menq, P. Chidamparam, and J. Griffin, "Friction damping of two-dimensional motion and its application in vibration control," *Journal of sound and vibration*, vol. 144, no. 3, pp. 427–447, 1991.

[83] C. Menq and B. Yang, "Non-linear spring resistance and friction damping of frictional constraint having two-dimensional motion," *Journal of Sound and Vibration*, vol. 217, no. 1, pp. 127–143, 1998.

[84] K. Sanliturk and D. Ewins, "Modelling two-dimensional friction contact and its application using harmonic balance method," *Journal of sound and vibration*, vol. 193, no. 2, pp. 511–523, 1996.

Appendix A

Remarks on Numerical Computation of Nonlinear Forced Response Levels

The reduced equations of motion of a generic bladed disk with friction interfaces can be expressed as:

$$M_{rom}\ddot{\mathrm{x}}_{\mathrm{rom}}(t) + C_{rom}\dot{\mathrm{x}}_{\mathrm{rom}}(t) + K_{rom}\mathrm{x}_{\mathrm{rom}}(t) = F_{nl}(\mathrm{x}_{\mathrm{rom}}(t), \dot{\mathrm{x}}_{\mathrm{rom}}(t)) + F_{ex}(t) \quad \text{(A.1)}$$

where

- $\mathrm{x}_{\mathrm{rom}}(t)$ is the vector of DOFs of the reduced bladed disk and in general it comprises nonlinear contact DOFs, active DOFs (e.g. force and response DOFs) and generalized coordinates associated with the vibration modes retained in the reduction basis.
- M_{rom} and K_{rom} denote reduced mass and stiffness matrices, respectively.
- C_{rom} denotes the reduced damping matrix and is usually assumed to be proportional to the reduced stiffness and mass matrices (i.e. $C_{rom} = \alpha \cdot M_{rom} + \beta \cdot K_{rom}$).
- F_{nl} denotes the state dependent vector of nonlinear contact forces acting on the retained nonlinear contact DOFs.
- F_{ex} represents the vector of external periodic excitation in the reduced coordinates. Depending on the employed reduction technique, F_{ex} can contain

physical forces acting on the retained forcing DOFs (e.g. the ROMs developed in chapters 2 and 3) or can represent the modal force vector acting on the ROM (e.g. RCCMS-based ROMs in chapter 4).

Contact surfaces are modeled using the state-of-the-art node-to-node contact elements. The employed contact models are imposed at each contact node pair and characterize:

i. *unilateral contact force* in normal direction based on an elastic unilateral contact law.

ii. *friction force* in tangential plane based on a regularized Coulomb's law (the regularization is achieved by introducing the penalty stiffness to the model).

The employed contact models are referred to as *semi-3D* [46, 80, 81] and *full-3D* [82–84] contact elements. The schematic plot of the contact elements can be seen in Fig. A.1. The semi-3D contact model is composed of two perpendicular Jenkins contact elements with variable normal loads and assumes that the tangential components of contact forces are independent from each other. The full-3D contact model avoids such an assumption and describes a fully coupled tangential contact.

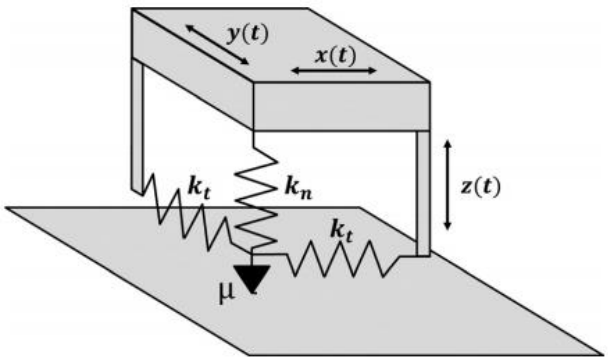

Fig. A.1 Schematic plot of a generic 3D contact element.

In general, blades can undergo a complex vibratory motion which is a combination of fundamental vibration motions in different planes (e.g. bending and torsion).

As a results, contact points at friction interfaces will experience an elliptical trajectory. Although a semi-3D contact element consists of two uncoupled perpendicular Jenkins elements, it is shown that (see [46, 80, 81]) they perform reasonably well compared to the more accurate full-3D contact elements.

Note that, the construction of the proposed ROMs in this thesis are independent of the contact models. In majority of the simulations performed, the semi-3D contact element is used due to efficiency reasons. It is intuitive that due to the complexity of the elliptical trajectory, more iterations is needed for the convergence of the contact model.

The nonlinear contact forces are computed using a predictor-corrector approach [46], and in general, the semi-3D contact model demands less iterations for convergence. The semi-3D contact model is employed in chapters 2 and 3 to reduce the computational burden.

The steady state response of the reduced system is computed using the HBM [22] and assuming that the response of the system under a periodic excitation remains periodic. Displacements and forces in Eq. (A.1) can be approximated as a sum of harmonic functions, as follows:

$$
\begin{aligned}
\mathrm{x}_{\mathrm{rom}}(t) &\approx X^0_{rom} + \Re\left(\sum_{h=1..H} \bar{X}^{(h)}_{rom} e^{ih\omega t}\right) \\
F_{ex}(t) &\approx F^0_{ex} + \Re\left(\sum_{h=1..H} \bar{F}^{(h)}_{ex} e^{ih\omega t}\right) \\
F_{nl}(x_{rom}(t), \dot{x}_{rom}(t)) &\approx F^0_{nl} + \Re\left(\sum_{h=1..H} \bar{F}^{(h)}_{nl} e^{ih\omega t}\right)
\end{aligned}
\tag{A.2}
$$

where $\Re$ indicates the real part of a complex valued function; H indicates the number of retained harmonics; ω denotes the frequency of the excitation force; and $\bar{X}^{(h)}_{rom}$, $F^{(h)}_{nl}$ and $F^{(h)}_{ex}$ are vectors of the hth Fourier coefficients corresponding to displacements, nonlinear friction forces and external excitation, respectively.

In Eq. (A.2), superscript 0 indicates zeroth harmonic terms. In details, X^0_{rom} denotes the static equilibrium position, F^0_{nl} and F^0_{ex} denote the static contact and the

static external force (e.g. centrifugal loads), respectively.

The static equilibrium is computed using either of following approaches [56, 57]:

- *Uncoupled static/dynamic approach*: in which, a preliminary nonlinear quasi-static analysis is performed. It is assumed that static equilibrium solutions are not affected by higher harmonic solutions, and thus, are solved separately from dynamic solutions. The solution of the static balance equations will give as an output the normal preload acting over the contact surfaces, used as an input in the dynamic analysis.
- *Coupled static/dynamic approach*: in which, the fully coupled balance equations are solved, simultaneously. No assumption is made, and thus, this method can capture the changes in the static equilibrium due to the system vibrations.

Since, in the coupled static/dynamic approach, static and dynamic balance equations are solved simultaneously, it is computationally more expensive. In this thesis, the coupled approach is only used in chapter 4 for some comparison purposes.

By introducing Eq. (A.2) into Eq. (A.1) and performing a Galerkin projection, the algebraic balance equations for each harmonic index, can be expressed as:

$$\bar{D}^{(h)}_{rom}\bar{X}^{(h)}_{rom} - \bar{F}^{(h)}_{nl} - \bar{F}^{(h)}_{ex} = 0 \tag{A.3}$$

where $\bar{D}^{(h)}_{rom} = [-(h\omega)^2 M_{rom} + ih\omega C_{rom} + K_{rom}]^{(h)}$ denotes the ROM dynamic stiffness corresponding to the hth harmonic.

The nonlinear balance equations in Eq. (A.3) can be solved using an iterative (predictor-corrector) Newton-Raphson method and the alternating frequency/time domain(AFT) algorithm [45]. In nonlinear forced response simulations, the pseudo-arclength path following technique [46] is used to compute the evolution of nonlinear forced response levels with respect to the excitation frequency.

The ROM dynamic stiffness in Eq. (A.3) can be partitioned as:

$$\begin{bmatrix} \bar{D}_{NN} & \bar{D}_{NL} \\ \bar{D}_{LN} & \bar{D}_{LL} \end{bmatrix}^{(h)} \begin{Bmatrix} \bar{X}_N \\ \bar{X}_L \end{Bmatrix}^{(h)} - \begin{Bmatrix} \bar{F}_{nl} \\ 0 \end{Bmatrix}^{(h)} - \begin{Bmatrix} \bar{F}^n_{ex} \\ \bar{F}^l_{ex} \end{Bmatrix}^{(h)} = 0 \tag{A.4}$$

where $\bar{X}_N$ denotes the vector of nonlinear DOFs and contains the relative displacements of contact node pairs; and $\bar{X}_L$ indicates the vector of linear DOFs and contains, in general, the remaining physical DOFs and generalized coordinates.

Note that, depending on the construction of the ROM, the $\bar{X}_{rom}$ vector may already contain the relative displacements between contact node pairs (e.g. RCCMS-based ROMs developed in chapter 4), and thus the $\bar{X}_N$ partition is readily available. Nevertheless, the absolute displacements of nonlinear contact DOFs, can be represented in terms of relative displacements between contact node pairs [19, 40] and afterwards the $\bar{X}_N$ partition will be available. Note that, the application of the relative notation, reduces the number of unknowns in the nonlinear core by half and considerably increases the computational efficiency.

Equation (A.4) can be first solved for the nonlinear DOFs by condensing the linear partitions on nonlinear DOFs), as follows:

$$\left[D_{NN} - D_{NL}D_{LL}^{-1}D_{LN}\right]^h \bar{X}_N^h = \bar{F}_{nl}^h + \left[\bar{F}_{ex}^n - D_{NL}D_{LL}^{-1}\bar{F}_{ex}^l\right]^h \tag{A.5}$$

and the solution of linear DOFs can be obtained outside of the iterative solver (offline solution) using the already calculated nonlinear solutions:

$$\bar{X}_L^h = D_{LL}^{-1\,h}\left(\bar{F}_{ex}^{l\;h} - D_{LN}^h \bar{X}_N^h\right) \tag{A.6}$$

It should be noted that, the nonlinear friction forces are dependent on all harmonic functions of the displacement vector. So, the algebraic balance equations $(h = 1..H)$ are coupled to each other through the nonlinear $\bar{F}_{nl}^h$ terms, and they should be solved simultaneously.

It is worth mentioning that the efficiency of solving the nonlinear core of balance equations can be further increased by employing the spectral expansion of the dynamic stiffness and avoiding its inversion. For instance, the nonlinear core of balance equations in Eq. (A.3), that is associated with relative displacements of nonlinear contact DOFs, can be obtained by:

$$\bar{X}_N^{(h)} = \Phi_{r,N} diag\left(\frac{1}{\omega_{r,s}^2 - (h\omega)^2 + i2h\zeta_{r,s}\omega_{r,s}\omega}\right)\left(\Phi_{r,N}^T \bar{F}_{nl}^{(h)} + \Phi_{r,E}^T \bar{F}_{ex}^{(h)}\right) \tag{A.7}$$

where

- $\Phi_{r,N}$ denotes a partition of the ROM normal modes corresponding to relative nonlinear contact DOFs.
- $\Phi_{r,E}$ denotes a partition of the ROM normal modes corresponding to forcing DOFs (where modal forces are nonzero).
- $\omega_{r,s}$ denotes the sth natural frequency of the ROM.
- $\zeta_{r,s}$ denotes the damping ratio associated with the sth normal mode of the ROM and can be expressed in terms of mass and stiffness proportional damping by $\zeta_{r,s} = \frac{\alpha}{2\omega_{r,s}} + \frac{\beta}{2}\omega_{r,s}$.

Note that the continuation scheme demands calculation of the Jacobian matrix at each iteration step, which can become a rigorous task. The computational burden was extremely reduced by implementing the analytical Jacobian as described in [15, 55].

Appendix B

Construction of the Reduced Mass Matrix Based on the Fixed-Boundary Component Mode Substitution Technique

B.1 Reduced Mass Matrix Construction

Mass matrices in each reduction step are partitioned exactly in the same way as their corresponding reduced stiffness matrices. A more detailed description for mass matrices are given here. Accordingly, different partitions of M_{CB} are:

$$M^b_{cb} = \begin{bmatrix} m^b_{cb,NN} & m^b_{cb,N\gamma} \\ m^b_{cb,\gamma N} & m^b_{cb,\gamma\gamma} \end{bmatrix} \tag{B.1}$$

where

$$\begin{aligned}
m^b_{cb,NN} &= m^b_{NN} + \left(k^b_{NI}k^{b^{-1}}_{II}\right) m_{II} \left(k^{b^{-1}}_{II}k^b_{IN}\right) - m_{NI}\left(k^{b^{-1}}_{II}k^b_{IN}\right) - \left(k^b_{NI}k^{b^{-1}}_{II}\right) m_{IN} \\
m^b_{cb,\gamma\gamma} &= m^b_{\gamma\gamma} + \left(k^b_{\gamma I}k^{b^{-1}}_{II}\right) m_{II} \left(k^{b^{-1}}_{II}k^b_{I\gamma}\right) - m_{\gamma I}\left(k^{b^{-1}}_{II}k^b_{I\gamma}\right) - \left(k^b_{\gamma I}k^{b^{-1}}_{II}\right) m_{I\gamma} \\
m^b_{cb,N\gamma} &= \left(k^b_{NI}k^{b^{-1}}_{II}\right) m_{II} \left(k^{b^{-1}}_{II}k^b_{I\gamma}\right) - m_{NI}\left(k^{b^{-1}}_{II}k^b_{I\gamma}\right) - \left(k^b_{NI}k^{b^{-1}}_{II}\right) m_{I\gamma} \\
m^b_{cb,\gamma N} &= \left(k^b_{\gamma I}k^{b^{-1}}_{II}\right) m_{II} \left(k^{b^{-1}}_{II}k^b_{IN}\right) - m_{\gamma I}\left(k^{b^{-1}}_{II}k^b_{IN}\right) - \left(k^b_{\gamma I}k^{b^{-1}}_{II}\right) m_{IN}
\end{aligned} \tag{B.2}$$

Implementing the same procedure as for stiffness matrix, final reduced mass matrix of a single sector yields:

$$M_{rom} = \begin{bmatrix} I & m_{\eta N} & 0 \\ m_{N\eta} & m^b_{cb,NN} & m^b_{cb,N\gamma}\tilde{\varphi}_\gamma \\ 0 & \tilde{\varphi}^T_\gamma m^b_{cb,\gamma N} & [\hat{m}] \end{bmatrix} \tag{B.3}$$

where

$$\hat{m} = \begin{bmatrix} \tilde{\varphi}_\gamma \\ \tilde{\varphi}_O \end{bmatrix}^T \begin{bmatrix} m^b_{cb,\gamma\gamma} + m^d_{\gamma\gamma} & m^d_{\gamma O} \\ m^d_{O\gamma} & m^d_{OO} \end{bmatrix} \begin{bmatrix} \tilde{\varphi}_\gamma \\ \tilde{\varphi}_O \end{bmatrix} \tag{B.4}$$

One may obtain the final reduced stiffness matrix of the full system, as follows:

$$\begin{aligned} M_{ROM} &= \begin{bmatrix} I \otimes \Lambda^b_i & I \otimes m_{N\eta} & 0 \\ I \otimes m_{N\eta} & I \otimes m^b_{cb,NN} & \left(I \otimes m^b_{cb,N\gamma}\right)\tilde{\Phi}_\gamma \\ 0 & \tilde{\Phi}^T_\gamma \left(I \otimes m^b_{cb,\gamma N}\right) & [\hat{M}] \end{bmatrix} \\ \hat{M} &= \begin{bmatrix} \tilde{\Phi}_\gamma \\ \tilde{\Phi}_O \end{bmatrix}^T \begin{bmatrix} \underset{n=1..N}{Bdiag}[m^{rom^{(n)}}_{\gamma\gamma}] & I \otimes m^d_{\gamma O} \\ I \otimes m^d_{O\gamma} & \bar{m}^d_{OO} \end{bmatrix} \begin{bmatrix} \tilde{\Phi}_\gamma \\ \tilde{\Phi}_O \end{bmatrix} \end{aligned} \tag{B.5}$$

where $\underset{n=1..N}{Bdiag}[m^{rom^{(n)}}_{\gamma\gamma}] = I \otimes m^{rom}_{\gamma\gamma} = I \otimes \left(m^b_{cb,\gamma\gamma} + m^d_{\gamma\gamma}\right)$.
Finally, the alternative formulation for $\hat{M}$ is expressed below. Using the operator introduced by Eq. (2.30), the compact notation for $\hat{M}$ takes the following form:

$$\hat{M} = \tilde{\Phi}^T \left(M_D + blkdg[m^b_{cb,\gamma\gamma}]\right)\tilde{\Phi} \tag{B.6}$$

By adding and subtracting the Guyan mass matrix of the tuned blades to the interface DOFs of the $\hat{M}$ central core and using Eq. (B.6), one may cast $\hat{M}$ as follows:

$$\begin{aligned} \hat{M} &= \tilde{\Phi}^T \left(M_D + blkdg[m^b_{Guyan}] - blkdg[m^b_{Guyan}] + blkdg[m^b_{cb,\gamma\gamma}]\right)\tilde{\Phi} \\ &= \tilde{\Phi}^T \left(\tilde{M} - blkdg[m^b_{Guyan}] + blkdg[m^b_{cb,\gamma\gamma}]\right)\tilde{\Phi} \\ &= [I] - \tilde{\Phi}^T_\gamma \underset{n=1..N}{Bdiag}[m^{b^{(n)}}_{Guyan}]\tilde{\Phi}_\gamma + \tilde{\Phi}^T_\gamma \underset{n=1..N}{Bdiag}[m^{b^{(n)}}_{cb,\gamma\gamma}]\tilde{\Phi}_\gamma \end{aligned} \tag{B.7}$$

Note this alternative formulation enables constructing the final reduced mass matrix by sector level calculations.

B.2 Direct Sum of Matrices

The direct sum of two matrices of arbitrary size is defined as:

$$A \oplus B = \begin{bmatrix} A & 0 \\ 0 & B \end{bmatrix} = \begin{bmatrix} a_{11} & \dots & a_{1n} & 0 & \dots & 0 \\ \vdots & \ddots & \vdots & \vdots & \ddots & \vdots \\ a_{m1} & \cdots & a_{mn} & 0 & \cdots & 0 \\ 0 & \dots & 0 & b_{11} & \dots & b_{1q} \\ \vdots & \ddots & \vdots & \vdots & \ddots & \vdots \\ 0 & \cdots & 0 & b_{p1} & \cdots & b_{pq} \end{bmatrix} \tag{B.8}$$